UNIVERSITÀ DEGLI STUDI DI NAPOLI FEDERICO II

Scuola politecnica e delle scienze di base
Dipartimento di Ingegneria Industriale

Scuola di Dottorato di Ricerca in Ingegneria Industriale
XXVIII Ciclo

Tesi di dottorato di ricerca
in Ingegneria Aerospaziale, Navale e della Qualità

Aerodynamic design of stall regulated wind turbines to maximize annual energy yield

Relatore
Ch.mo Prof. Domenico Coiro

Dottoranda
Nadia Bizzarrini

Anno accademico 2015/2016

Contents

List of Figures

Introduction

Looking back in wind turbines history, pitch-regulated machines gradually substituted stall-regulated systems. In fact, the possibility to optimize the power production for each wind condition by regulating the pitch angle of the blade, proved to be a key feature to maximize the Annual Energy Production (AEP) of the wind turbines. Nowadays, all the modern MW-class wind turbines are “by default” pitch-regulated and several innovations are implemented by Industry to improve the pitch performance (e.g. individual pitch control IPC, fine regulation mechanisms/algorithms) and extract more power.

In apparent contradiction with MW machines however, small and medium kW wind turbines are still largely stall-regulated machines. The reasons of this are easy to explain. In fact, the advantages of the pitch system come with some costs. The first is the direct cost of the pitch system and its maintenance. Secondly, the pitch system increases the weight of the machine and the general complexity of the system, together with the development costs and the issues related to the system robustness/reliability. Extra components, such onboard anemometers and pitch bearings, are necessary to operate the pitch of the blade correctly. All these costs and complications can be too much significant for small machines and it explains why a robust and easy-to-maintain solution is preferred even with some AEP sacrifice.

However, from the design point of view, the stall-regulated machines still turn out to be a challenging task, especially concerning the aerodynamics of the blade that should ensure the power performance and it is also the only component to provide the machine control.

In particular the aerodynamics of the airfoils along the blade plays a crucial role and, compared to pitch control wind turbines, more characteristics have to be considered and carefully treated.

Regarding the AEP maximization, a single point optimization can be sufficient for pitch controlled wind turbines, that means optimization of the aerodynamic efficiency of the airfoils along the blade. Whereas, for stall regulated machines a multi-point optimization of blade and airfoils turns out to be necessary, because these work in a wide range of angles of attack depending on the wind speed.

Furthermore, regarding the overall design of the rotor, it’s fundamental to take into account several difficulties related to stall and post-stall regimes, where the power peak of the wind turbine and, then, the power control are obtained.

First of all, to predict turbine performances the Blade Element Momentum Theory (BEM) is widely used in preliminary design phases because of a reasonably velocity and accuracy compared to CFD or other methods, but it lacks of the same accuracy in these regions for reasons related to limitations in predicting airfoil performances, which are used by the BEM, and limitations of the theory itself.
Regarding prediction of airfoil performances, both experimental and numerical analyses are more delicate in this zones and not always good predictions can be obtained. CFD and experimental analyses would often be necessary, with related high time costs.
Experimental data of drag coefficient in the deep post-stall region are not accurate or even not available for most of the published airfoils, thus specific experimental tests would be needed to use these airfoils on a stall regulated wind turbine.
Furthermore, in stall and post-stall regions the effects of blade rotation (also known as 'stall delay' or 'centrifugal pumping') have to be taken into account, especially in the inner part of the blade, but this issue, nowadays, is still to be investigated in depth. The main effect of blade rotation is a stall delay and higher stall and post stall lift coefficient values for the inner airfoils of the blade, with a consequent less power control of the turbine.
Regarding the limitations of BEM Theory itself in stall and post stall regions, these are caused by the simplifying assumptions of the theory, which are the force, but also the problem of the theory at the same time (as for any simplified model).
Finally, design challenges in the structural dynamics of the whole machine are peculiar of stall regulated wind turbines and are deeply depending on the airfoils characteristics and the blade shape.
In particular, difficulties related to dynamic stall and, most importantly, to stall-induced vibrations have to be taken into account.
As deeply outlined by Petersen et al. in [1],the main problem is that a gentle slope of lift coefficient curve of the tip airfoils of the blade is necessary to reduce stall induced vibrations but at the same time it causes a less power control of the turbine.
Finding a good compromise between vibrations problem and power control can be considered the main issue in the design of stall regulated wind turbines.

The main objective of this work has been the study of all the issues briefly presented, to properly design an experimental stall regulated wind turbine, maximizing the Annual Energy Production and minimizing the rotor weight.
In particular, the issue of stall induced vibrations turned out to be critical for this turbine because it is intended to produce energy at low wind speeds and needs slender and highly deformable blades.

First of all, some fast methods and codes for a correct prediction of airfoils and turbine performances in a preliminary design have been investigated.

For the airfoils performances, some corrections have been proposed and validated through a comparison with 3D-CFD results on a rotating blade. Furthermore, BEM shortcomings have been analyzed.
The stall induced vibrations phenomenon and its sources have been investigated and some solutions have been tested.
Finally, desirable airfoils characteristics have been individuated both for the AEP maximization and the compromise between stall induced vibrations and power control, and have been used to design an airfoil specifically suited to the new wind turbine.
The final purpose of this work is to give suggestions for a reasonably fast and accurate predesign about computing methods and design choices for stall regulated wind turbines.

Summary of the work

In Chapter 1 a brief overview of the working principle of stall regulated wind turbines is reported, with the main differences, advantages and disadvantages respect to pitch regulated machines.
In Chapter 2 the Blade Element Theory is outlined, with its limitations, but also its advantages, compared to other methods for computing wind turbines performances.
Chapter 3 addresses the issues in predicting performances of airfoils on a rotating blade and the method adopted in this work is introduced.
Chapter 4 presents the BEM code used in this work to predict wind turbine performances in steady operating conditions, and its results are compared to those obtained with a CFD simulation and with an aeroelastic analysis in unsteady conditions.
In Chapter 5 the issue of stall induced vibrations is presented in detail and the results obtained during the optimization process developed in this work are reported.
Finally, in Chapter 6 the blade design developed in this work is presented together with the main results obtained.

Chapter 1
Stall regulated wind turbines

Wind turbines are designed to produce electrical energy as cheaply as possible.
At high wind speeds it is necessary to waste part of the energy of the wind in order to avoid excess power which would overload the turbine generator, as well as excess forces on the blades which would damage the wind turbine. All wind turbines are therefore designed with some sort of power control.
Section 1.1 reports a brief overview of various strategies for limiting power aerodynamically, while in Section 1.2 a more detailed presentation of stall regulated wind turbines is performed.
Finally, Section 1.3 reports the method used to evaluate the Annual Energy Production, which is one of the objective functions optimized within the design process developed in this work.

1.1 Power control strategies

1.1.1 Pitch control

Pitch regulated wind turbines have blades that can be turned around their longitudinal axis (to pitch) usually by means of an hydraulic pitch actuator system.
The wind turbine is provided with an electronic controller which checks the power output several times per second. When the power output becomes too high, it sends an order to the blade pitch mechanism which immediately pitches the rotor blades slightly out of the wind, thus modifying the angle of attack to reduce lift and torque. Conversely, the blades are turned back into the wind whenever the wind drops again.
This machines offer better control options than the stall regulated ones. Nevertheless, the hub results in a more complicated structure as pitch bearings as well as the pitch actuation system need to be incorporated.
In some wind turbines, only the outer part of the blade can be pitched. This mechanism is known as ‘partial span pitch control’.

1.1.2 Stall control

- **Passive stall control**

Contrary to pitch regulated wind turbines, passive stall controlled machines have the rotor blades rigidly fastened to the hub.
The airfoils along the blade work at angles of attack increasing with the increase of wind speed, until at some point they starts to stall.
Passive stall control takes advantage of reduced aerodynamic lift of stalled airfoils to limit power output and loads at high wind speeds. (A more detailed explanation is reported in Section 1.2.)
Anyway, passive stall controlled machines incorporate separate braking systems to ensure that the turbine can be shut down under all eventualities.
The basic advantage of passive stall control is that it avoids moving parts and a complex control system. On the other hand, it requires a highly complex aerodynamic design, with several challenges regarding the structural dynamics of the whole wind turbine.
In this work a passive stall regulated wind turbine has been optimized and the related issues are addressed in this report. In the following chapters, 'passive stall control' will be simply reported as 'stall control'.

- **Active stall control**

The active stall machines resemble pitch controlled machines, since they have pitchable blades, but they work in the opposite manner to control the power at high wind speeds.
When a machine reaches its rated power, it will pitch the blades in the opposite direction respect to a pitch controlled machine. In other words, it will increase the angle of attack of the rotor blades in order to make the blades go into a deeper stall, thus wasting the excess energy in the wind.

1.1.3 Yaw control

Yaw control consists in the rotor being turned away from the wind for achieving the necessary power reduction.
The hub must be able to withstand gyroscopic loads due to yawing motion. Thus, this system requires a robust yaw system which results in yaw control being a far less common power regulation method compared to pitch and stall control. It is in practice used only for little wind turbines (1 kW or less).

1.1.4 Aerodynamic surfaces

Aerodynamic surfaces - e.g. ailerons - can also be added to the blades to control or modify power.

1.2 Stall regulated wind turbines - Working principle and performances

As briefly said in Introduction, nowadays pitch control is the most commonly used power control strategy since it can reach the highest performances in terms of Annual Energy Production (AEP).
For this reason, stall regulated wind turbines will be presented comparing their working principle to pitch control strategy, to highlight their advantages and shortcomings with respect to pitch controlled machines.
Figure 1.1 shows the scheme of a blade section at the generic local radius r, with the angle and velocities that determine the forces on the element and also the induced velocities on the airfoil (that will be explained in more detail in Chapter 2).

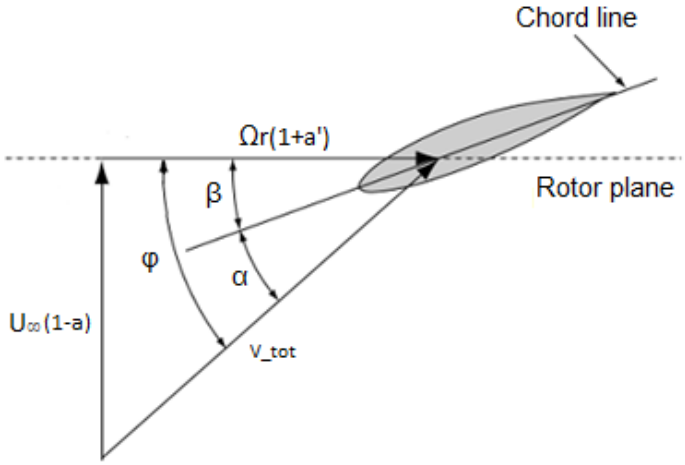

Figure 1.1: Local element velocities and flow angles. Adapted from [2]

In figure:
Ω is the rotational speed of the blade,
U_∞ is the wind speed,
Vtot is the total velocity relative to the airfoil, defined as:
$\mathrm{Vtot} = \sqrt{(U_\infty(1-a))^2 + (\Omega r(1+a'))^2}$
β is the local pitch angle,
ϕ is the inflow angle,
α is the angle of attack (and α= ϕ- β),
a is the axial induction factor and
a' is the tangential induction factor
(aU_∞ and $a'U_\infty$ are the induced velocities in the axial and tangential direction respectively).

Figure 1.2 shows the local aerodynamic forces (lift (L) and drag (D)) on the blade element and their components perpendicular and parallel to the rotor plane. These forces, integrated along the blade, produce the thrust (T_{tot}) and torque (Q_{tot}) of the rotor, respectively.

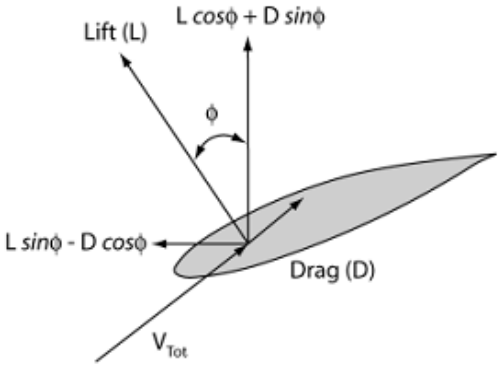

Figure 1.2: Local element forces. Extracted from [2]

As shown in Figure 1.2, the angle relating the lift and drag of the airfoil element to the thrust and torque forces is the local inflow angle ϕ, which depends on wind speed, rotational speed and induced velocities.

The local pitch angle (β) depends on the static blade geometry (twist) and the variable or fixed blade pitch.

Finally, the local angle of attack can be obtained as α=ϕ-β.

Thus, on pitch controlled wind turbines α can be set at any desired value, varying the pitch of the blade (and thus the local pitch angle β).

On the contrary, stall regulated wind turbines have fixed pitch blades and are normally operated at an almost constant rotational speed, thus the angle of attack increases as the wind speed increases.

The angles of attack along the blade of a fixed pitch wind turbine, at different wind speeds, are shown in the following figure.

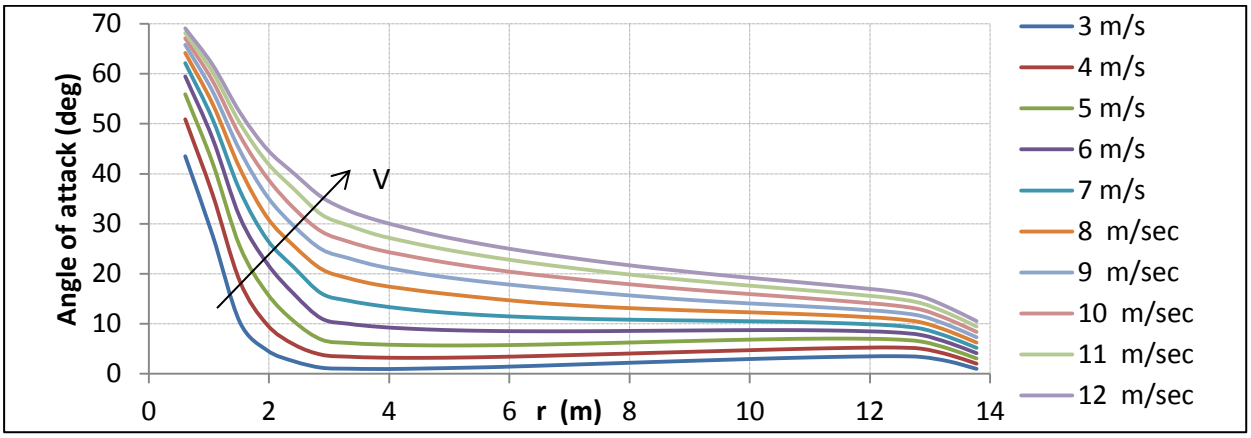

Figure 1.3: Angles of attack along the blade of a stall regulated wind turbine

Furthermore, in the following figures the working points of the airfoil at the station r=75%R, for different wind speeds, are reported on the lift curve, drag curve and efficiency curve of the airfoil.

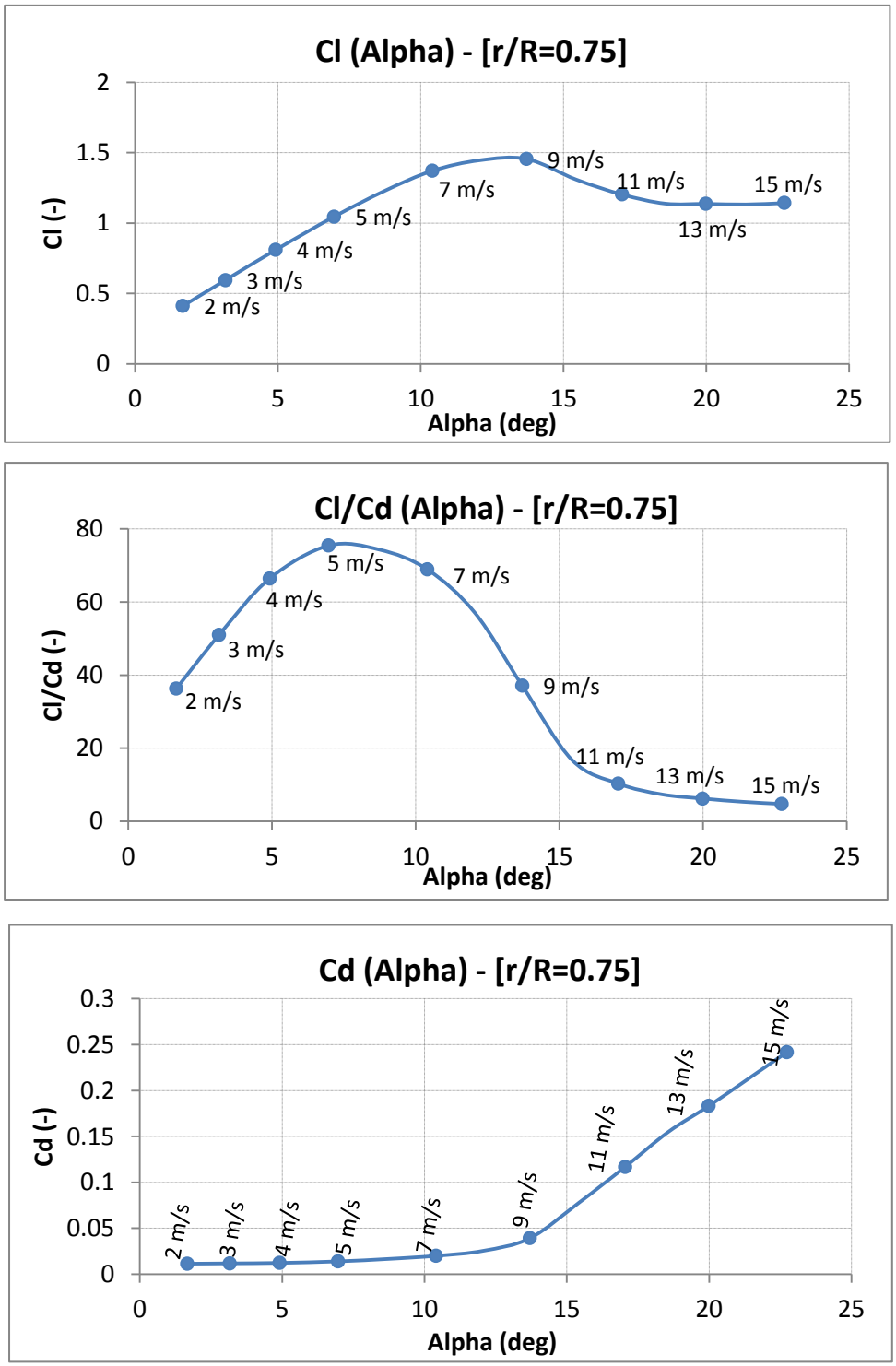

Figure 1.4: Aerodynamic performance of the representative airfoil (r=75%R) with the increasing of wind speed

With the increasing of wind speed, the airfoils along the blade gradually reach their own stall angle of attack, beyond which the lift starts to decrease with a consequent reduction of the produced torque and thrust.
Stall controlled wind turbines use this mechanism to limit and control power output and loads at high wind speeds, without the need of the complex and expensive devices to be provided in the case of pitch controlled wind turbines.
However, a fixed pitch causes lower performances with respect to the variable pitch system.
Global performances of wind turbines essentially depend on the rotor-size and the power coefficient, defined as:

$$Cp = \frac{P}{\frac{1}{2}\rho U_{\infty}^{3}\pi R^{2}} \qquad (1.1)$$

where:
P is the power output of the wind turbine,

ρ is the air density,

V is the wind speed

and

R is the rotor radius.

This coefficient represents the efficiency of a wind turbine, not depending on the rotor size, and actually it is the parameter to optimize within a design process.
Betz demonstrated that it is not possible to obtain a power coefficient higher than 0.59, the so called “Betz limit”.
Looking at next figure, which reports the power coefficient of a stall regulated wind turbine as function of wind speed, compared to the power coefficient of a pitch regulated turbine, it is possible to understand the main difference between this two kinds of machine.
It has to be noticed that the ideal curve of power coefficient is reported for both of them, that means maximum power coefficient equal to the Betz limit value.
Since pitch regulated wind turbines can continuously adapt the pitch of the blades to make the airfoils produce the maximum torque at different wind speeds, they can always work at the maximum power coefficient until the Vrated (the wind speed at which the desired power (Prated) is achieved); at higher wind speeds, the pitch is varied to obtain a constant power output and limited loads on the blades.

On the contrary, stall controlled turbines can reach the maximum power coefficient at only one wind speed.

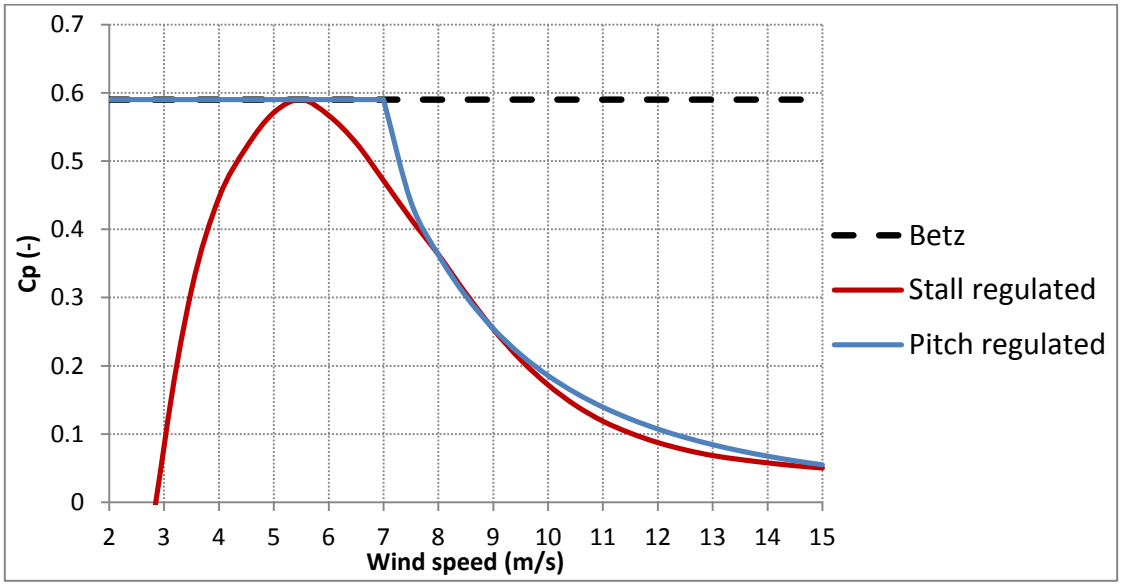

Figure 1.5: Power coefficient curve of a stall regulated and a pitch regulated wind turbine

(Cp max=Betz limit)

In terms of power curves, this means that stall control leads to a loss of power output in different operating conditions (with a related loss of annual energy production) respect to pitch control (rotor-size being equal), as shown in the following figure.

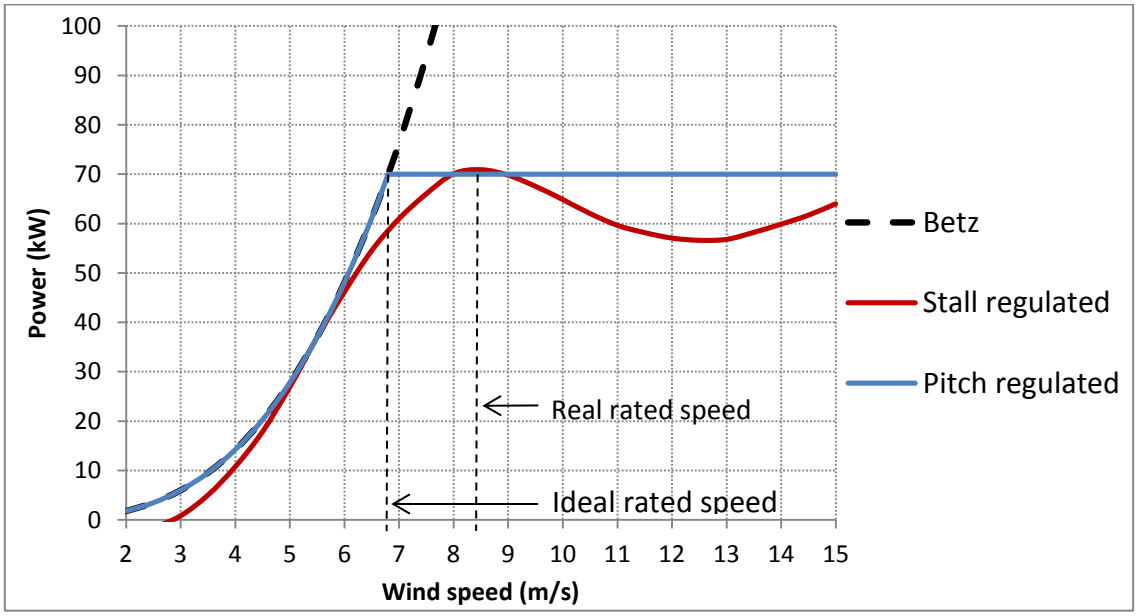

Figure 1.6: Power curve of a stall regulated and a pitch regulated wind turbine

(Cp max=Betz limit)

Thus, the ideal curve of the pitch regulated wind turbine represents the 'optimum' in the optimization process of both pitch and stall regulated machines but in the latter case the aerodynamics of the blades can't ensure a power output that matches this curve, not even in ideal conditions.
For this reason, nowadays pitch control is the most used solution.
Nevertheless, as said in introduction, the pitch system increases the weight and the general complexity of the machines, together with the development costs and the issues related to the system robustness/reliability. All these costs and complications can be too much significant for small machines and it explains why a robust and easy-to-maintain solution like stall controlled wind turbines is preferred even with some AEP sacrifice.
However, from the design point of view, stall-regulated machines turns out to be a challenging task because of several counteracting aerodynamic and structural issues to be taken into account during the design of a new machine.
Some of these issues have been addressed in this work and reported in detail in the following chapters.

1.3 Calculation of Annual Energy Production (AEP)

To evaluate the Annual Energy Production of a wind turbine, it is necessary to define the probability distribution of wind speed on a specific site, which can be expressed by a typical Weibull distribution.
We can define the probability density function of the wind speed as:

$$f(V_0) = \frac{k}{c}\left(\frac{V_0}{c}\right)^{k-1} exp\left(-\left(\frac{V_0}{c}\right)^{k}\right) \tag{1.2}$$

and the cumulative distribution function as :

$$F(V_0) = 1 - exp\left(-\left(\frac{V_0}{c}\right)^{k}\right) \tag{1.3}$$

where c is the scale parameter and k is the shape parameter
Both of these parameters are used to model corrections for the specific local conditions - meteorological data, landscape, and obstacles such as vegetation or buildings.
Usually, the wind speed is discretized in N values and a local probability is used, which is expressed as:

$$f(V_i < V_0 < V_{i+1}) = exp\left(-\left(\frac{V_i}{c}\right)^{k}\right) - exp\left(-\left(\frac{V_{i+1}}{c}\right)^{k}\right) \tag{1.4}$$

and represents the probability that the wind speed lies between the two discrete values *Vi* and *Vi+1.*

Multiplying this with the total number of hours per year (8760 hours), the number of hours per year that the wind speed lies in the interval (Vi< V0< Vi+1) can be obtained.

Thus, the Annual Energy Production can be computed as in the following expression:

$$AEP = \sum_{i=1}^{N=1} \frac{1}{2}(P(V_{i+1}) + P(V_i)) \cdot f(V_i, V_0, V_{i+1}) \cdot 8760 \quad (1.5)$$

where P is the electrical power produced by the wind turbine.

The following figure shows a typical 'relation' between a wind Weibull distribution and a power curve of a wind turbine.

It can be noticed that, in most cases the main contribution to the AEP is given by the region before the power peak of the wind turbine.

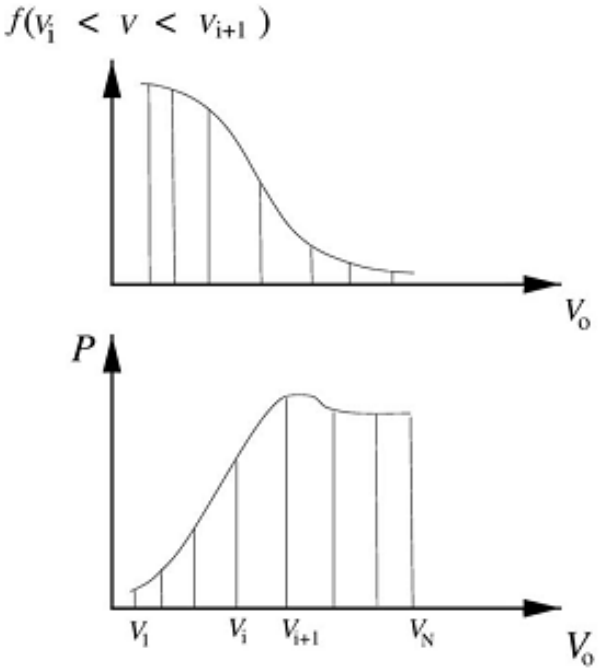

Figure 1.7 Example of a typical Weibull distribution of the wind speed and a typical power curve of a stall regulated wind turbine

Chapter 2
Steady performance prediction of stall regulated wind turbines – BEM and related issues

Wind turbine power production depends on the interaction between the rotor and the wind, which may be considered to be a combination of the mean wind and turbulent fluctuations about that mean flow.
In the first stage of a wind turbine design, only mean aerodynamic loads and power production need to be evaluated, and experience has shown that these are determined by the aerodynamic forces generated by the mean wind.
Periodic aerodynamic forces - caused by wind shear, off-axis winds, and blades rotation - and randomly fluctuating forces - induced by turbulence and dynamic effects - are the sources of fatigue loads and are a factor in the peak loads experienced by a wind turbine.
These are, of course, important, and have to be taken into account in a later stage of the design to evaluate the dynamic response of the turbine, but they can only be understood once the steady state aerodynamics of the wind turbine has been clearly defined.

Furthermore, in a preliminary design phase, the design method should be reasonably fast, produce results that are reasonably accurate, and only rely on input parameters that can be known or guessed in an early phase.

For this reasons, because of its simplicity and reliability, the Blade Element Momentum Theory (BEM) has always been one of the most commonly used methods for predicting rotor performances within aerodynamic design processes.
In fact, as it will be shown later, with the use of the BEM theory, rotor performance can be quickly predicted just knowing the shape of the blade and the aerodynamic characteristics of the airfoils along the blade.
However, to properly apply this method, some issues have to be taken into account and, as explained later, most of them become crucial for stall regulated wind turbines, being more important in the post stall region.
However, to properly apply this method, it is necessary to take into account several issues which, as explained later, are crucial for stall regulated wind turbines, since they become more important in the post stall regime of the blade.

Some of these issues are related to simplifying assumptions of the BEM theory itself and others are related to uncertainties in modelling airfoils performances along the blade.
In this work these issues have been analysed to define a simple and reliable procedure of preliminary design of a stall regulated wind turbine using the BEM theory.

A detailed explanation of the BEM method is not reported here because it is readily available in literature. Just a brief overview is made to introduce the advantages and limitations of this method.

2.1 Blade Element Momentum Theory (BEM)

Blade Element Momentum Theory (BEM) is an iterative method used to evaluate the loads and thus the power output of a rotor, whose size, blade shape (twist and chord distributions) and airfoils aerodynamic performances are known.
This theory is an extension of actuator disk theory, first proposed by the pioneering propeller work of Rankine and Froude in the late 19th century.
It was originally developed for propeller design by Betz and Glauert [3] in the 1930s. Subsequently, the theory was expanded and adapted for use with wind turbines for example by Wilson and Lissaman [4], Burton et al. [5],and Hansen [6].
A number of authors have derived different BEM methods during the years adding corrections and modifications.
All of these methods are based on the combination of the Momentum Theory and the Blade Element Theory.

The Momentum Theory derives loads on the rotor disc applying equations of continuity and conservation of momentum and angular momentum in a control volume analysis constituted by a divergent stream tube from far upstream to far downstream of the rotor.
The work done on the blade elements by the airflow passing through the rotor plane causes a sudden momentum variation of the flow (or pressure drop) in the axial and tangential directions.
Thus, the Momentum Theory can furnish the loads applied by the airflow on the blade elements in terms of velocities induced from the momentum variation in the axial and tangential directions.
On the other hand, Blade Element Theory divides the blades into small elements that act independently of surrounding elements and operate aerodynamically as two-dimensional airfoils.

The term two-dimensional implies that no three dimensional flow effects are assumed to occur around each blade element.
Thus, the forces exerted by the flow stream on each element are expressed solely in terms of the two-dimensional lift (Cl) and drag (Cd) characteristics of the blade local airfoil and its angle of attack (α) relative to the local incoming flow (Vrel), which is affected by velocities induced by the wake.
Figure1.1 is reported again to shows the scheme of velocities and angles on a blade section, and how the forces along the blade can be obtained.

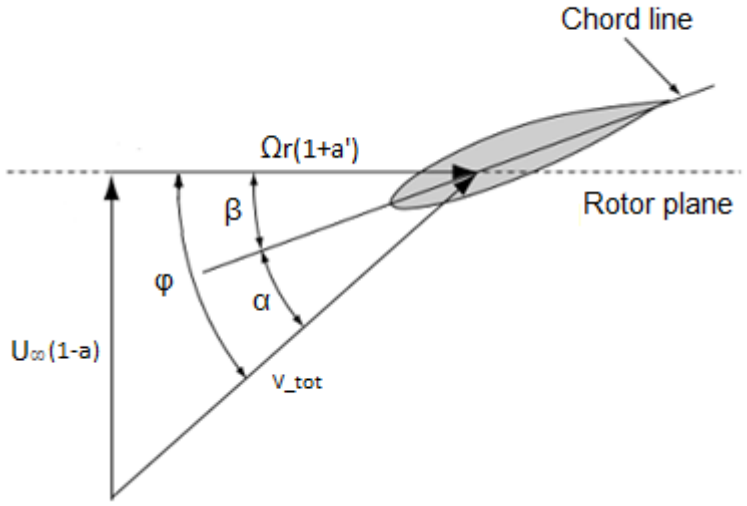

Figure 2.1: Local element velocities and flow angles. Adapted from [2]

In figure:
Ω is the rotational speed of the blade,
U_∞ is the wind speed,
Vtot is the total velocity relative to the airfoil, defined as

$$\text{Vtot} = \sqrt{(U_\infty(1-a))^2 + (\Omega r(1+a'))^2}$$

a is the axial induction factor
and
a' is the tangential induction factor.
(aU_∞ and $a'U_\infty$ are the induced velocities in the axial and tangential direction respectively).
φ is the inflow angle, defined as the angle between Vrel and the rotor plane, and determined by the expression:

$$tan\varphi = \frac{U_\infty(1-a)}{\Omega r(1+a')} = \frac{(1-a)}{(1+a')\lambda_r} \qquad (2.1)$$

where λ_r is the local tip speed ratio, defined as the ratio between the components of the relative wind speed (Vrel) respectively parallel and perpendicular to the rotor plane:

$$\lambda_r = \frac{\Omega r}{U_\infty} \qquad (2.2)$$

Finally, β is the local pitch angle,
α is the angle of attack at which the airfoil operates and can be obtained as: α= φ-β.

Thus, the angle of attack α only depends on the local pitch angle β, that is defined by the blade geometry, and the inflow angle φ that is a function of the induced velocities in both the axial and tangential directions, as well as of the local tip speed ratio λ_r.
Also Figure 1.2 is reported again shows the resultant aerodynamic forces on the element and their components perpendicular and parallel to the rotor plane, that are respectively the contribute to thrust and torque of the blade element.

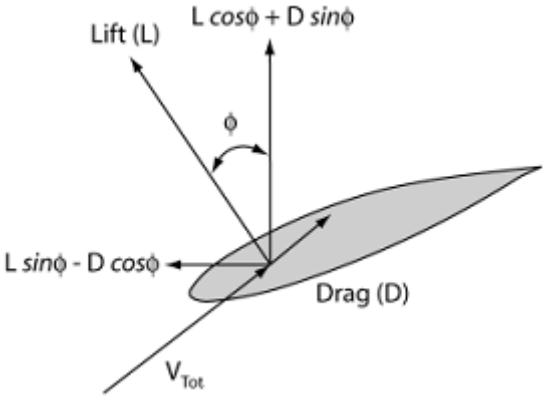

Figure 2.2: Local element velocities and flow angles. Extracted from [2]

From blade element theory, the thrust distributed around an annulus of width dr is equivalent to:

$$dT = B\frac{1}{2}\rho V_{tot}^2(C_l cos\varphi + C_d sin\varphi)cdr \qquad (2.3)$$

and the torque produced by the blade elements in the annulus is equivalent to:

$$dQ = B\frac{1}{2}\rho V_{tot}^2(C_l sin\varphi - C_d cos\varphi)cdr \quad (2.4)$$

where

$$Vtot = \sqrt{(U_\infty(1-a))^2 + (\Omega r(1+a'))^2} \quad (2.5)$$

Finally, the elemental forces are summed along the span of the blade to calculate the total forces and moments exerted on the turbine.

The induced dimensionless velocity components a and a' in the equations of both the theories illustrated, are functions of the forces on the blades themselves.
Thus, an iterative method is needed to compute them and Blade Element Momentum Theory (BEM) is used for this purpose.

BEM couples the Momentum Theory with the Blade Element Theory and sets up an iterative process to determine the aerodynamic forces and also the induced velocities near the rotor.
In practice, BEM is implemented by breaking the blades of a wind turbine into N elements of width dr along the span as in the blade element theory. As these elements rotate in the rotor plane, they trace out annular regions, shown in the following figure.

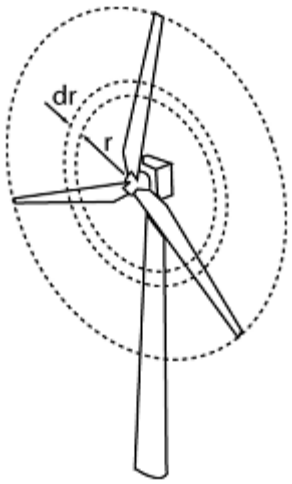

Figure 2.3: Annular sector used in blade element momentum theory. Extracted from [2]

At the same time, the original stream tube of the Momentum Theory is subdivided into N non interacting annular sectors of thickness dr, intersecting the rotor plane in the annular regions traced by the rotating elements as shown in the figure.

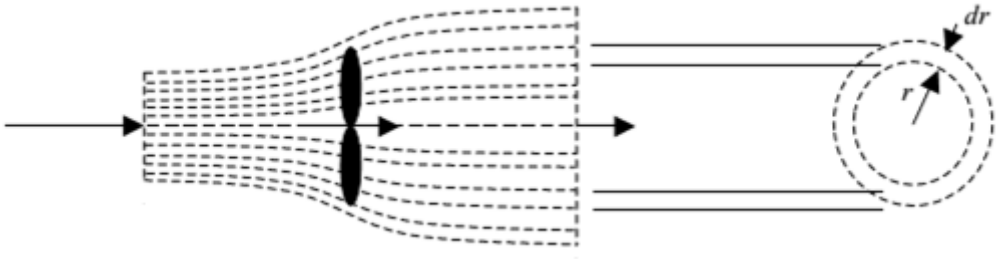

Figure 2.4: Annular stream tube control volumes used in blade element momentum theory. Extracted from [7]

On each annular sector momentum balance is applied to determine the differential rotor thrust (dT), and differential rotor torque (dQ) in terms of the local velocities induced by the wake, with the following expressions:

$$dT = 4\pi r \rho U_{\infty}^{2}(1-a)a dr \qquad (2.6)$$

$$dQ = 4\pi r^{3} \rho U_{\infty} \Omega (1-a)a' dr \qquad (2.7)$$

BEM theory is based on the fact that the differential loads derived from Momentum Theory and Blade Element Theory must be equivalent.
Thus, equating the differential thrust and torque derived with the two methods, a set of two equations is obtained that relates the local induction factors a e a' and local Cl and Cd values of the airfoils.
As previously explained, Cl and Cd, and thus the forces, are functions of the angle of attack that depends on the induced velocities, but, at the same time, a and a' depend on the same forces.
Thus the set of equations has to be iteratively solved for the induced velocities and the forces on each blade element.

Once the differential loads on each element blade are found, the total forces on the entire blade can be obtained by simple integration (or summation for the case of a finite number of elements).
Finally the overall power output (P) of the wind turbine and rotor power coefficient (Cp) can be evaluated using the following expressions:

$$P = \int_{0}^{R} \omega dQ \qquad (2.8)$$

$$Cp = \frac{P}{\frac{1}{2}\rho U_{\infty}^{3}\pi R^{2}} \qquad (2.9)$$

2.1.1 BEM inherent shortcomings

In BEM the following simplifying assumptions are used:

1) The force from the blades on the flow is constant in each annular element; this corresponds to a rotor with an infinite number of blades.
2) The flow of each sector is independent of adjacent circular sector flows. Thus, each radial section of the blade is analysed independently of the others (using two dimensional airfoil data) and what happens at one element cannot be felt from the others (the forces acting on the blade element are essentially two dimensional, meaning that span-wise flow is neglected).
   Furthermore no flow passes across the walls of the whole stream tube

These assumptions produce errors that have to be corrected or, at least, taken into account for a correct performance prediction.

Regarding the first assumption, for a rotor with an infinite number of blades the vortex system in the wake is different from that of a real rotor and this results in incorrect computations of velocity induction values.
The real local induction for each annulus is greater at each blade than the average of the annulus because of induced effects from the blade trailing vorticity.
Greater local induction leads to lower angle-of-attack distributions, greater induced drag and lower torque relative to BEM (see BEM expression for torque).
This can become critical for stall regulated wind turbines at high wind speeds, because they have fixed pitch blades, thus the airfoils encounter increasing angles of attack with related higher loads and higher vorticity with the increase of the speed.

Regarding the second assumption, it can become critical especially in the post stall regime of a stall regulated wind turbine, where the airfoils are stalled, the flow becomes turbulent, and a strong three-dimensional flow occur. This also invalidates the assumptions of stream tube flow of the BEM.

At high wind speeds the BEM assumptions lead to an over prediction of power and loads beyond the power peak of stall regulated wind turbines.

Furthermore, in the original theory no modelling of tip or hub vortex influence on the induced velocities are included, that causes an overestimation of loads and performance.
Because a blade has a suction surface and a pressure surface, air tends to flow over the blade tip from the lower (pressure) surface to the upper (suction) surface, effectively reducing the resulting forces in the vicinity of the tip.

The errors resulting from these BEM simplifications could be overcome through the use of a more physically accurate approach, like prescribed-wake vortex theory or free-wake vortex theory, that model the rotor blades with a lifting surface and the resulting vortex wake, and automatically include effects of tip losses, hub losses, finite number of blades.

However, numerous model comparisons with experimental data of rotating wind turbines, for instance those presented in [8] and [9] show that vortex-wake analysis is apparently no more accurate than BEM theory for ordinary blades.
Furthermore it requires higher amount of computer time compared to BEM.
For this reasons it is not recommended for design of ordinary blades. It might possibly be useful for special rotors with two section blades, surface effects, dynamic tip inducers, etc.

Thus, BEM method is usually preferred for preliminary design but, as previously said, corrections are needed to properly use it.

The main corrections to the BEM method are the classical Prandtl's tip loss factor, which corrects the assumption of an infinite number of blades and accounts for tip vortex influence (in particular, it predicts losses to occur for a rotating device of finite number of blades due to the circulation flow which takes place at the tip of the lifting device) and the Glauert's correction, which is an empirical relation between the thrust coefficient (Ct) and the axial induction (a) for a greater than approximately 0.4 (beyond this value the BEM method is no longer valid).
Like most engineering models they have limitations that affect the accuracy.
For each of these corrections several modifications have been proposed during the years, and adopted in different BEM codes.

However, the validation studies of different tools in [8] and [9] also showed that for stall regulated wind turbines discrepancies between different BEM tools are mainly caused by differences in the methods to model the airfoils aerodynamic characteristics.

Thus, modifications of the original Prandtl's and Glauert's corrections, that distinguish one BEM code from another, have effects on predicted rotor performances that are negligible (in a preliminary design) if compared with the effects of the airfoils.
For this reason, this work has been mainly focused on the issues related to a correct modelling of airfoils aerodynamic characteristics on a rotating blade.

Chapter 3
Prediction of airfoil aerodynamic performances and related issues

In the previous chapter it has been seen that airfoil data accuracy is considered to be the greatest potential source of error in BEM codes.
Thus, BEM can be a reliable tool for preliminary design only with a correct modelling of airfoil performance along the blade.
In particular, for stall regulated wind turbines it is necessary to obtain accurate information on airfoils performances nearby and beyond the stall, since the power peak and then the power control are obtained when most part of the blade is stalled.
Unfortunately, it is difficult to know airfoils behaviour in these regimes and even more their behaviour on a 3D rotating blade.

In fact, for existing airfoils not always accurate experimental data are available for angles of attack much beyond stall (in the deep post-stall regime).
Furthermore, if the experimental tests are not performed by means of force balances, usually drag coefficient beyond the stall is underestimated.
Thus, specific experimental tests would be needed to use airfoils on a stall regulated wind turbine.

Furthermore, if experimental data are not available at all, for example for a new airfoil, it is necessary to predict airfoil performances using numerical methods. This has been the case of the present work.
To get accurate results, CFD analyses of the airfoils should be performed. However, CFD codes in general are not yet considered practical tools for design processes because they are highly time consuming.
For this reasons panel codes based on integral solution of the boundary layer equations are usually used to predict airfoils aerodynamic performances.

In the next section a brief overview of the panel code used in this work is reported and in the last section the issue of predicting airfoils performances on a rotating blade is treated.

3.1 Prediction of 2D airfoil aerodynamic performances – Rfoil

To predict airfoils performances along the blade in this work Rfoil ([10], [11]) has been used, which is a modified version of the MIT aerodynamic analysis programme Xfoil [12], featuring an improved accuracy in predicting the maximum lift coefficient, its position and the airfoil characteristics beyond the stall (that is the main region of interest for stall regulated wind turbines).
Furthermore, Rfoil gives the possibility of modelling rotational effects, as it will be explained in the next section.

XFOIL was originally written by Mark Drela in 1986. and has been further developed during the years. The main goal of the code was to combine the speed and accuracy of high-order panel methods with a fully-coupled viscous/inviscid interaction method. For the inviscid formulation of XFOIL, a simple linear-vorticity stream function panel is used; a finite trailing edge base thickness is modeled with a source panel and the equations are closed with an explicit Kutta condition.
The boundary layer and the wake are described with an integral boundary layer formulation and an envelope e^n transition criterion.
The entire viscous solution (boundary layer and wake) is strongly interacted with the incompressible potential flow via the surface transpiration model, permitting proper calculation of limited separation regions.
The drag is determined from the wake momentum thickness far downstream. A special treatment is used for a blunt trailing edge which fairly accounts for base drag.
The local velocity at each point of the airfoil surface and the wake , the airfoil surface vorticity and the equivalent viscous source distribution, are obtained by using the panel solution with the Karman-Tsien correction. This is incorporated into the viscous equations, yielding a nonlinear elliptic system which is readily solved by a full-Newton method.
For a viscous calculation the wake trajectory is taken from an inviscid solution.
This is not strictly correct, since viscous effects will in general change the trajectory and decrease lift.
The effect of this approximation on the overall accuracy is small, and will be felt mainly near or past stall, where accuracy tends to degrade anyway. In attached cases, the effect of the incorrect wake trajectory is imperceptible.

The Rfoil code has been developed through a cooperation between the Dutch institutes: DUT (TuDelft: Delft University of Technology), ECN and NRL, by modifying the aerodynamic

analysis code Xfoil to make it converge toward higher angles of attack and to include the possibility of modelling rotational effects.
Thus, in a first stage, Van Rooij (DUT) [10] modified the governing equations in Xfoil to improve its numerical stability making it converge at higher angles of attack.
To get this results a manipulation of the boundary layer parameters was used from the stagnation point to the trailing edge, and especially the calculation of the turbulent boundary layer was enhanced in order to improve the results at higher angles of attack. (The most important adjustment was made to the closure relation which determines the connection between the adopted equilibrium relations derived by Green and the actual non-equilibrium flow.)
This process improved the accuracy of the code in predicting the maximum lift coefficient, its position and the airfoil characteristics beyond the stall, which is the main region of interest in wind energy applications.
The rotational effects were treated and implemented by Bosschers (NRL) [13] in a second stage. The modifications of Xfoil for rotational effects will be discussed in the next chapter in detail.

3.2 Extrapolation of airfoil aerodynamic performances

Another issue of the airfoils performance prediction originates from the inability of most of the methods to converge to a solution at very high angles of attack and give correct representation of lift and drag coefficients.
This is crucial for stall regulated wind turbines since the airfoils can reach angles of attack up to 40-50 degrees also in normal operating conditions.
Thus, in practical performance prediction the individual analyst applies his individual ”post stall-model”.
The choice of the curve to apply in this zone is a difficult task which has been identified in the Blind Comparison for the NREL/Ames wind turbine ([9],[14]) as one of the main source of errors, and specific studies are still ongoing.

The Viterna-Corrigan post-stall model [15] is commonly used, but it should be applied with caution.
In fact, the curves obtained using this method represent the curves that would guarantee a constant power output beyond the peak of the wind turbine power curve, which for most of the airfoils are lower than the real ones.

For all these reasons, the accuracy of Rfoil at high angles of attack results fundamental, since it permits to use Viterna-Corrigan only at very high angles of attack.
Furthermore, in normal operating conditions these angles of attack are reached only by inner airfoils whose contribution to the power output is lower with respect to outer airfoils.
The outer airfoils usually reach at most angles nearby 30 degrees, where Rfoil still gives good results in most of the cases.
Finally, in the post-stall regime the flow becomes decreasingly dependent on the airfoil and at angles of attack beyond approximately 45 degrees behaves similarly to flow around flat plates.
Thus, usually the airfoil is considered equivalent to a flat plate beyond 45 degrees to extrapolate the available airfoil data across the entire 360°range of potential angles of attack.
On the basis of various attempts made in this work, the best approach found is to apply the Viterna-Corrigan method after the last angle of convergence of Rfoil and the flat plate theory beyond 45 degrees.

3.3 Prediction of 3d airfoil aerodynamic performances on a rotating blade – Rotational effects

Airfoil characteristics used in BEM calculations are typically based on 2-D airfoil performances.
However, for stall regulated wind turbines a direct application of the 2-D characteristics shows poor agreement between measured and calculated loads and power in high winds, when much of the blade is stalled and the flow is separated.
Since a stall-regulated wind turbine works in stall regime in a considerable part of its life, this must be taken into account during the design and dimensioning.
Flow separation and rotation of the blades cause secondary flows that play a key role in the aerodynamic behaviour of the rotor. These effects, being highly three-dimensional (3D), limit substantially the applicability of two-dimensional (2D) airfoil polars for their use in the design process.
Therefore, there is a need of corrections of the 2-D airfoil characteristics to include 3-D rotation effects, which have become a design item in the last years and have been the subject of investigation for decades.
The main effects of rotation are a stall delay to larger angles of attack for the inner airfoils of the blades, the suppression of separation bubbles and leading edge stall (stall starts at the trailing edge and develops to the leading edge in most of the cases) and significant increase

in lift and drag coefficients in the post stall region compared to the nonrotating (or ’2D’) values, with consequent larger aerodynamic power and loads beyond the power peak, compared to predictions based on 2D airfoil coefficients.

These effects can be clearly observed in the next figure, that reports the aerodynamic characteristics extracted (using pressure-tap data during tests in the wind tunnel NASA/AMES) from rotating blades of the NREL UAE (Unsteady Aerodynamics Experiment) Phase VI wind turbine [14], compared to 2D data of the airfoils.

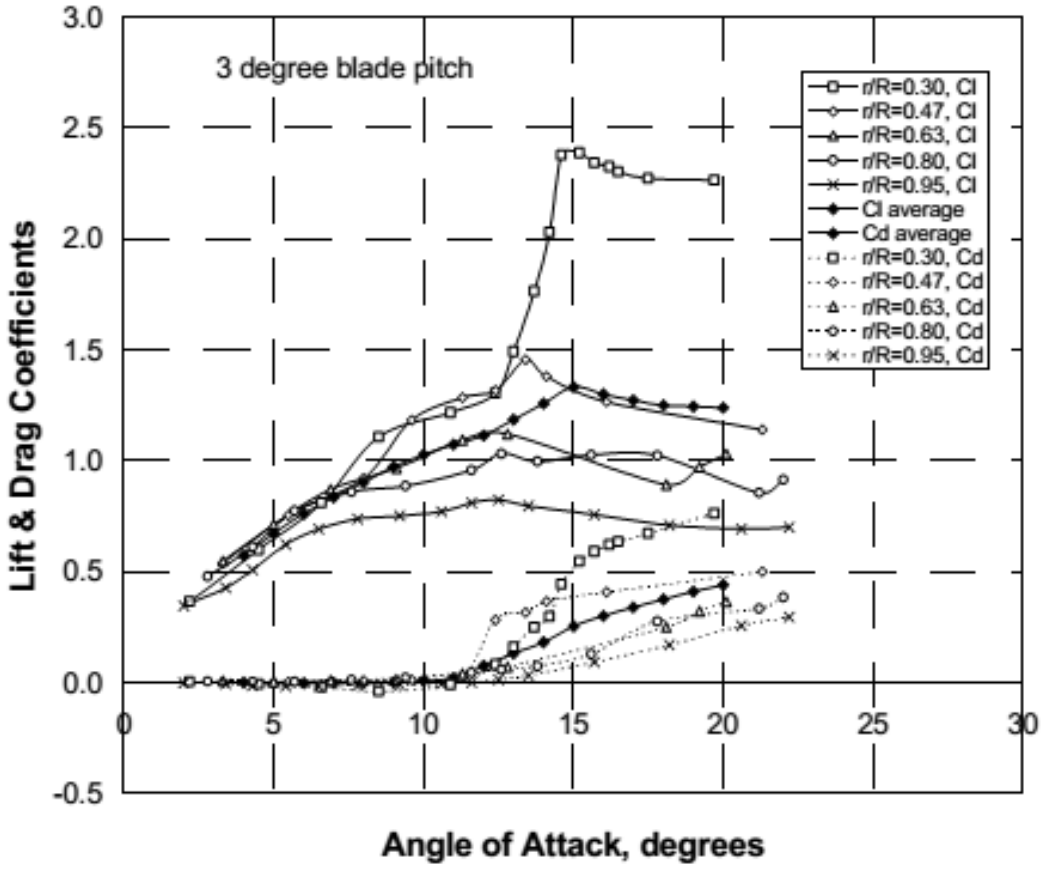

Figure 3.1: Experimental aerodynamic performances of airfoils along a rotating blade of the NREL/UAE Phase VI wind turbine. Extracted from Tangler [74]**.**

It can be noticed that the experimental 3D Cl characteristics are almost identical to the 2D case until the 2D airfoil begins to stall and that the effect is greater on the inboard region of rotor blades and decreases with radius until it becomes negligible on the outer half of the blade.
Accurately predicting the occurrence and severity of stall is slightly more complicated when introducing rotational effects imparted by the rotor.
A full understanding and modelling of these problems has been the cause of much discussion and is the subject of ongoing research.

Simms et al. in [9] reported the results of a blind test comparison in which different aerodynamic models were used for simulating the NREL UAE Phase VI turbine. The computed results, which were obtained with numerical tools ranging from blade element momentum (BEM) theory to wake and computational fluid dynamics (CFD) codes, showed a great level of uncertainty. The discrepancies observed between experiments and computations were attributed to the difficulty of predicting correctly the effect of rotation on rotor blades.
This highlights the importance of improving the correction models for rotational effects, and at the same time, it stresses the necessity of gaining a deeper understanding of the underlying physical mechanisms.
A complete model has not yet been developed but a lot of insight is obtained from both experimental and computational studies.

3.3.1 Centrifugal forces and radial flow

A very much simplified explanation of rotational effects can start from seeing that the boundary layer air rotates with the blade and so it is subject to centrifugal forces that accelerate it radially outwards and that are proportional to the radial location of the section. This holds for the attached and for the separated flow areas.
Furthermore in the rotating reference frame of the blade Coriolis forces appear and act on the air particles with components both in the radial and azimuthal directions.
So, an observer in the reference frame of the blade could notice an acceleration along the radial direction and another one along the azimuthal direction on passing air particles.
Therefore, centrifugal and Coriolis forces have to be considered for the aerodynamic analysis.

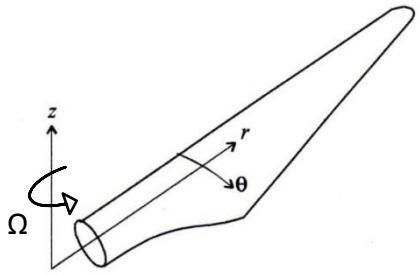

Figure 3.2: Rotating reference frame of the blade

The expressions or centrifugal and Coriolis forces can be obtained as hereinafter.
Let's call Ω the angular velocity of the rotational reference frame; the centrifugal force on the air particle of volume $d\tau$ is:

$$F_{centr} = \rho \, d\tau \Omega^2 \, r \tag{3.1}$$

and, when the particle is moving in the rotating system with a vector velocity $\vec{v}$, the Coriolis force acting on the particle is:

$$F_{cor} = 2\rho \, d\tau \vec{\Omega} \times \vec{v} \tag{3.2}$$

The vector $\vec{\Omega}$ only has a z-component, thus the Coriolis force per unit mass is:

$$f_{cor} = 2v_r \Omega \vec{\theta}_1 - 2v_\theta \Omega \vec{r}_1 \tag{3.3}$$

where $\vec{\theta}_1$and $\vec{r}_1$ are the unit vectors in the azimuthal and radial directions respectively.
In short, the relevant external forces per unit mass are:

$$f_\theta = 2\Omega v_r \tag{3.4}$$

$$f_r = \Omega^2 \, r - 2v_\theta \Omega \tag{3.5}$$

$$f_z = 0 \tag{3.6}$$

These two kind of "apparent" forces and the related accelerations have various effects on the airflow and the boundary layer along the blade.

The main effect is that the Coriolis forces push the flow towards the trailing edge, thus acting as a negative chord-wise pressure gradient which is favourable for the stability of the

boundary layer encouraging the flow to remain attached. Therefore, (either) separation is delayed or, in the case of separated flow, the separated region becomes thinner and shorter (the separation point is shifted towards the trailing edge), resulting in the lift coefficient being higher beyond the stall than what would be obtained on a non-rotating blade.

Suction on the separated flow area gives an increased lift for a given separation-point location, while a given separation-point location may occur at a larger angle-of-attack.
This phenomenon is usually referred to as **"stall delay",** or **"centrifugal pumping"** by some authors, because the rotating blade can be viewed as a centrifugal pump pushing boundary layer air in the direction toward the tip.
As the velocity - and hence also the momentum - is low in the separated boundary layer compared with the centrifugal force, a stronger radial flow appears in that region of the blade, as shown in the following figure.
In particular, the figure reports the flow simulated by a CFD run on a rotating blade (of one of the tentative wind turbines obtained during this work) for two wind speeds. The first (7 m/s) refers to a condition for which the flow is still attached on most of the blade, and the latter (10 m/s) refers to a condition beyond the stall of the blade.

7 m/s

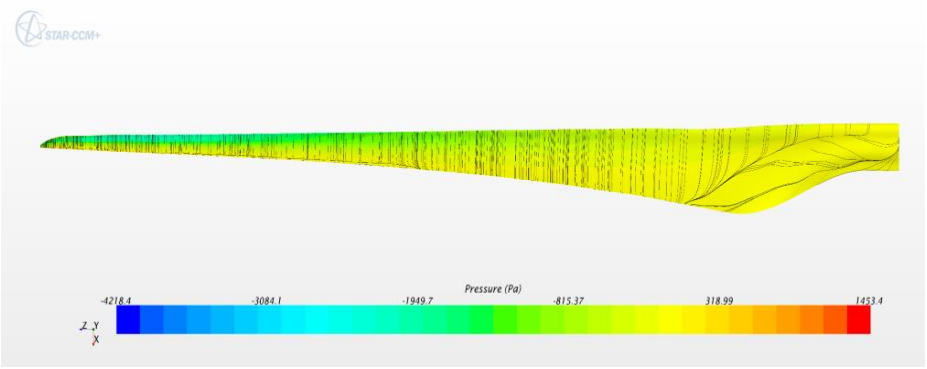

10 m/s

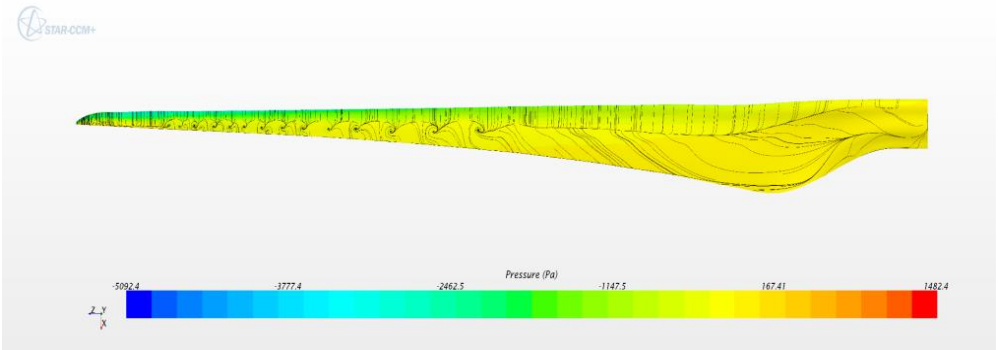

Figure 3.3: Airflow on a rotating blade before stall (7m/s) and post stall (10 m/s)

Under stall conditions, the separation line is clearly recognizable along the span as the location where the flow coming from the leading edge ceases to be oriented in chord-wise direction.

It is also evident that under stall conditions, large regions of the suction side are dominated by radial flows and a recirculation component towards the leading edge.

Root vortex

The combination of the recirculation and the radial flow in the inboard region creates a standing vortex on the separated area whose intensity decreases going toward the outboard part of the blade, as in the following figures.

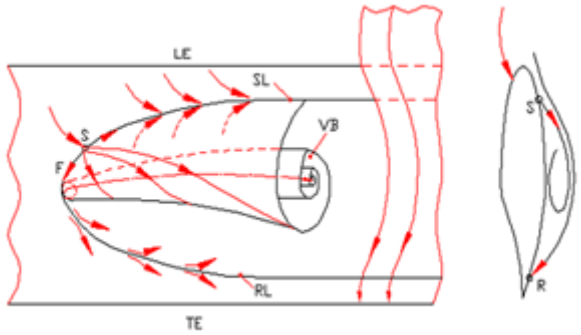

Figure 3.4: Formation of the standing vortex in the radial direction. Extracted from Tangler [16]

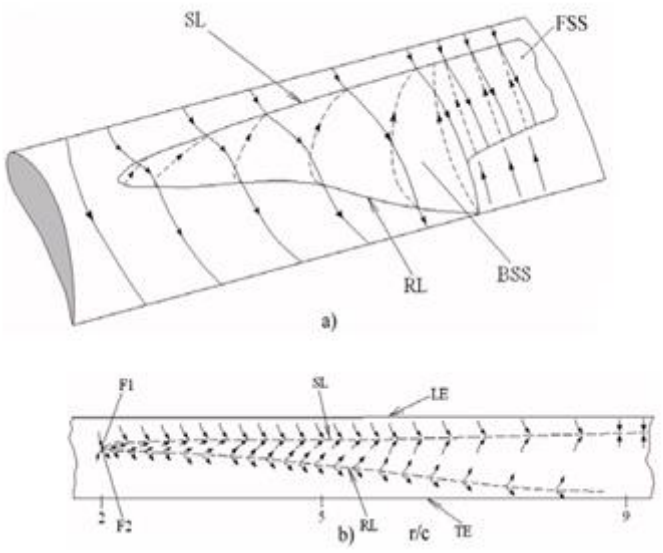

Figure 3.5: Topological structures of separation on rotating blade: a) types of separation surface; b) separation/reattachment. Extracted from Tangler [16]**.**

This effect, has been observed both experimentally (for instance in [17], [18] and [19]) and numerically (for instance in [20] and [21]) in other turbines operating under stall conditions, and it is usually considered to be intrinsically related to the existence of rotational effects.
Dumitrescu et al. [22] also showed that this inboard standing vortex structure is produced by Coriolis action and may augment the aerodynamic forces.

The decreasing of the rotational effect with the increasing of the radius can be related to the decreasing of the vortex intensity.
Actually, the parameter that influences rotational effects predominantly is not the radius but the local blade solidity (chord/radius). In particular, rotational effects decrease with the decrease of local solidity (going from the root to the tip).

Reduction of Rotating Sectional Coefficients near the Tip

The effects of rotation in the tip-region are opposite to that for the mid-span and root region of the blade: the lift coefficients on the tip of a rotating blade are smaller than those on a non-rotating blade.
An explanation was given by Lindenburg [23], who suggested that the radial flow caused by the centrifugal effects and the span wise gradient of dynamic pressure results in a reduction of the negative pressure on the suction side of tip airfoils, compared to the non-rotating case. Tip airfoils will never develop very strong negative pressures.
(It should be stressed that this reduction of the aerodynamic coefficients is of a different nature than the reduction in angle of attack due to the flow around the blade tip.)
However, often this effect is not considered because it is reasonable to neglect rotational effects near the tip of a utility-scale blade.

Effects on drag

An increase of the drag coefficient was found on the NREL UAE Phase-VI rotor and by many other researchers. Uncertainties are still high about that, because the influence on the drag seems to be airfoil-type dependent.

3.3.2 Modelling of rotational effects

The study of rotational effects dates back to the mid-20th century for helicopter rotors and aircrafts and their role on the overall performance of a wind turbine rotor has been investigated extensively.

The first investigations were performed by Himmelskamp in 1947 [24] (from which the phenomenon is sometimes reported as "Himmelskamp effect") who studied experimentally the rotational effects on aircraft propellers. He observed lift enhancement and stall delay in rotating blades as compared to non-rotating blades and addressed them to the occurrence of radial flow.
Banks and Gadd [25] in 1963 performed a theoretical analysis for steady boundary layers and inferred that rotation helps to delay stall, especially in the blade root region.
Klimas [26] (1986) described radial flow based on the Euler-equations including the centrifugal and Coriolis-effects on the flow in the trailing-edge separation bubble.
Schreck and Robinson [27] (2002) investigated surface pressure measurements from the NREL UAE Phase VI experiment concluding that rotational augmentation is connected to radial surface pressure gradients.
Tangler [28] (2004) also studied the experimental data from the same wind turbine and highlighted the importance of the trailing vorticity and rotational effects for the aerodynamic performance.

CFD simulations have also been commonly used for the last 15 years for the analysis of rotor aerodynamics.
Aerodynamic analyses of rotating blades using computational fluid dynamic techniques have been performed for example by Wood [29] (1991) and Snel et al. [30] (1993).
Wood described stall delay in terms of pressure changes to the external inviscid flow and observed that it depends on the local solidity of the blades.
Snel developed a set of equations including centrifugal and Coriolis terms. It turned out that it was possible to capture the problem in two-dimensional equations of boundary layer integral type.
In [31] a deep investigation has been performed on the MEXICO wind turbine [32] using a CFD model in conjunction with experimental data.
The characteristics of rotational effects are studied by comparing 2D and 3D airfoil polars and Cp distributions. A deeper insight into the sources of the rotational effects is gained through the study of distinctive flow features in the near wake and the boundary layer of the rotor blades.

The need to correct 2D, quasi-steady airfoil coefficients for rotational effects has resulted in several (mainly empirical) models in which the lift coefficient, and for some models also the drag coefficient and even the moment coefficient, are corrected in the case of flow separation from the airfoil sections, but a rigorous approach is lacking.
Using these models, 2-D airfoil characteristics are corrected with a limited input.
Snel, Houwink, and Bosschers derived a so-called '3D correction' method [33]using boundary-layer equations similar as those reported by Banks & Gadd [25], in which the rotational effects are proportional to (c/r)^2.
This correction has to be applied for locations up to 80% radius and for angles-of-attack up to 30deg. For larger angles-of-attack the correction on the lift coefficient was reduced linearly to zero at a 50 deg angle of-attack.
Other models have been developed by Du and Selig ([34],[35]), Chaviaropoulos [36], Lindenburg [37], Corten [38].
The derivation of these models is outside the scope of this project and will not be pursued here.
In general, most of them are formulated as function of the ratio c/r , sometimes called 'local solidity', which is the ratio between the local chord length and the radius at a certain blade span-wise position (local blade solidity).
In the following expressions a general formulations of some of the models is reported, both for Cl and Cd.

$$c_{l,3D} = c_{l,2D} + f_{cl}\left(\frac{c}{r}, \dots\right)\Delta_{Cl} \quad (3.7)$$

$$\Delta_{Cl} = C_{l,P} - C_{l,2D} \quad (3.8)$$

$$C_{l,P} = 2\pi(\alpha - \alpha_0) \quad (3.9)$$

$$c_{d,3D} = c_{d,2D} + f_{cd}\left(\frac{c}{r}, \dots\right)\Delta_{Cd} \quad (3.10)$$

$$\Delta_{Cd} = C_{d,2D} - C_{d0} \quad (3.11)$$

$$C_{d0} = C_{d,2D}(\alpha = 0) \quad (3.12)$$

The expression f(c/r,…) means that all models are a function of c/r, but that they also can be a function of other parameters. The function f(c/r,…) varies from model to model, as shown in the following expressions.

Snel et al.:

$$f_{cl} = 3\left(\frac{c}{r}\right)^2 \quad (3.13)$$

$$f_{cd} = 0 \quad (3.14)$$

Lindenburg:

$$f_{cl} = 3.1\left(\frac{\omega r}{V_{rel}}\right)^2\left(\frac{c}{r}\right)^2 \quad (3.15)$$

f_{cd} =0 (3.16)

Du and Selig:

$$f_{cl} = \frac{1}{2\pi}\left[\frac{1.6(c/r)}{0.1267}\frac{a-(c/r)^{\frac{dR}{\Lambda r}}}{b+(c/r)^{\frac{dR}{\Lambda r}}} - 1\right] \quad (3.17)$$

$$f_{cd} = \frac{1}{2\pi}\left[\frac{1.6(c/r)}{0.1267}\frac{a-(c/r)^{\frac{dR}{2\Lambda r}}}{b+(c/r)^{\frac{dR}{2\Lambda r}}} - 1\right] \quad (3.18)$$

where:

$$\Lambda = \frac{\omega R}{\sqrt{U_\infty^2+(\omega r)^2}} \quad (3.19)$$

and

a=b=d=1

Chaviaropoulos and Hansen:

$$f_{cl,cd} = a\left(\frac{c}{r}\right)^h cos^n(\theta) \quad where\ a=2.2,\ h=1 and\ n=4 \quad (3.20)$$

It has to be noticed that the models have a linear c/r dependency, excepting the Snel model which has a quadratic c/r dependency.

Some models for the rotational effects are formulated in terms of ' stall delay', such as the method of Corrigan & Schillings [39], obtained using equations similar as those by Banks & Gadd [25].

The method of Corrigan & Schillings has been investigated by Tangler & Selig [40] for constant-chord and tapered rotor blades with S809 airfoils.

Comparison of models

Breton et al. [41] compared six different correction models for rotational effects using a lifting-line prescribed wake vortex code for simulating the NREL UAE Phase VI turbine, and they showed that none of the models was able to predict the measured data satisfactorily, and the loads under stall conditions were generally overestimated.

Guntur et al. [42] performed a similar test with experimental data from the MEXICO wind turbine.

In the following figure the comparison between different methods and experimental data extracted from the (experimental test wind turbine of the MEXICO project) MEXICO test [43], [32] is reported.

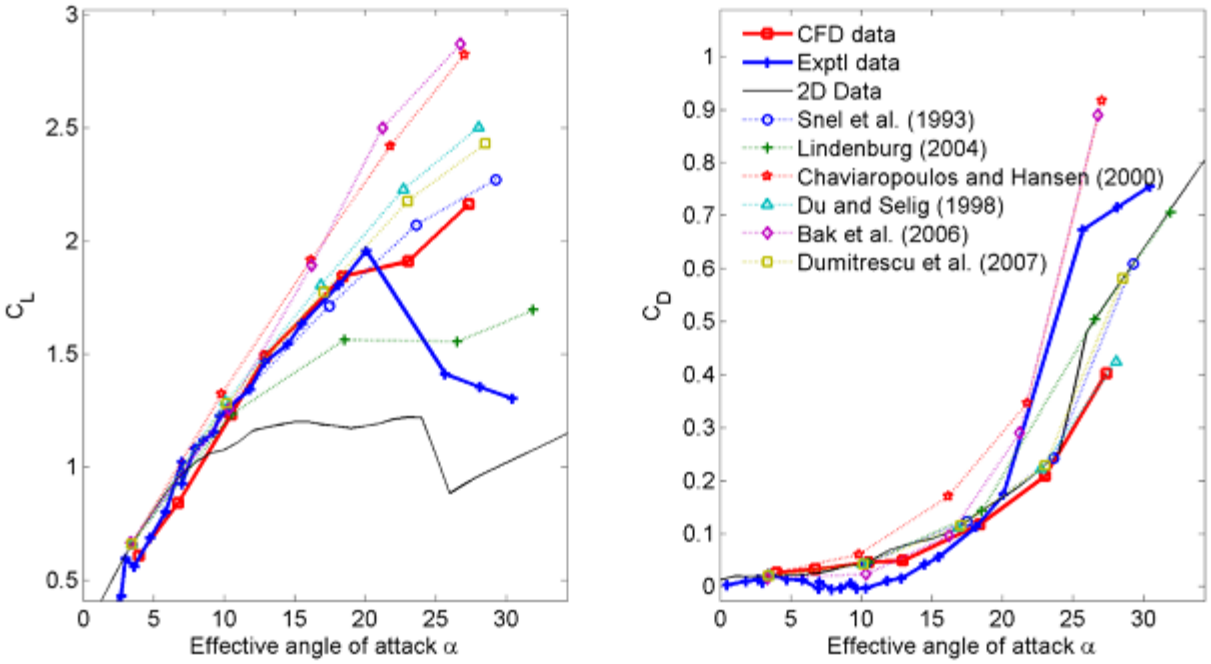

Figure 3.6: Lift and drag polars from experimental data, CFD data and predicted polars from various rotational augmentation models on the MEXICO rotor at r/R=0.25. Extracted from [44]

From this comparison it can be seen that most of the models over predict lift coefficient and under predict the drag coefficient, the model by Chavariopoulos and Hansen over predict both the lift and drag coefficients and the model by Lindenburg under predicts them, while the best agreement with the experimental data is given by the Snel et al. model.

In [45] it is reported that the model of Snel can reproduce quite well rotational effects and in [46] it is said that it gives realistic results also for the NREL/AMES wind turbine.

Difficulties in modelling rotational effects

Knowing that 'stall delay' is related to the location of the separation point, the 'amount' of angle-of-attack delay may show a strong dependency on the airfoil shape, most likely for thick airfoils. The result is that most correction models have one or more parameters or a scaling factor.

Furthermore, in [31] it is observed that the subsequent phenomena of stall delay and lift enhancement can exist independently of each other, although they tend to manifest themselves together.

Finally, it should be noted that in the literature (for example Schreck and Robinson [27] with respect to the NREL UAE Phase VI wind turbine) also span wise pressure gradients due to the difference in dynamic pressure along the blade, are mentioned to be responsible for the rotational effects, but nowadays "centrifugal pumping" is the most accredited explanation

Nevertheless, the higher uncertainties concern the aerodynamic drag coefficient.
Most correction models for rotational effects predict a Cd increase, while others describe a Cd reduction or no influence at all on Cd.
Almost all the models give a reduction of the aerodynamic drag coefficient but the measurements on both the UAE phase-VI rotor in the NASA-Ames wind tunnel and the MEXICO wind turbine give a serious increase of the aerodynamic drag coefficient for the inner airfoils . Also Himmelskamp [24] and other authors reported this same effect.
This can derive by the fact that 'centrifugal pumping' of air requires energy (as explained by Lindenburg in [37]), but there is still no consensus about that.
Furthermore, such effect seems to be highly dependent on the airfoil.
At the same time, modelling the drag coefficient on the basis of pressure-tap measurements can be highly delicate because they are very sensitive to small errors in the measured sectional angle-of-attack.

These findings show the lack of generality of the state-of-the-art knowledge about rotational effects and more research in this field would be necessary.

Concluding remarks

Modelling rotational effects is difficult because they highly depend on the type of airfoil, the type of loading distribution along the blade and also on the transitioning airfoils, when the blade has been built using different airfoil shapes.

For all these reasons, all the models cannot be used with confidence but fortunately they at most overestimate the power and loads beyond the power peak, where we are not interested in having high power and the overestimation is conservative compared to power control and structural design of stall regulated wind turbines. Thus, their results can be accepted in a preliminary design phase.

3.3.3 Evaluation of rotational effects by using RFOIL

In this work the software Rfoil has been used to obtain the aerodynamic coefficients of the airfoils along the blade taking into account rotational effects.

The rotational effects have been implemented in this code on the basis of the work of Snel [47] describing the three-dimensional flow past a wind turbine rotor blade in the form of quasi two-dimensional boundary layer equations in which centrifugal and Coriolis terms are included.

This implementation was carried out by Bosschers at NLR [48],who extended the “rotating” boundary layer equations developed by Snel [33] with higher order terms, put them into an integral form to be implemented in the Xfoil code and described in more detail radial pressure differences along the blade.

RFOIL, like XFOIL is valid for steady flow and allows one to calculate lift, drag and moment coefficients of an airfoil rotating about an axis parallel to the axis perpendicular to the airfoil section’s chord. The two input parameters are the local solidity (i.e. the ratio of the chord length and the radial position) and the non-dimensional free-stream velocity

$f_0 = \frac{Vtot}{\Omega r}$ (which depends on the rotor speed and the wind speed).

The RFOIL code turns out results that crudely speaking are proportional to the factor (c/r)**2 (as seen for the Snel model).

ECN has been testing RFOIL with a first intent to assess its usefulness for wind turbine performance prediction.

A comparison of pressure distributions and lift curves from RFOIL and two experimental wind turbines (a small -scale wind turbine tested in a wind tunnel ([49],[50]) and a full scale wind turbine in the field [51] showed that computations on basis of 2/3 of the local solidity give the better agreement between measurements and calculations.

3.3.3.1 Rfoil validation

To analyse the accuracy of Rfoil in evaluating rotational effects, in this work the airfoils performances obtained by this code in the rotational mode have been compared to those extracted from a 3D-CFD analysis of a rotating wind turbine (obtained during the optimization process), for different stations along the blade.
Furthermore the Rfoil curves have been used in a BEM code, WtPerf [52] (developed by NREL) to predict the turbine performances and the results have been compared to those obtained by the CFD computations.
Hereinafter, a brief overview of the CFD analysis is reported.
Then, the comparison of the results furnished by Rfoil and the CFD is shown.

CFD analysis

The CFD analysis in this work has been performed with the use of the software STAR-CCM+ in steady and axisymmetric operating conditions.
The K-ω SST model for the turbulence has been applied with a viscosity ratio equal to 10 and a turbulence level equal to 0.01.
A validation of the CFD procedure has been previously performed, using it to analyse the performances of the NREL/Ames experimental wind turbine [14] and comparing the results to the experimental data.
The comparison of the two power curves is reported in the next figure , which shows a good agreement between CFD and experimental results.

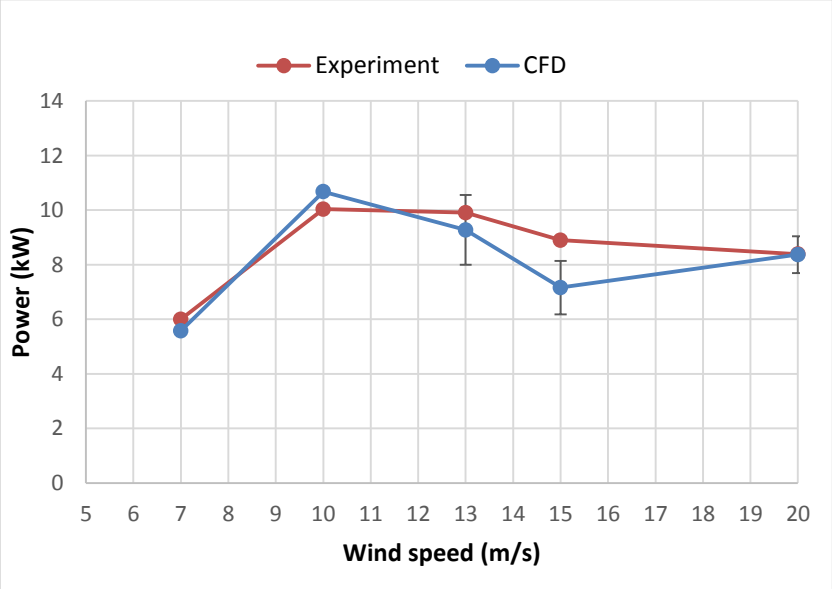

Figure 3.7: NREL-UAE Phase VI - Power curve - Experimental data VS CFD

Comparison between 3D-CFD results and Rfoil results

As previously said, the comparison between Rfoil and 3D-CFD results has been performed for one of the wind turbines obtained during the optimization process in this work (turbine 'V00_backtwist'), in steady and axial symmetric operating conditions.
The 3D-CFD polars of the airfoils along the blade have been extracted from the CFD results following an inverse BEM method reported in [53].
With this method, the normal force coefficient (Cn) and tangential force coefficient (Ct) are computed from the surface pressure coefficient (Cp) distributions and then transformed into Cl and Cd after calculating the angle of attack. The calculation of the angle of attack is based on an iterative procedure also reported in [53].
The following figures show the comparison between Cl(α) and Cd(α) coefficients obtained by using Rfoil and those extracted from the 3D-CFD analysis, at different stations along the blade.

The airfoils adopted in the inner part of the blade are:

- $r = 20 \div 25\%R$: 'D30'; maximum thickness τ_max=30%c;
- $r = 35 \div 60\%R$: 'G25b'; maximum thickness τ_max=25%c;

The airfoils are interpolated in the transition sections of the blade (between two different airfoils). (See Chapter 6 for details).

For each station the 2D airfoil's curve in rough conditions are also reported.
The presence of roughness is simulated in Rfoil by fixing the transition point at 0.01%c on the suction side of the airfoil and at 10%c on the pressure side.

For section r=56.22%R Rfoil gives a lift curve practically identical whether or not rotation effects are taken into account; thus, for the Rfoil data at this station the only 2D lift curve is reported.
Furthermore, 2D lift curve at r=43.25%R is not reported since it is interpolated between the 2D curves of the airfoil 'D30' and 'G25b'.

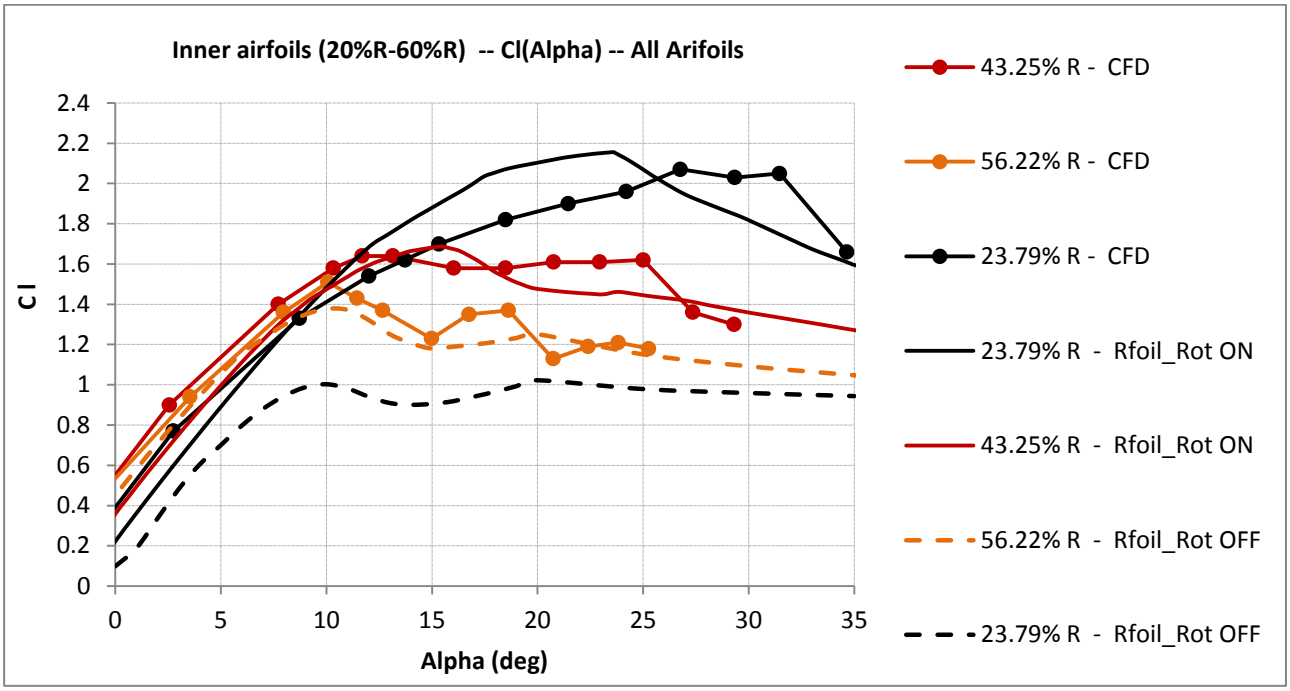

Figure 3.8: Lift curves of inner airfoils of wind turbine 'V00_backtwist'.

(Data extracted from 3D-CFD) VS (Rfoil data)

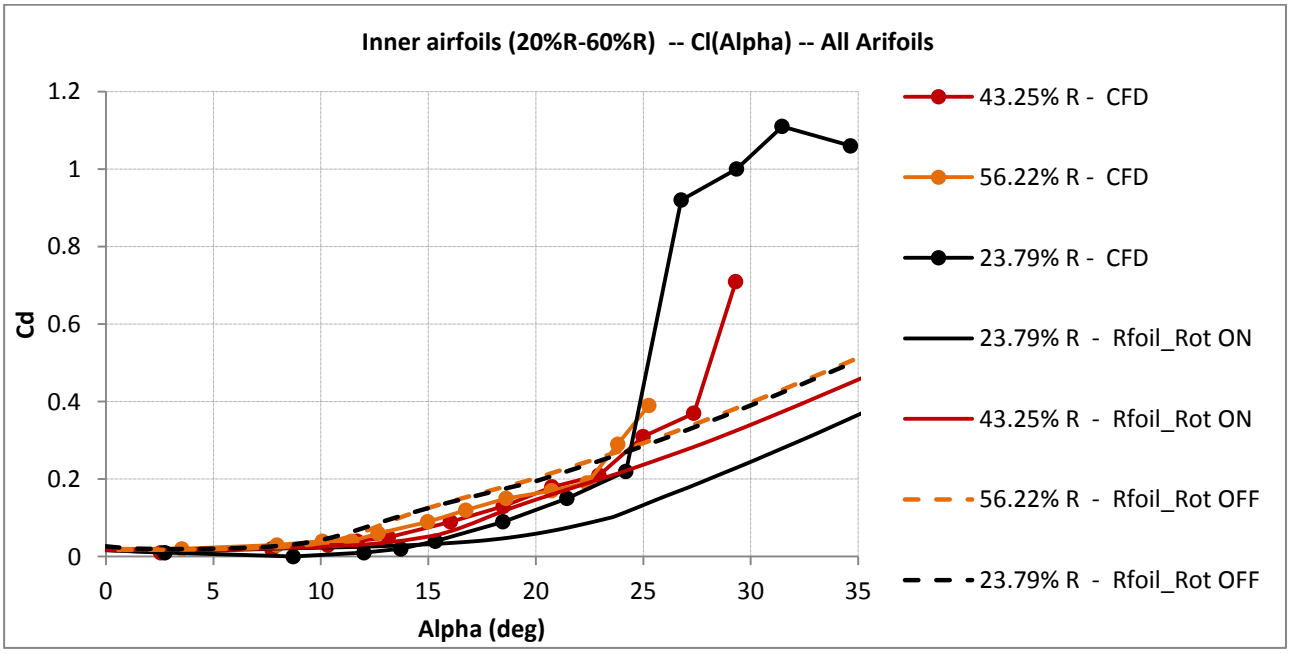

Figure 3.9: Drag curves of inner airfoils of wind turbine 'V00_backtwist'.

(Data extracted from 3D-CFD) VS (Rfoil data)

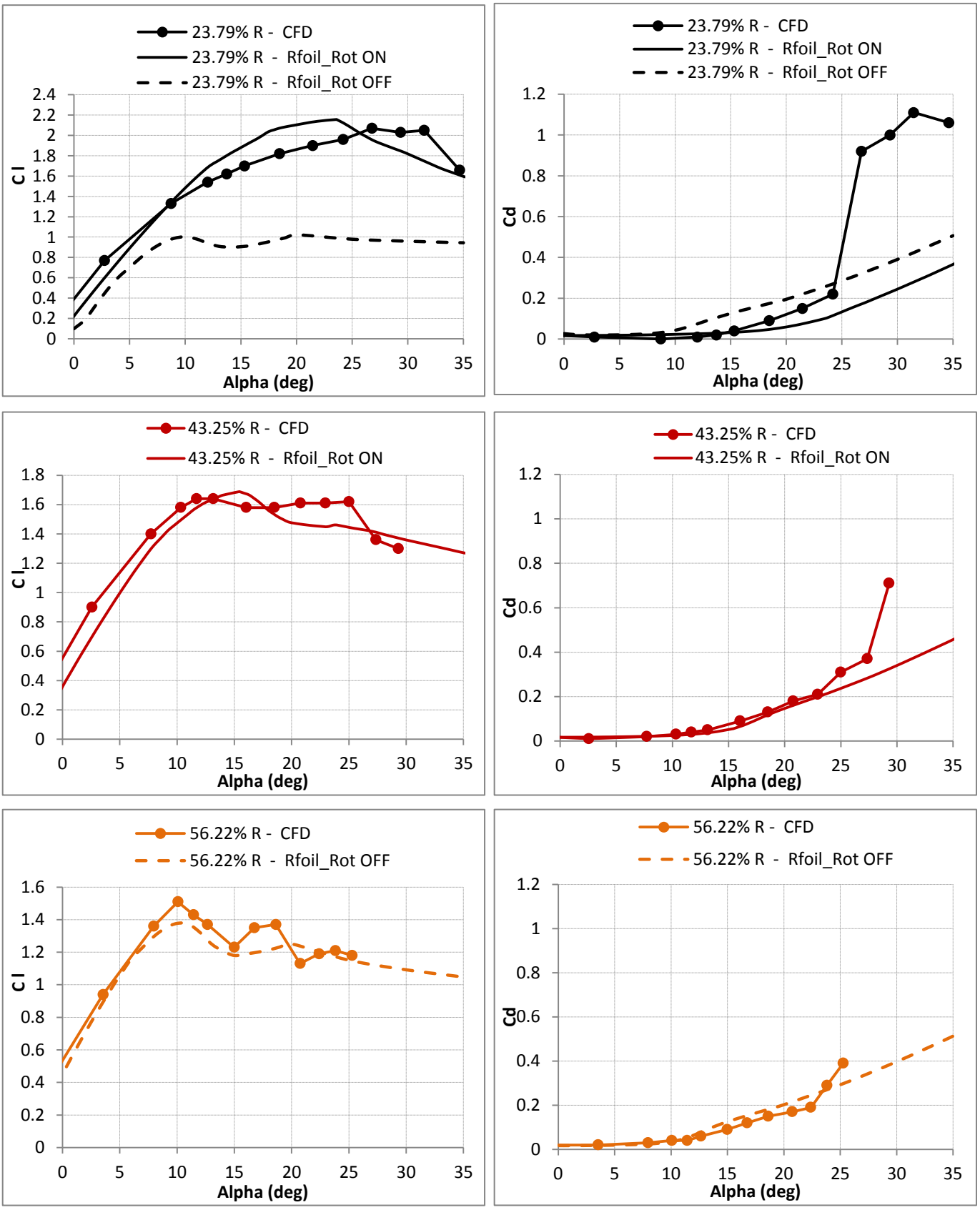

Figure 3.10:Lift and drag curves of inner airfoils of wind turbine 'V00_backtwist'.

(Data extracted from 3D-CFD) VS (Rfoil data)

From the figures it can be observed that:

- both Rfoil and CFD give decreasing rotational effects along the blade with the increasing of the radius,

and

- both of them give considerable modifications of the airfoils aerodynamic characteristics with rotational effects only at angles of attack beyond the 2D stall according with experimental results from the NREL-UAE tests.

In particular:

- both the methods give an increase of lift coefficients compared to 2D values, and the results agree quite well for all the stations.

- CFD gives an increase of drag coefficients compared to 2D values , according with experimental data on the NREL-UAE wind turbine in while Rfoil gives a decrease of drag coefficient.

Furthermore, at approximately the half of the blade span rotational effects can be considered negligible, thus 2-dimensional characteristics of the airfoils can be considered.
The following figure reports the comparison between Rfoil and CFD results in terms of global power output of the blade.
As previously said, airfoil curves obtained by using Rfoil have been used in the BEM code Wt_Perf to evaluate the wind turbine performances.

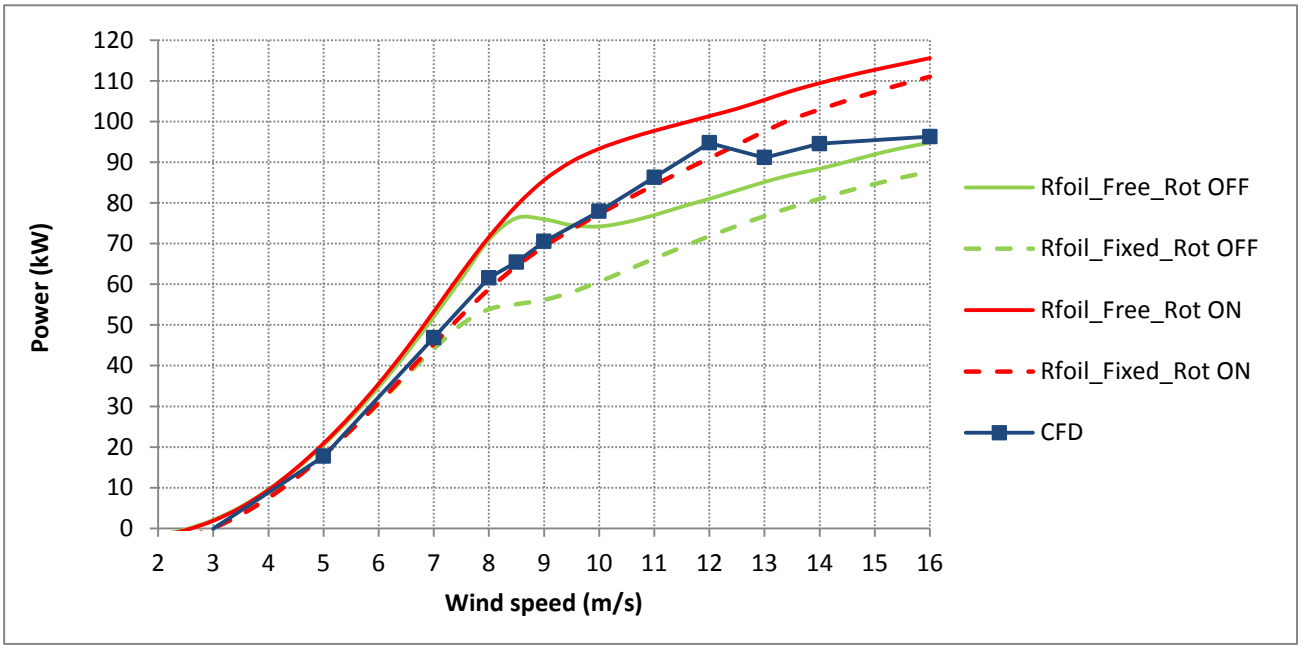

Figure 3.11: Power curve of wind turbine 'V00_backtwist'.

CFD curve compared to Wt_Perf curves obtained using airfoils data from Rfoil, with and without taking into account rotational effects, in clean (free) and rough (fixed) conditions.

From this figure it can be observed how the underestimation of drag coefficients results in an overestimation of the power at wind speeds beyond the power peak.
Furthermore, CFD power curve and the power curve obtained using WT_Perf with airfoils computed in Rfoil in rough conditions are almost coincident, excepting the region far beyond the power peak.

From this results, it can be concluded that Rfoil can be used with quite some confidence, giving at most an acceptable and conservative (both for power control and maximum loads) over prediction of power and loads beyond the power peak, to take into account.

Chapter 4
Wind turbine performance prediction in steady and unsteady operating conditions

This chapter reports an overview of the tools used to predict wind turbines performances and loads within the optimization process developed in this work, both in steady and unsteady operating conditions.
In steady operating conditions the BEM based code WTPerf [52],[54],[55] developed by NREL has been used and the analysis of its accuracy is reported in the following sections.
In particular, results obtained by using Wt_Perf, in terms of wind turbine power curves, are compared to those obtained with a CFD analysis of a rotating wind turbine rotor, in steady operating conditions, for one of the wind turbines obtained during the optimization process.
For unsteady operating conditions, the BEM-based aeroelastic code FAST ([56],[7]) has been used to analyze performances, maximum loads and the structural dynamic behavior of the wind turbines also taking into account the deformation of the blades.
In this chapter, the results furnished by WT_Perf in steady operating conditions and those obtained by FAST in unsteady conditions are compared to verify the reliability of WT_Perf steady results within an optimization process.
Finally, WT_Perf results are compared to those obtained with field experimental tests performed on a scaled wind turbine prototype.

4.1 Steady operating conditions

4.1.1 WT_Perf

WT_Perf is a free tool widely used for the analysis of steady-state horizontal axis wind turbine (HAWT) performance, developed by M. Buhl of the National Wind Technology Center (NWTC) and maintained by the National Renewable Energy Laboratory (NREL).
It is based on BEM theory with capabilities to account for yawed and tilted operation as well as operation in the turbulent windmill and propeller brake states.
WT_Perf is a descendant of the PROP code; the original theory can be found in several papers [4], [57], [58], [59].

In Wt_Perf an iteration routine is used to solve the axial and tangential velocities acting on a blade element, so that the forces on that element can be calculated based on airfoil lift and drag data.
WT_Perf iterates on axial induction factor (a) and the tangential induction factor (a') for each blade element until convergence is reached for both of them.
Then, the final forces are computed and the code moves radially outward to iterate between the velocities and forces of the next blade element.
The following characteristics distinguish the WT_Perf code:

- each blade element iteration begins with initial values a and a' set equal to the converged value from the previous neighboring blade element;
- the newest release of the code uses a two-dimensional Newton-Raphson iteration routine, iterating on both a and a' rather than separating them into two separate iteration loops.
- the tip-loss factor is implemented using the Wilson and Lissaman method as described in [60]. In particular, the a(l-a) term in the induction equation is transformed by the tip-loss factor, F, to aF(1-aF) for the Wilson and Lissaman model (to aF(1-a) for the linearized model)
- in the turbulent wake state (a>0.5) a modified implementation of the Glauert empirical relationship is adopted, as described in the paper by Buhl [61].

As shown in Chapter 2, the rotor enter the turbulent wake state typically at low wind speeds, where the wake has large amounts of mixing with the outer flow and the axial induction factor can have values greater than 0.5.
The blade element moment theory is not valid in this region and under predicts the thrust of a rotor because it is not able to model the momentum transfer in the vortex ring state, due to the BEM assumption of radial independence.
Thus, empirical data, typically the Glauert empirical relationship (sometimes modified by authors as in this case) are used to account for the difference between the real thrust and thrust predicted by classical momentum theory.

WT_Perf code gives, as output file, the aerodynamic data and performances of the whole wind turbine. In particular it furnishes power, power coefficient, torque, flap bending moment and thrust values for each wind speed and for different blade pitch angles at a fixed rotational rate.
In addition, it can give the blade elements data – local aerodynamic data and loads – for different rotation rates, blade pitch angles and wind speeds.

4.1.2 Comparison between WT_Perf and CFD steady results.

As seen in Chapter 2, errors in predicting wind turbine performances can be caused by an incorrect modelling of the airfoils performances along the blade or by simplifying assumptions of the BEM method.
Furthermore, it has been seen that the main errors are caused by a wrong modelling of rotational effects on performances of the inner airfoils of the blade.
Finally it has been noted that CFD analyses, in general, give the most accurate results.
For all these reasons, to analyze the accuracy of WT_Perf, the power curve predicted by this code for a wind turbine obtained during the optimization process developed in this work (the turbine 'V00_backtwist' analyzed in Chapter 3) has been compared to the curve predicted with a CFD analysis in steady operating conditions on the same turbine (and already presented in Chapter 3). The comparison is reported in the next figure.
Furthermore, the airfoils curves extracted from the CFD analysis (shown in Chapter 3) have been used for the inner airfoils, while 2D aerodynamic curves have been used for the outboard airfoils (between the station at about 50% of the blade span and the blade tip) where rotational effects can be neglected, as shown in Chapter 3.
This way, it's possible to override the errors caused by rotational effects modelling, and to analyze the inaccuracies caused by the only simplifying assumptions of the BEM code.

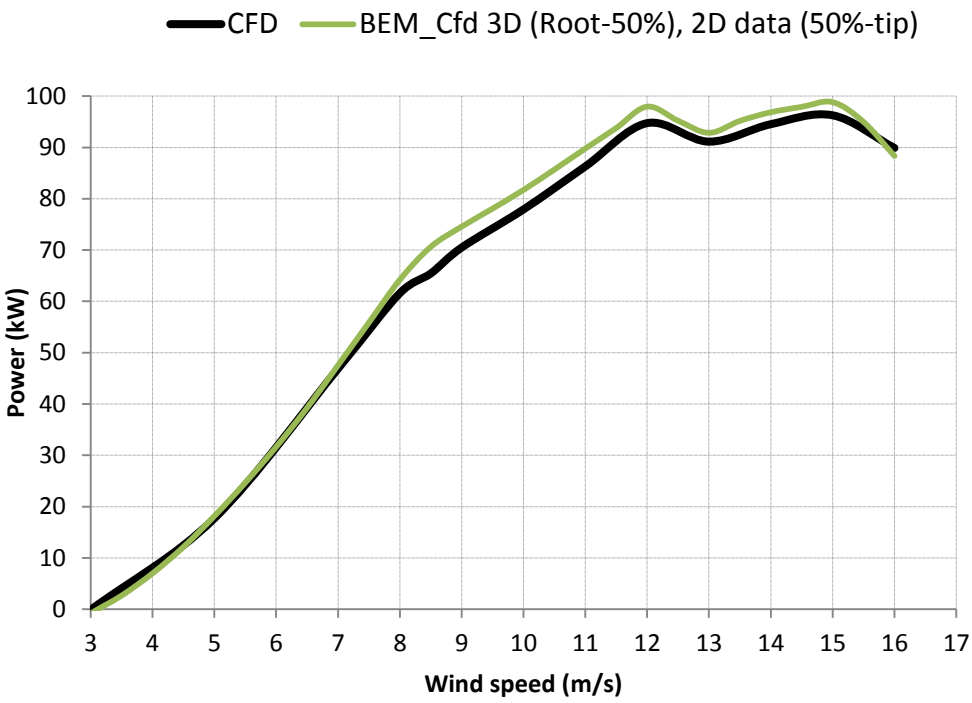

Figure 4.1: Validation of Wt_Perf

CFD power curve VS Wt_Perf power curve implementing aerodynamic curves of inner airfoils extracted from CFD (wind turbine 'V00_backtwist')

The figure shows a good agreement between the two curves, and an acceptable power overestimation of WT_Perf at high wind speeds, nearby the cut-out wind speed of the wind turbine.
This result demonstrates that it is possible to have a good performance prediction even if 2D aerodynamic characteristics are used in the BEM code for the outer airfoils; thus, it is possible to change the aerodynamics of the outer part of the blade with a little computing effort during the optimization process, without the need of rotational effects evaluation at each step. This can be useful to speed the design process.
In fact, the outer half of the blade gives the main contribution to performances and loads of a wind turbine since local velocities are higher; furthermore, the outer airfoils are the main responsible of the structural dynamic issues of stall regulated wind turbines, as it will be shown in Chapter 5. Thus, the main effort within the design process has to be made in the aerodynamic optimization of this part of the blade.
In the inner part of the blade, the aerodynamics of the airfoils is less important, while principally structural requirements have to be satisfied (that essentially means having high maximum thickness airfoils).
This means that here the choice of the airfoil can be simpler and faster with respect to the outboard airfoils; thus, the inner part of the blade can be designed and fixed in a first phase of the optimization process, with the related rotational effects evaluation.
Then, in a second phase the outer half can be optimized simply using 2D aerodynamic characteristics of the airfoils in the BEM code.

4.2 Unsteady operating conditions

BEM theory assumes that the flow field around the wind turbine rotor is in equilibrium at every time step considered (quasi-equilibrium). During the operation of a real wind turbine, however, the flow field is always changing in intensity and direction, even during normal operation. Consequently, BEM theory computations may not reflect reality when examining unsteady events.
Furthermore, flexibility of the components of wind turbines has to be taken into account.
To evaluate wind turbines performances in unsteady operating conditions and to account for flexibility of the different components of the wind turbines, aero-elastic simulations in the time domain have been performed in this work by using the BEM-based aeroelastic code Fast_AD [56], [7].
The same code has also been used to evaluate extreme loads and fatigue loads within the design process developed in this work, including extreme events like gusts and rapid direction changes.

The following sections contain a brief overview of the main advanced aerodynamics topics that address these conditions (main unsteady aerodynamic effects), a presentation of Fast_AD and the different codes and subroutines used by Fast_AD.

4.2.1 Unsteady and asymmetric aerodynamic phenomena

A number of unsteady and asymmetric aerodynamic phenomena such as yawed flow, inflow turbulence and wind shear, have a large effect on wind turbine operation. These can cause rapid changes in speed and direction of the air flow encountered by the airfoils along the blades of a wind turbine. These changes cause fluctuating aerodynamic forces, increased peak forces, blade vibrations, and significant material fatigue. Additionally, the transient effects of tower shadow (for downwind rotor configurations), dynamic stall, dynamic inflow, explained below, change turbine operation in unexpected ways.
Many of these effects occur at the rotational frequency of the rotor or at multiples of that frequency. Effects that occur once per revolution are often referred to as having a frequency of 1P. Similarly, effects that occur at three or n times per revolution of the rotor are referred to as occurring at a frequency of 3P or nP.

Yaw condition

When wind directions change, or when the rotor exhibits a yaw error, the axial induction is affected by both a cyclic variation in axial flow velocities relative to the blades and a deflected rotor wake. The cyclic variation in axial flow is accounted for by including the axial component of the blade velocity in the equations for the relative velocity of the incoming flow stream. The deflected wake is accounted for by multiplying the axial induction factor, a, by a so-called skewed-wake correction factor.

Tower shadow

For downwind rotor configurations, aerodynamic loads on the blades are affected by the tower wake, commonly called the tower shadow, which causes a wind speed deficit behind the tower.
The blades of a downwind rotor with B blades will encounter the tower shadow once per revolution, causing a rapid drop in power and BP vibrations in the turbine structure.
Thus, the tower shadow or wake is modelled as a reduction in wind velocity according to a cosine law.

Dynamic stall

For blades that are downwind of the tower (which are affected by tower shadow), turbines that are operating in yawed conditions, or even turbines operating in a turbulent flow, the aerodynamic environment is rapidly changing.

Rapid changes in wind speed cause sudden changes in the angle of attack of the airfoils along the blade, that can result in a detachment and then reattachment of air flow along the airfoil.

During such dynamic conditions, stall may be delayed or may take place earlier than expected (known as dynamic stall).

Furthermore, a difference in Cl can be observed for the same angle of attack, depending on whether the Cl is ascending or descending, and can be seen as hysteresis (see g. 2.8) [8] with a corresponding variation in the aerodynamic forces on the blade compared to the ones that should be experienced for steady conditions.

Thus, dynamic stall can result in high transient forces as the wind speed increases, and stall is usually delayed.

Research has not yet come to an agreement on this point so, usually semi-empirical models for dynamic stall are used in computer rotor performance codes.

The most common dynamic stall models are those Beddoes-Leishman model, summarized by Leishman and Beddoes [62]), and Gormont [63].

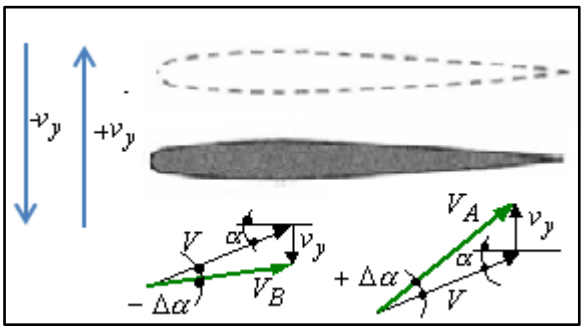

Figure 4.2: Variation of local velocity and related variation of angle of attack

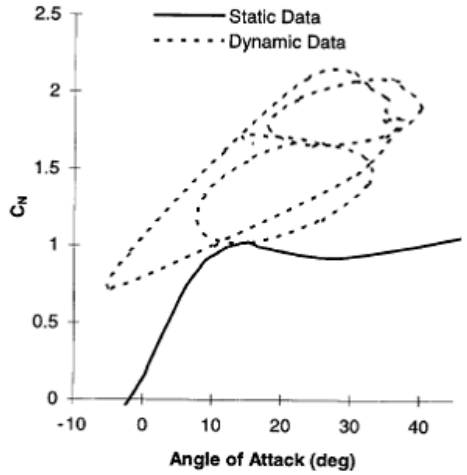

Figure 4.3: Dynamic stall events Experimental data from (Pierce,1996)

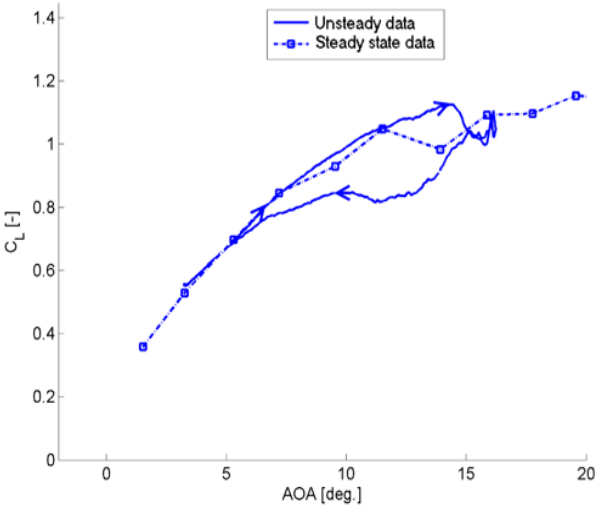

Figure 4.4: Dynamic stall. Extracted from [44]

Dynamic inflow

The term dynamic inflow is used to indicate the dynamic response of the inflow velocities in the rotorplane to turbulence and changes in rotor operation caused, for example, by pitch or rotor speed changes, wind gusts and also yawed flow, for which the loading of the turbine blades changes periodically, and the inflow will respond with time delay.

Steady state aerodynamics suggest that increased wind speed and, thus, increased power production should result in an instantaneous increase in the axial induction factor and changes in the flow field upstream and downstream of the rotor. During rapid changes in the flow and rapid changes in rotor operation, extended flow field around the rotor cannot react promptly enough to establish steady-state conditions instantaneously.

Thus, the aerodynamic conditions at the rotor are not necessarily the expected conditions, but an ever-changing approximation as the flow field changes.

For more information on dynamic inflow see Snel and Schepers [64] and Pitt and Peters [65], Suzuki and Hansen [66].

4.2.2 Analysis code used for unsteady and asymmetric operating conditions – Fast_AD

FAST is a free code for aerodynamic and dynamic analysis of horizontal axis wind turbines for both two- and three-bladed turbine configurations, with a teetering or rigid hub.

This code uses the BEM theory with modifications to improve the results for unsteady events and it is capable to simulate wind turbines behaviour in many different operating conditions.

It was developed by Oregon State University, NREL, and Windward Engineering.

The code models the wind turbine as a combination of rigid and flexible bodies, and models flexible elements, such as the tower and blades, using a linear modal representation.

FAST allows to account for multiple degrees of freedom including yaw, teeter, drive train torsion, four different bending modes for the tower (two fore-aft modes and two side-to-side modes), and three blade-bending modes (two flap-wise modes and one edgewise mode).

Any combination of the available DOFs and features can be enabled for each analysis.

Blades and tower are treated as cantilever beams, that means zero deflection and slope at the blade root; thus, the mode shapes take the form of a sixth-order polynomial with the zeroth and first terms being zero.

The modes of the blades are defined with respect to the local structural twist, that is, the shapes twist with the blade, are three dimensional, and do not lie within a single plane. In the case of a twisted blade, the tip will deflect in both the in-plane and out-of-plane

directions due to a pure flap-wise deflection or a pure edge-wise deflection. Flap-wise and edge-wise deflections can usually lie in a range of directions as shown in the next figure.

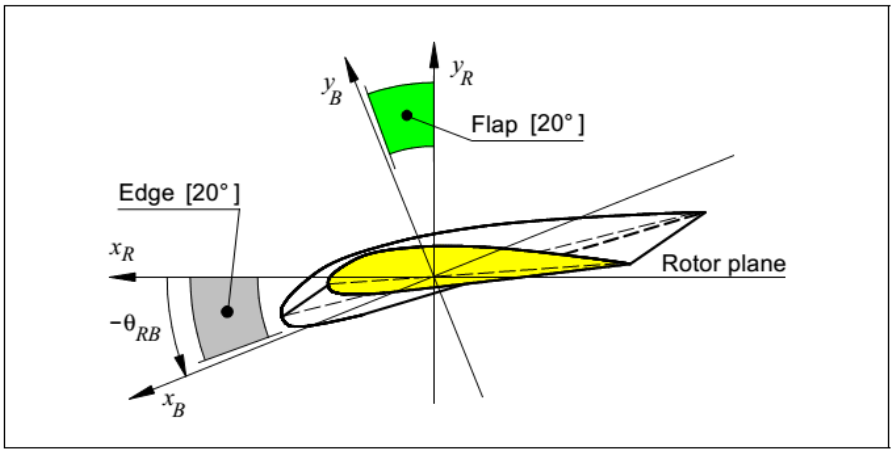

Figure 4.5: Typical ranges of flap-wise and edge-wise local directions. Extracted from [1]

FAST was evaluated by Germanischer Lloyd Wind Energie and has been approved for the calculation of onshore wind turbine loads for design and certification [67] in combination with the ADAMS software.
FAST incorporates the AeroDyn [2],[68] aerodynamic subroutine library to calculate the aerodynamic forces on the blades.
A brief overview of the codes used in this to generate all the input files necessary to run FAST_AD is reported hereinafter.

Aerodyn

Aerodyn [2],[68] is a code which calculates aerodynamic loads developed by NREL and incorporated in FAST_AD.
As WT_Perf, AeroDyn is based on blade element momentum theory, but it is more detailed in many ways.
It includes the following features: dynamic inflow, dynamic stall, tower shadow, vertical wind shear, horizontal wind shear, vertical wind, tower shadow, and unsteady inflow (turbulence).
AeroDyn contains two wake models: the blade element momentum theory and a dynamic inflow model based on the Generalized Dynamic Wake (GDW) theory.
These methods are used to calculate the axial induced velocities from the wake in the rotor plane.
The user also has the option of turning off the wake completely.
If the user chooses blade element momentum theory, he can choose to incorporate the aerodynamic effects of tip losses, hub losses, and skewed wake. With the generalized dynamic wake, all of these effects are automatically included.

The GDW uses a series solution to describe the induced velocity field in the rotor plane, which includes Legendre functions in the radial direction and trigonometric functions in the tangential direction. The AeroDyn GDW model is based on the work of Suzuki [69].
The dynamic stall model implemented in AeroDyn is based on the semi-empirical Beddoes-Leishman model [62].
Finally, for the tower shadow AeroDyn implements a model based on potential flow around a cylinder and an expanding wake.
The theory used for AeroDyn can be found in [68], [2].

TurbSim

TurbSim is used to synthesize time series of turbulent wind data, including coherent structures, for input to codes such as FAST, and developed by NREL.
Simple uniform wind shear is modelled using a power-law profile, in which the incoming wind speed becomes dependent on the elevation above the ground. Horizontal variation in incoming wind speed is usually modelled with a linear velocity profile. Wind-inflow data are usually stored in files that permit modellers to specify wind parameters that change with time (time-series inputs).
Alternatively, several models have been developed to simulate full field turbulent flow. In these models, inflow data can have velocity components in three dimensions that vary across the entire rotor plane.

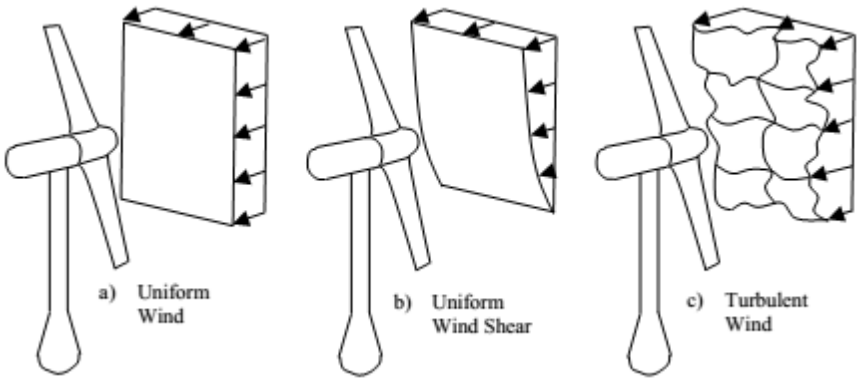

Figure 4.6: Natural wind characteristics. Extracted from [7]

BModes

BModes is a pre-processor which calculates mode shapes and frequencies of cantilevered beams, particularly blades and towers, and it is used to generate FAST input files containing tower and blades structural information.
The beam is divided into a number of finite elements.

Each element has three internal and two boundary nodes and is characterized by 15 degrees of freedom. Inputs for a blade include geometric and structural properties, rotational speed, and pitch angle.
More details on this code can be found in [70].

PreComp
This code is a pre-processor which calculates section properties of composite blades, such as inertias and stiffness, and it is used to generate BMODES input files. Inputs for PRECOMP are external blade shape and internal lay-up of composite layers.

4.2.3 Comparison between WT_Perf and FAST results

The following picture shows the comparison between a power curve evaluated in steady operating conditions by using WT_Perf, and the results for the same wind turbine obtained by using Fast_AD in unsteady operating conditions. The power curves refer to the last wind turbine obtained in this work (see Chapter 6 for details).
It can be noticed that WT_Perf steady results almost match the mean values of power obtained in unsteady conditions, thus it can be used with quite confidence to perform a preliminary design of a wind turbine.
On the other hand, the picture also shows that there is a huge variation of power values in unsteady conditions, that has to be taken into account for computing extreme and fatigue loads in a second phase of the design process.

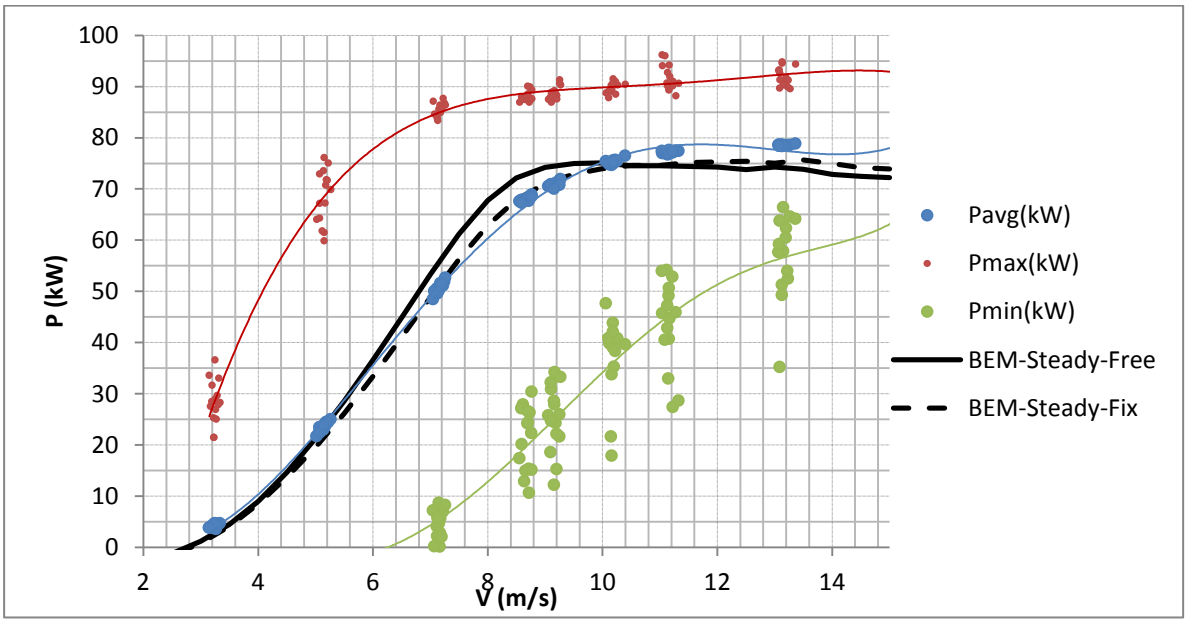

Figure 4.7: Example of power curve computed in unsteady conditions (FAST_AD) and steady conditions (WT_Perf).

4.3 Comparison between WT_Perf and field experimental tests results

To be more confident of the power overestimation of the BEM method, an experimental test campaign has been performed for a scaled model of the first wind turbine obtained during the optimization process developed in this work.
Due to very low values of Reynolds number for the scaled prototype and some uncertainties about the accuracy of the tests, the campaign was limited to a few initial attempts, whose results are quite scattering. Nevertheless, the main objective of the tests was achieved, since the results of all the tests gave decreasing power curves beyond the power peak, as shown as an example in the next figure.

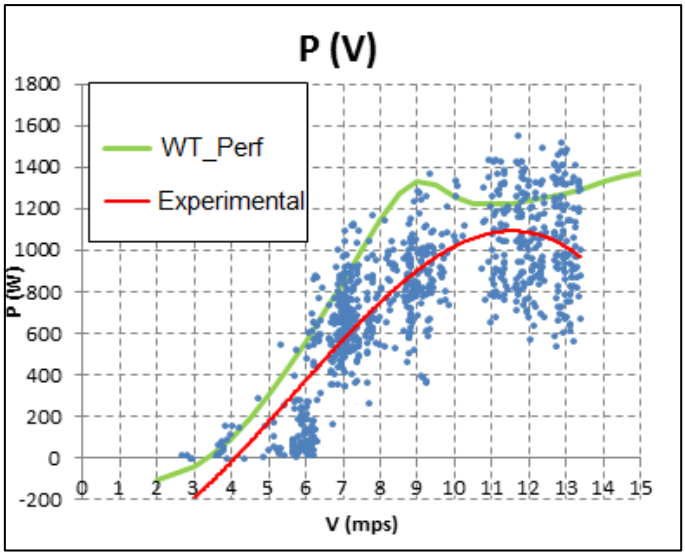

Figure 4.8: Field test power curve VS WT_Perf power curve (Scaled model)

Figure 4.9: Field experimental test

Chapter 5
Stall induced vibrations

When a wind turbine blade vibrates, the aerodynamic forces have an additional component originated by the vibration velocity, which has to be taken into account for a correct prediction of the loads and the dynamic behaviour of the blade.
Such component with good approximation can be considered proportional to vibration velocity, thus it actually acts as a viscus damping force, usually denoted as “aerodynamic damping”.
When the airfoils are in stall conditions, the slope of the lift curve becomes negative and can cause a local negative aerodynamic damping in the lift direction.
As in instance, a descending airfoil will see an increasing angle of attack that will cause a lower value of lift coefficient; this will be equivalent to have a component of the aerodynamic force promoting the descent of the airfoil, thus acting as a negative damping force.
If global aerodynamic damping of the blade is both negative and bigger in magnitude than the structural damping, any disturbance can cause divergent oscillations which can dramatically increase fatigue loads and can even lead to rapid failure in the worst cases.
This phenomenon is usually reported as “stall induced vibrations” and represents a key issue for stall regulated wind turbines, which work in stalled conditions in a significant part of the lifetime.
In particular, Petersen at al. in [1] demonstrated that on the single blade section the damping in the in-plane direction will always be negative if the blade section produces power and the slope of the power curve as function of wind speed is negative or zero, which is a typical operating condition of stall regulated wind turbines beyond the power peak.
The same can be said regarding the out-of-plane damping on the section, which is positive if the slope of the thrust is positive.

In the first phase of this work the optimization of a stall regulated wind turbine has been carried out only accounting for annual energy production and weight requirements.
Then, a full aeroelastic analysis of the optimized wind turbine has been developed in unsteady conditions by using the aeroelastic code Fast_AD, to verify extreme loads, fatigue loads and thus the lifetime of the machine.
The results of the analysis showed high vibrations at some wind speeds beyond the power peak, leading to unacceptable fatigue loads and lifetime.

Thus, in the second phase of this work, this issue has been carefully addressed, in order to develop a new optimization process aiming at preventing the occurrence of vibrations.
First of all, a specific investigation has been performed to individuate the main sources of these vibrations and the main parameters influencing the dynamic behaviour of stall regulated wind turbines.
A simplified method to predict the dynamic behaviour of the blades in a preliminary design phase has been individuated and validated by comparing its predictions with results obtained by using the aeroelastic code FAST_AD.
Finally, this simplified method has been implemented within the new optimization process, aiming at optimizing both the annual energy production and the dynamic behaviour of the wind turbine, preventing the occurrence of vibrations.

In the following sections results obtained by FAST_AD for the wind turbine optimized in the first phase of this work are supplied, to show the extent of the phenomenon and its main characteristics.
Then, the simplified method used to predict the dynamic behaviour of the blades is shown together with its validation with FAST_AD results and the influence of different parameters will be shown.

5.1 FAST_AD results for a low damped wind turbine

The following figures show the results of the analysis performed by using the aeroelastic code FAST_AD for the wind turbine optimized in the first phase of this work, which presents a severe amplification of stall induced vibrations at wind speeds beyond the power peak.
The following settings in FAST_AD have been used for all the cases:

- Only the first mode in the flap-wise direction is enabled
- No modes in the edge-wise direction are enabled
- Structural damping (1st flap-wise mode): 0.5 %
- Tower shadow disabled
- Dynamic effects disabled (dynamic stall and dynamic inflow)
- Tilt=0 degrees (Tilt angle is intended as the angle between the rotor plane and a vertical plane)
- Yaw angle =0
- No wind shear
- Steady inflow conditions

This settings have been used to neglect all the other effects that could cause vibrations, to highlight the effects of the steady aerodynamics of the airfoils.

The wind turbine behaviour in terms of bending moments at the root section of the blade and in terms of shaft bending moment (Mys, 'tilt' direction) are reported for two wind speeds, 9 m/s and 11 m/s.
The first corresponds to a wind speed where relevant vibrations still have not occurred, while in the second case divergent oscillations are observable for all the loads reported.

Shaft bending moments and root bending moments of the blades use the coordinate systems reported in the following figures.

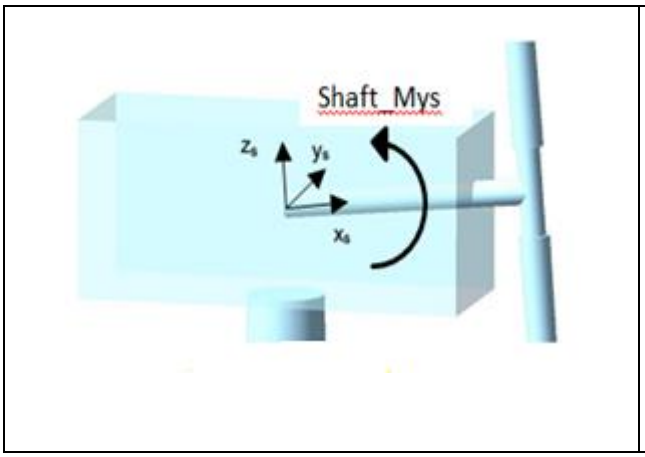

Figure 5.1: Shaft coordinate system

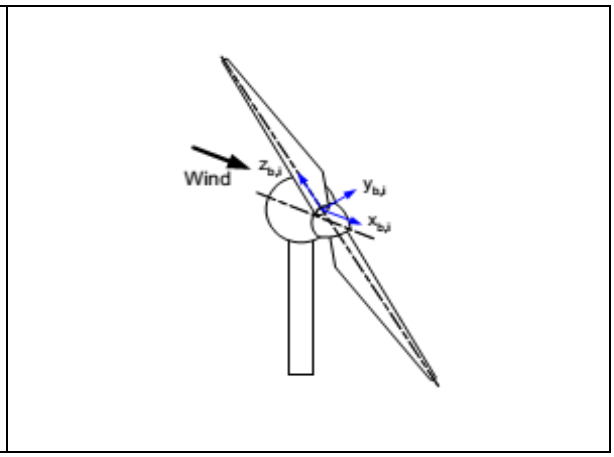

Figure 5.2: Blade coordinate system

Lift curves of the airfoils at three representative stations along the blade are reported for both the cases to show the operating condition of each airfoil in both the conditions.
These two conditions are also highlighted on the power curve.

The figures show that the oscillations have the highest amplitude when the outer airfoil reaches the maximum negative slope, at 11 m/s.

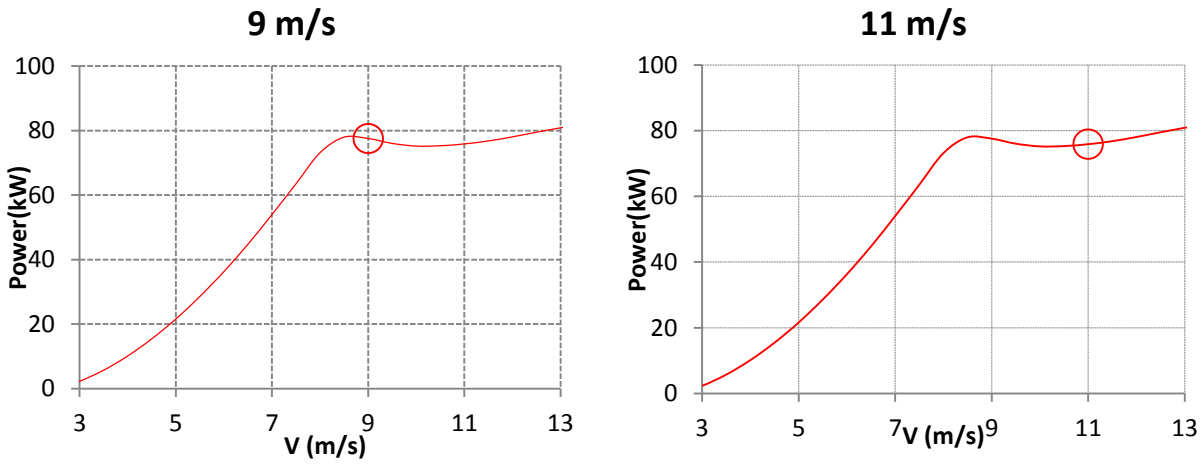

Figure 5.3: Power curve

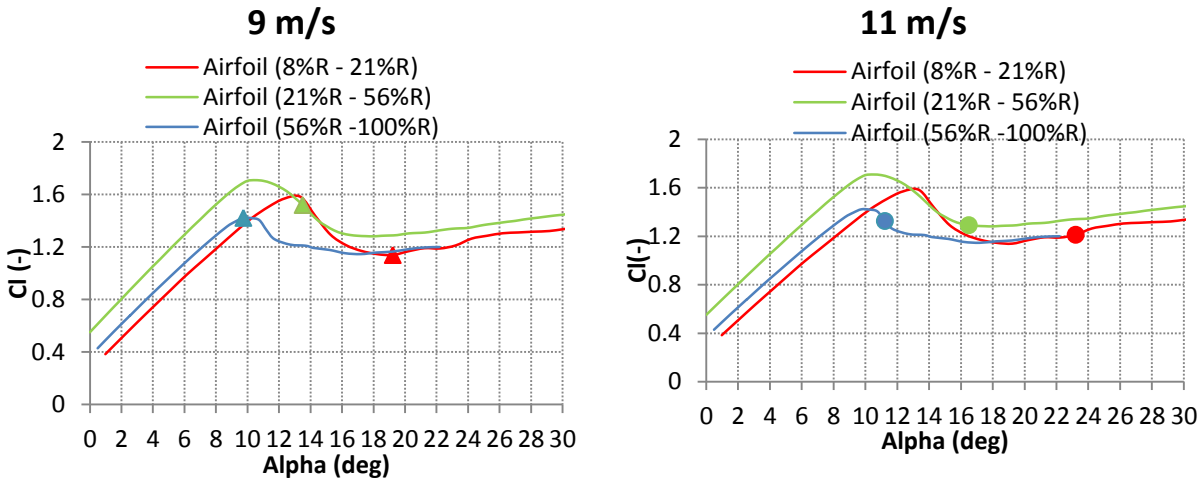

Figure 5.4: Lift coefficient of airfoils along the blade and working points at 9 m/s and 11 m/s

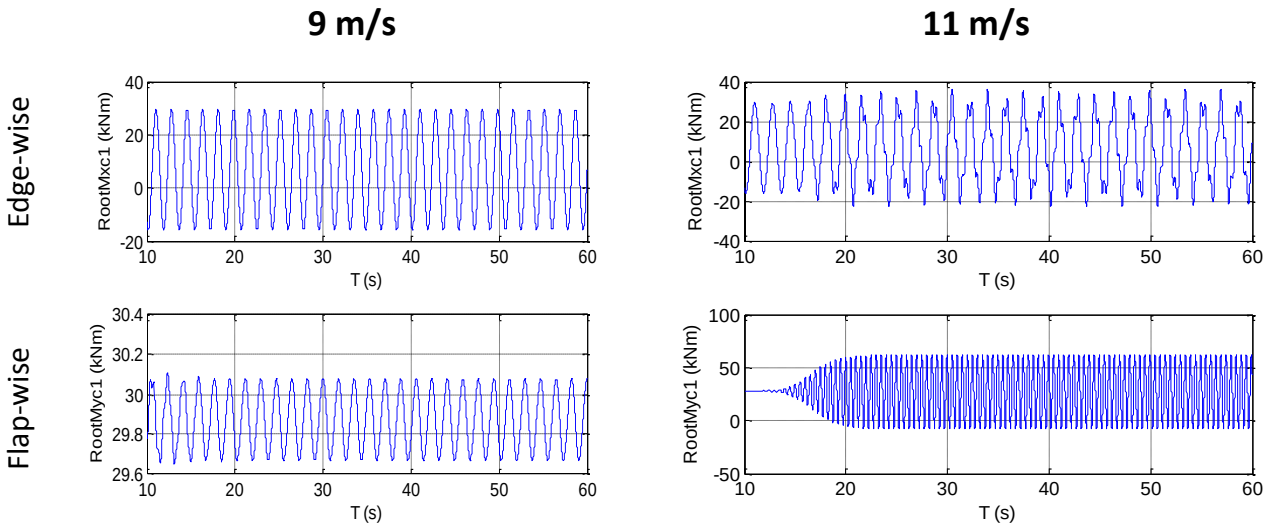

Figure 5.5: Blade Root Bending Moments (t)

(RootMxc1=Edge-wise direction; RootMyc1=Flap-wise direction)

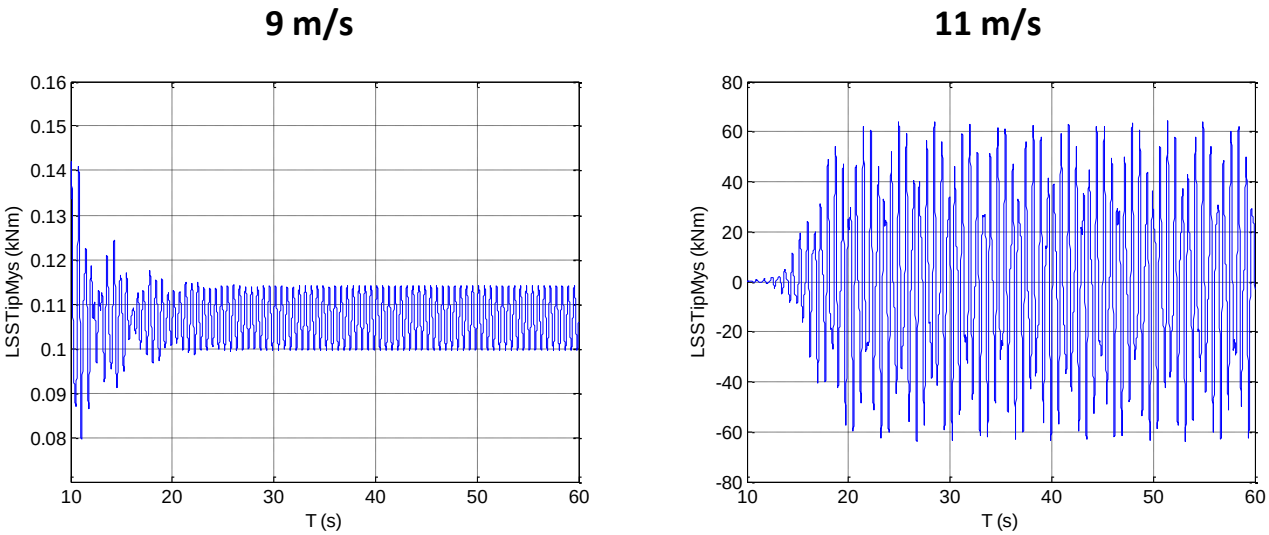

Figure 5.6: Shaft Bending Moment (t)

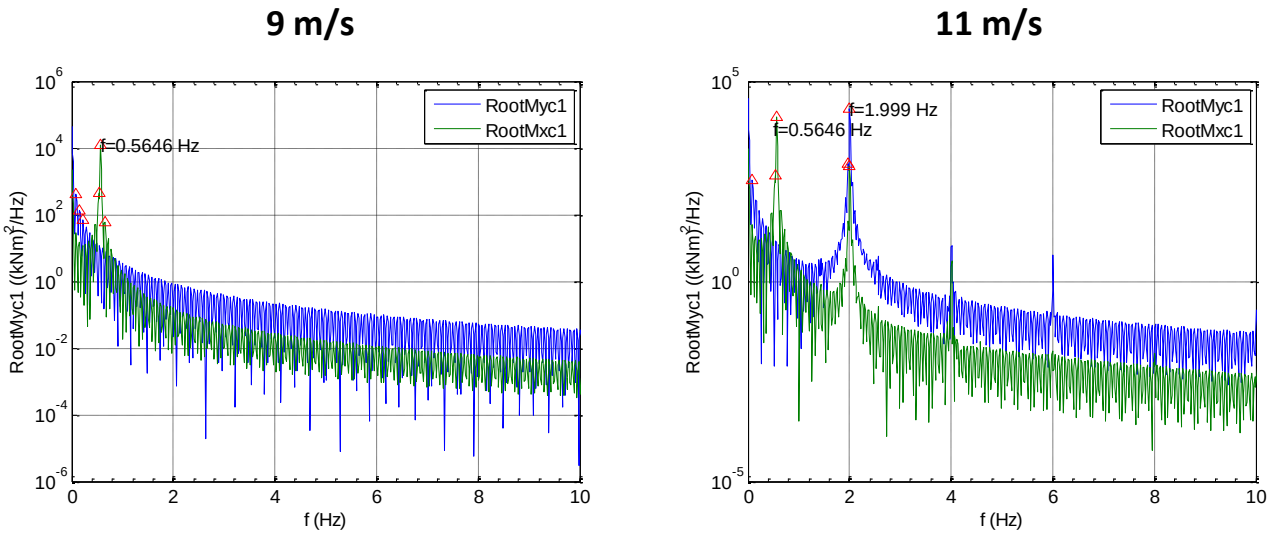

Figure 5.7: FFT Root Bending Moments (Edge-wise direction (Mxc), Flap-wise direction (Myc))

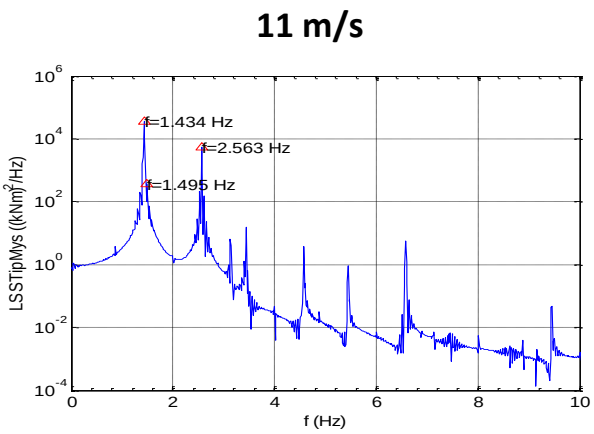

Figure 5.8: FFT Shaft Bending Moment

Similar graphs are reported for 13 m/s and 15 m/s in the following figures.
For these wind speeds the outer airfoil will reach higher angles of attack, where the slope of the lift curve is less negative or positive, and the oscillations decrease.

V=13 m/s

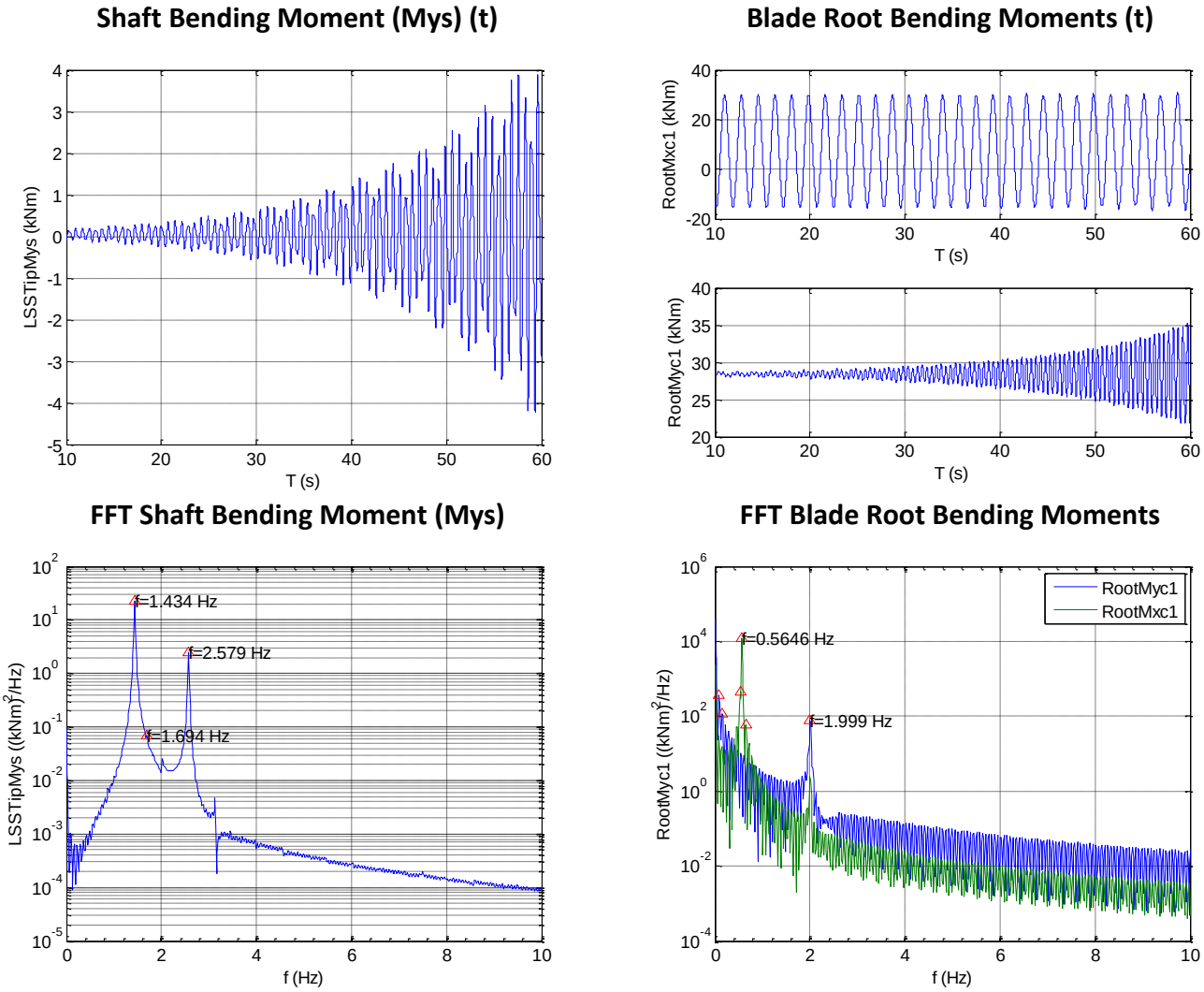

Figure 5.9: V=13 m/s

V=15 m/s

Shaft Bending Moment (Mys) (t)

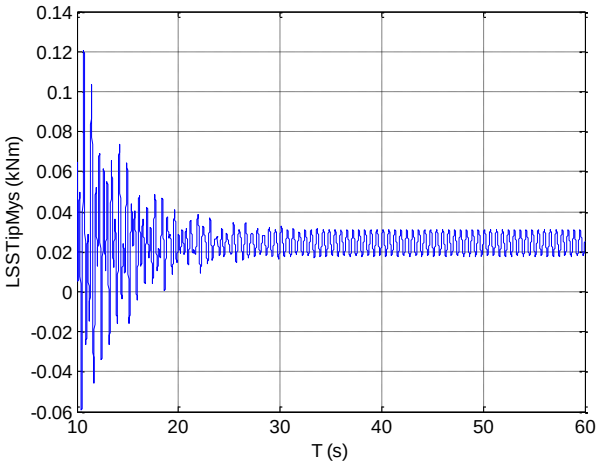

Blade Root Bending Moments (t)

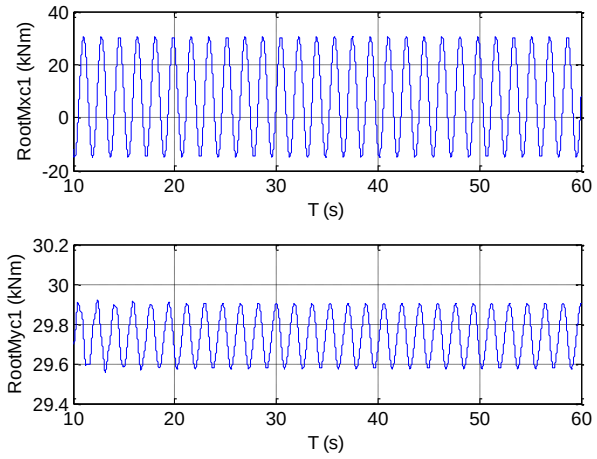

FFT Shaft Bending Moment (Mys)

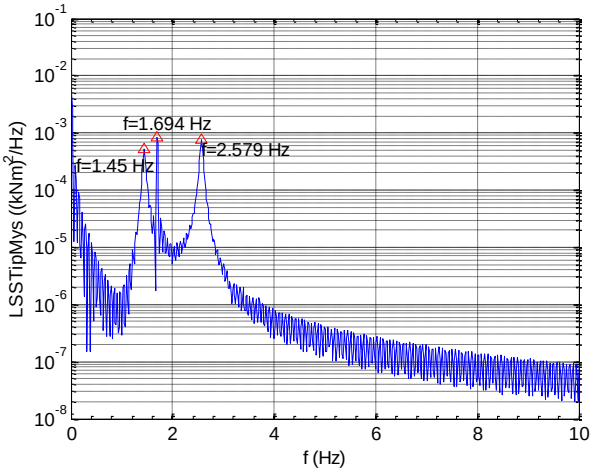

FFT Blade Root Bending Moments (f)

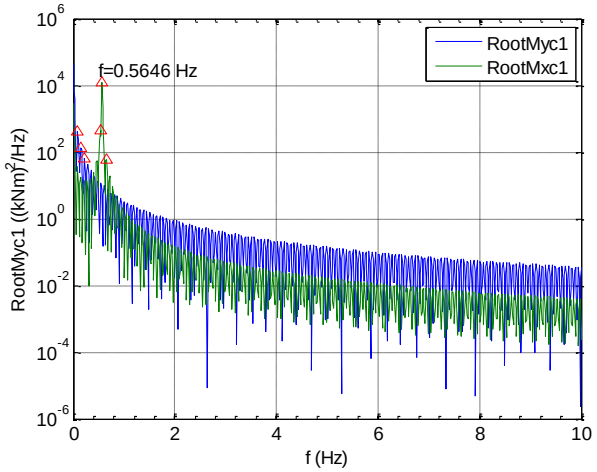

Figure 5.10: V=15 m/s

It should be highlighted that in [1] edge-wise vibrations are given more attention, while the following results show that flap-wise vibrations seem to be more dangerous.

Furthermore, stall induced vibrations occur even if the wind turbine is working in steady inflow conditions.

This highlights that stall induced vibrations have to be intended as instabilities of the blades, that can take place due to any initial disturbance.

Furthermore, vibrations occur even if all the sources of variable or asymmetric flow (tower shadow wind shear, tilt, yaw) are neglected.

In these conditions, vibrations could be caused by asymmetric flap-wise displacements between the upper half of the rotor disk and the lower half, that could cause the initial oscillations of the blades.

These asymmetric displacements could be caused by the weight of the blade, which can cause – when the blade is deflected - a further deflection in downwind direction when the blade passes through the upper half of the rotor disk, and in upwind direction when the blade passes through the lower half, as shown in the following figure (which refers to a downwind configuration).
Furthermore, they could be caused by a component of the weight of the blade in flap-wise direction (due to the twist of the blade).

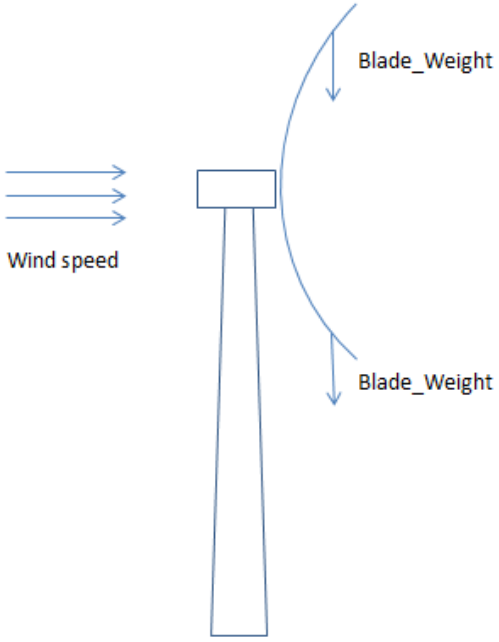

Figure 5.11: Weight on deflected blades

In the following figure structural and aerodynamic damping in flap-wise and edge-wise directions are shown for each wind speed.
It is also reported the shaft bending moment to show that divergent oscillations of its amplitude occur when the aerodynamic bending on flap-wise direction reaches negative values.

Modal aerodynamic and structural damping of the blades

V= 9 m/s

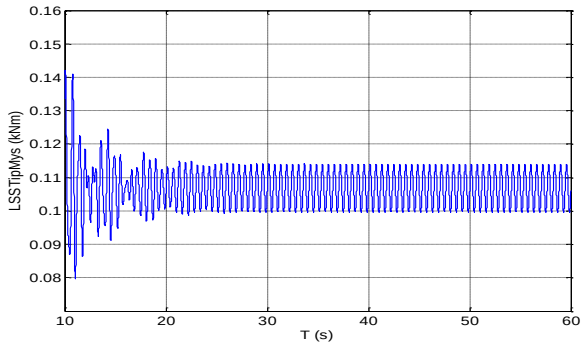

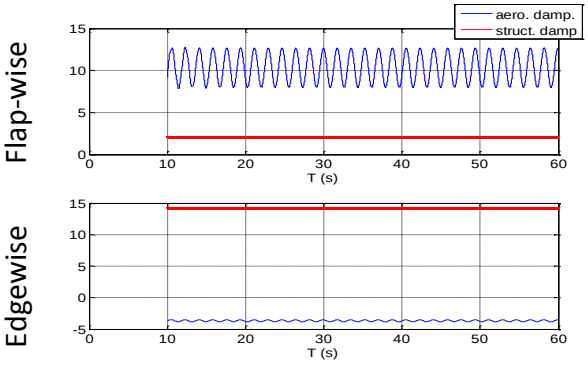

V= 11 m/s

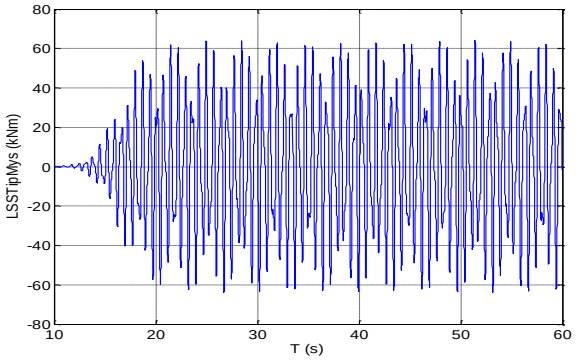

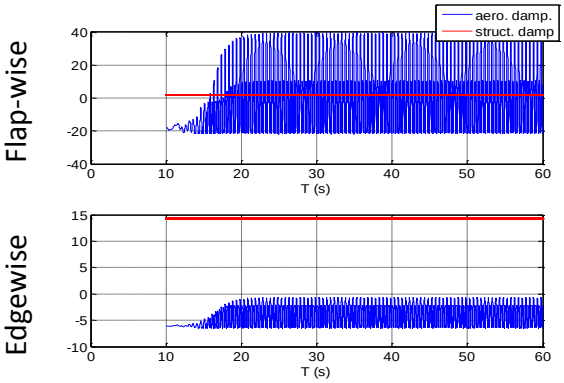

V= 13 m/s

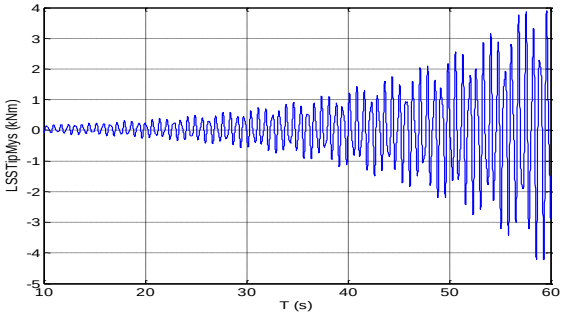

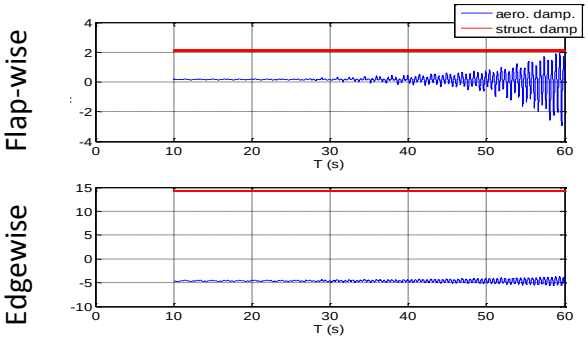

V= 15 m/s

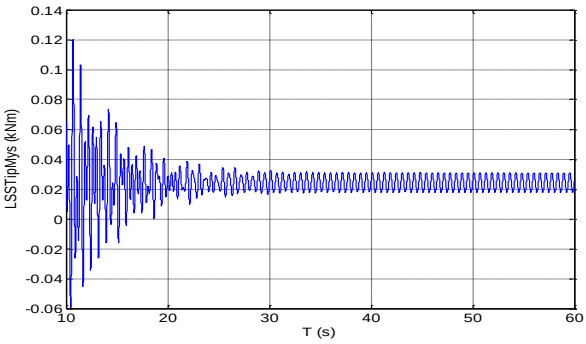

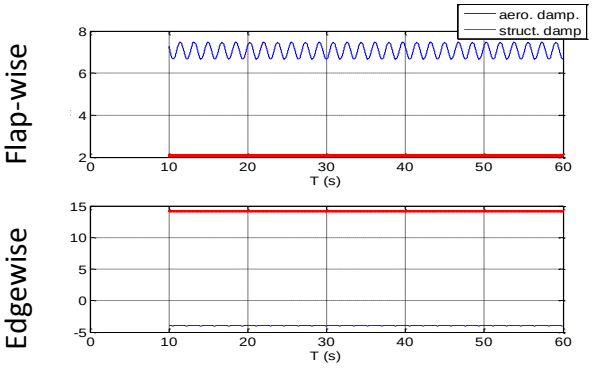

5.2 Simplified expression of aerodynamic damping of the blade

As previously said, in the second phase of this work a new optimization process has been carried out to optimize both the annual energy and the dynamic behaviour of the blades, avoiding the occurrence of stall induced vibrations.
During the preliminary design phase, a simplified expression of the aerodynamic damping of the blade has been used as an index of oscillations amplitude without the need of any aeroelastic analysis with FAST_AD, to make the design as fast as possible.
A linearized approach presented by Petersen et al. in [1] has been applied and briefly reported in the following section, to obtain a simplified expression for the local aerodynamic damping on the different sections of the blades.
Then, a modal approach has been used to evaluate the aerodynamic damping of the complete blade, also presented in this chapter.

5.2.1 Local aerodynamic damping

5.2.1.1 Local aerodynamic damping coefficients Out-of-plane and in-plane directions

Petersen et al. in [1] derived two linearized expressions of the aerodynamic damping for a blade section, using quasi-steady, 2-D aerodynamics.
The first expression is in terms of 2-D aerodynamic characteristics (Cl and Cd) of the airfoil, while the second is in terms of local power and axial force.
Both the expressions are reported because they can be useful to understand the main parameters influencing the aerodynamic damping of a blade.

In the next figure a generic blade section is shown with the related velocities and aerodynamic forces.

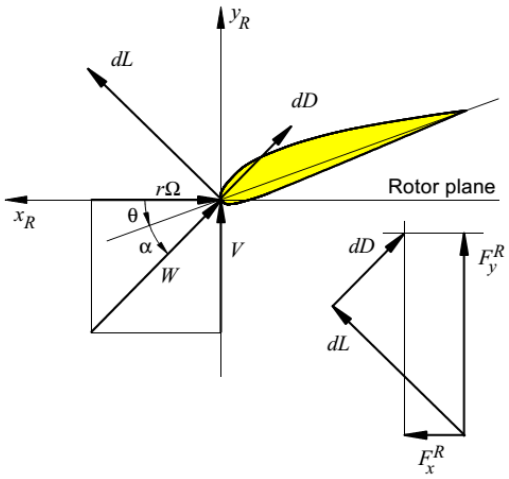

Figure 5.12: Local element - Velocities, flow angles and forces

In the figure:
x_R and y_R represent the in-plane and out-of-plane directions respectively,
F_x^R is the resulting force per unit length in the x_R-direction
F_y^R the resulting forces per unit length in the y_R-direction
Ω is the angular velocity of the rotor,
r is the actual blade radius, i. e. the radial position of the considered cross section,
V is the wind speed, which is felt by the blade in the y-direction,
W is the resulting wind speed,
θ is the local pitch-setting, i.e. the angle between chord and rotor plane,
α is the angle of attack,
dL is the lift-force per unit length of the blade,
dD is the drag-force per unit length of the blade.

In the following equations the upper index *R* will always indicate that the equations refer to the rotor coordinate system $\{x_R, y_R\}$.
Induction velocities can be neglected for the purposes of this simplified approach.
The resulting forces per unit length in the in-plane and out-of-plane directions can be obtained as:

$$\begin{Bmatrix} F_x^R \\ F_y^R \end{Bmatrix} = \begin{bmatrix} \sin(\gamma) & -\cos(\gamma) \\ \cos(\gamma) & \sin(\gamma) \end{bmatrix} \begin{Bmatrix} dL \\ dF \end{Bmatrix} \tag{5.1}$$

where:
d*L* is the lift per unit length and d*D* is the drag force per unit length,
γ= θ+α is the local inflow angle, which is related to the main inflow velocities (V, rΩ and W) as in the following expressions:

$$\cos\gamma = \frac{r\Omega}{W} \tag{5.2}$$

$$\sin\gamma = \frac{V}{W} \tag{5.3}$$

When the blade section vibrates, both the velocity in the in-plane direction and in the out-of-plane direction have additional components, which can be expressed respectively as:

$$\Delta(r\Omega) = \dot{x}_R = \frac{dx_R}{dt} \tag{5.4}$$

$$\Delta V = -\dot{y}_R = \frac{dy_R}{dt} \tag{5.5}$$

The aerodynamic forces will be functions of both the main steady velocities (rΩ and V) and the vibration velocities (Δ(rΩ) and ΔV).

These forces can be linearized by expanding them in a Taylor series at a point corresponding to V_0=V and $r\Omega_0$=rΩ, as in the following equations:

$$F_x^R\big(\Delta V, \Delta(r\Omega)\big) \simeq F_x^R(V_0, r\Omega_0) + \frac{\partial F_x^R(V_0, r\Omega_0)}{\partial V}\Delta V + \frac{\partial F_x^R(V_0, r\Omega_0)}{\partial(r\Omega)}\Delta(r\Omega) \tag{5.6}$$

$$F_y^R\big(\Delta V, \Delta(r\Omega)\big) \simeq F_y^R(V_0, r\Omega_0) + \frac{\partial F_y^R(V_0, r\Omega_0)}{\partial V}\Delta V + \frac{\partial F_y^R(V_0, r\Omega_0)}{\partial(r\Omega)}\Delta(r\Omega) \tag{5.7}$$

In a matrix formulation:

$$\begin{Bmatrix} F_x^R \\ F_y^R \end{Bmatrix} \simeq \begin{Bmatrix} F_{x0}^R \\ F_{y0}^R \end{Bmatrix} + \begin{Bmatrix} \frac{\partial F_x^R}{\partial(r\Omega)} & \frac{\partial F_x^R}{\partial V} \\ \frac{\partial F_y^R}{\partial(r\Omega)} & \frac{\partial F_y^R}{\partial V} \end{Bmatrix} \begin{Bmatrix} \Delta(r\Omega) \\ \Delta V \end{Bmatrix} \tag{5.8}$$

or:

$$\begin{Bmatrix} F_x^R \\ F_y^R \end{Bmatrix} \simeq \begin{Bmatrix} F_{x0}^R \\ F_{y0}^R \end{Bmatrix} - \begin{Bmatrix} -\frac{\partial F_x^R}{\partial(r\Omega)} & \frac{\partial F_x^R}{\partial V} \\ -\frac{\partial F_y^R}{\partial(r\Omega)} & \frac{\partial F_y^R}{\partial V} \end{Bmatrix} \begin{Bmatrix} \dot{x}_R \\ \dot{y}_R \end{Bmatrix} \tag{5.9}$$

The matrix in the last equation represents the local aerodynamic damping matrix, since it relates the aerodynamic forces acting on the blade section to the section velocity itself:

In a more concentrated expression we obtain:

$$\{F_a^R\} \simeq \{F_{a0}^R\} - [c_a^R]\{\dot{u}^R\} \tag{5.10}$$

where:

$$\{\dot{u}^R\} = \begin{Bmatrix} \dot{x}_R \\ \dot{y}_R \end{Bmatrix} \tag{5.11}$$

$$[c_a^R] = \begin{bmatrix} c_{xx}^R & c_{xy}^R \\ c_{yx}^R & c_{yy}^R \end{bmatrix} = \begin{bmatrix} -\frac{\partial F_x^R}{\partial (r\Omega)} & \frac{\partial F_x^R}{\partial V} \\ -\frac{\partial F_y^R}{\partial (r\Omega)} & \frac{\partial F_y^R}{\partial V} \end{bmatrix} \tag{5.12}$$

c_{xx}^R corresponds to the contribute of F_x^R to the damping in the x_R direction;
c_{yy}^R corresponds to the contribute of F_y^R to the damping in the y_R-direction;
c_{xy}^R corresponds to the contribute of F_x^R to the damping in the y_R-direction;
c_{yx}^R corresponds to the contribute of F_y^R to the damping in the x_R direction.

Damping coefficients expressed in terms of 2D airfoil aerodynamic characteristics

Assuming that $\{F_{a0}^R\}=\{0\}$ (without loss of generality of the next equations) and using the following expressions of the lift force per unit length (dL) and the drag force per unit length (dD):

$$dL = dL(r,\alpha) = \frac{1}{2}\rho c(r) W^2 C_L(r,\alpha) \tag{5.13}$$

$$dD = dD(r,\alpha) = \frac{1}{2}\rho c(r) W^2 C_D(r,\alpha) \tag{5.14}$$

it is possible to obtain local damping coefficients as functions of 2D aerodynamic coefficients (Cl and Cd) of the airfoil:

$$c_{xx}^{R}(r,V) = \frac{1}{2} c\rho \frac{r\Omega}{W}\left[\left(\frac{V^2+2r^2\Omega^2}{r\Omega}\right) C_D - V\frac{\partial C_D}{\partial \alpha} - VC_L + \frac{V^2}{r\Omega}\frac{\partial C_L}{\partial \alpha}\right] \quad (5.15)$$

$$c_{xy}^{R}(r,V) = \frac{1}{2} c\rho \frac{r\Omega}{W}\left[-VC_D - r\Omega\frac{\partial C_D}{\partial \alpha} + \left(\frac{2V^2+r^2\Omega^2}{r\Omega}\right) C_L + V\frac{\partial C_L}{\partial \alpha}\right] \quad (5.16)$$

$$c_{yx}^{R}(r,V) = \frac{1}{2} c\rho \frac{r\Omega}{W}\left[-VC_D + \frac{V^2}{r\Omega}\frac{\partial C_D}{\partial \alpha} - \left(\frac{V^2+2r^2\Omega^2}{r\Omega}\right) C_L + V\frac{\partial C_L}{\partial \alpha}\right] \quad (5.17)$$

$$c_{yy}^{R}(r,V) = \frac{1}{2} c\rho \frac{r\Omega}{W}\left[\left(\frac{2V^2+r^2\Omega^2}{r\Omega}\right) C_D + V\frac{\partial C_D}{\partial \alpha} + VC_L + r\Omega\frac{\partial C_L}{\partial \alpha}\right] \quad (5.18)$$

From the expression of c_{yy}^{R} it is possible to notice that the out-of-plane damping coefficient decreases when the slope ($\frac{dCl}{d\alpha}$) of the lift curve becomes negative beyond the stall.
Thus, a gentle stall, that means a low value of the absolute value $|\frac{dCl}{d\alpha}|$ beyond the stall, would be desirable to avoid the occurrence of stall induced vibrations.

Damping coefficients expressed in terms of local power and local thrust

Using the following expressions of the local thrust (F_u) (force normal to the rotor plane) and the local power (P_u) as functions of 2D aerodynamic coefficients of the airfoil:

$$F_u = F_u(r,V) = F_y^R = \frac{1}{2}\rho cW(r\Omega C_L + VC_D) \quad (5.19)$$

$$P_u = P_u(r,V) = r\Omega F_x^R = \frac{1}{2}\rho cr\Omega W(VC_L - r\Omega C_D) \quad (5.20)$$

and rearranging the expressions of the damping coefficients, it is possible to eliminate airfoil data in the equations and obtain local damping coefficients as function of local power and thrust, as in the following expressions :

$$c_{xx}^{R} = -\frac{2}{r^2\Omega^2}P_u + \frac{V}{r^2\Omega^2}\frac{\partial P_u}{\partial V} \quad (5.21)$$

$$c_{yy}^{R} = \frac{\partial F_y^R}{\partial V} = \frac{\partial F_u}{\partial V} \quad (5.22)$$

$$c_{xy}^{R} = \frac{\partial F_x^R}{\partial V} = \frac{1}{r\Omega}\frac{\partial P_u}{\partial V} \quad (5.23)$$

$$c_{yx}^{R} = -\frac{2}{r\Omega}F_u + \frac{V}{r\Omega}\frac{\partial F_u}{\partial V} \quad (5.24)$$

Thus, we have:

$$c_{xx}^{R}(r,V) = -\frac{2}{r^2\Omega^2}P_u(r,V) + \frac{V}{r^2\Omega^2}\frac{\partial P_u(r,V)}{\partial V} \quad (5.25)$$

$$c_{xy}^{R}(r,V) = \frac{1}{r\Omega}\frac{\partial P_u(r,V)}{\partial V} \quad (5.26)$$

$$c_{yx}^{R}(r,V) = -\frac{2}{r\Omega}F_u(r,V) + \frac{V}{r\Omega}\frac{\partial F_u(r,V)}{\partial V} \quad (5.27)$$

$$c_{yy}^{R}(r,V) = \frac{\partial F_u(r,V)}{\partial V} \quad (5.28)$$

From these new expressions it is possible to observe that, on the single blade section, the damping in the in-plane direction will always be negative if the blade section produces power and the slope of the power curve as function of wind speed is negative or zero, which is a typical operating condition of sections of stall regulated wind turbines beyond the power peak.

The same can be said regarding the out-of-plane damping on the section, which is positive if the slope of the thrust is positive.

In terms of global performances of a wind turbine, this means that, beyond the power peak, a power curve as flat as possible and a thrust curve monotonically increasing would be desirable to reduce stall induced vibrations.

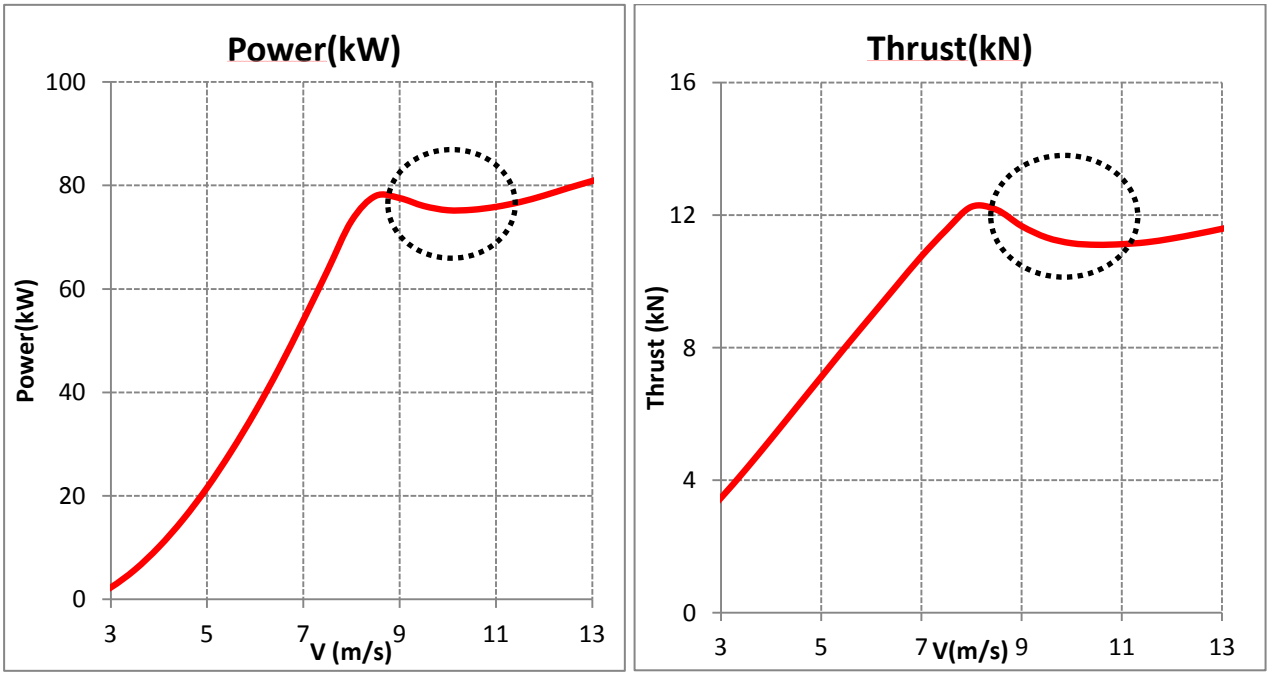

Figure 5.13: Typical power curve and thrust curve of a stall regulated wind turbine

5.2.1.2 Local aerodynamic damping coefficients Flap-wise and edge-wise directions

Usually, we are interested in analysing blade movements along the directions of the two principal bending axes of the blade, since they represent the directions of maximum and minimum deflection.
At each station along the blade, these directions depend on the local structural twist of the blade and are usually rotated relative the rotor reference system up to an angle $\theta_{RB}$of approximately 20-30 degrees, as shown in the following figure.

In particular, the direction of minimum moment of inertia is indicated as "flap-wise" direction (y_B in the figure); it represents the direction of maximum deflection and usually lies nearby the rotor out-of-plane direction.
The direction of maximum moment of inertia is indicated as "edge-wise" direction (x_B in the figure); it represents the direction of minimum deflection and lies nearby the rotor in-plane direction.

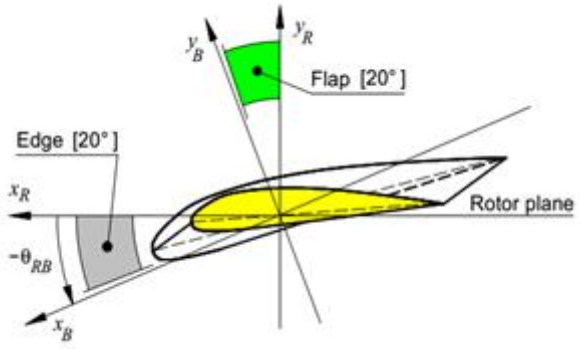

Figure 5.14: Typical ranges of flap-wise and edge-wise local directions. (Extracted from [1]**)**

To obtain local damping forces in flap-wise and edge-wise directions (B-coordinates) it is necessary to rotate both the local damping coefficients and the velocity vector expressed in rotor reference coordinates, by using the following rotation matrix:

$$[T_{RB}] = [T_{RB}(r)] = \begin{bmatrix} \cos[\theta_{RB}(r)] & \sin[\theta_{RB}(r)] \\ -sin[\theta_{RB}(r)] & cos[\theta_{RB}(r)] \end{bmatrix} \tag{5.29}$$

Thus, we have:

$$\{\dot{u}^B\} = [T_{RB}]\{\dot{u}^R\} \tag{5.30}$$

$$\{F_a^B\} = -[T_{RB}][c_a^R][T_{RB}]^{-1}\{\dot{u}^B\} \tag{5.31}$$

and finally:

$$\{F_a^B\} = -[c_a^R]\{\dot{u}^B\} = -\begin{bmatrix} c_{xx}^B & c_{xy}^B \\ c_{yx}^B & c_{yy}^B \end{bmatrix}\{\dot{u}^B\} \tag{5.32}$$

which defines the local damping matrix in B-coordinates.
Using the rotation matrix we obtain the following expression for the flap-wise local damping coefficient:

$$c_{yy}^B = c_{xx}^R \cos^2(\theta_{RB} + \frac{\pi}{2}) - \left(c_{xy}^R + c_{yx}^R\right)\cos(\theta_{RB} + \frac{\pi}{2})\sin(\theta_{RB} + \frac{\pi}{2}) + c_{yy}^R \sin^2(\theta_{RB} + \frac{\pi}{2}) \tag{5.33}$$

and for the edge-wise local damping coefficient:

$$c_{xx}^B = c_{xx}^R \cos^2\theta_{RB} - \left(c_{xy}^R + c_{yx}^R\right)\cos\theta_{RB}\sin\theta_{RB} + c_{yy}^R \sin^2\theta_{RB}\ . \tag{5.34}$$

5.2.2 Modal aerodynamic damping of the blade

5.2.2.1 Modal aerodynamic damping Out-of-plane and in-plane directions

To evaluate the global behaviour of the blade a modal approach has been used, obtaining the expression of the modal aerodynamic damping which has been used as an index of the damping of the blade within the preliminary design.

For many purposes a wind turbine blade can be considered as a one-dimensional structure, in the sense that the structural properties and the loading vary only with the radial coordinate, r.
Thus, as an instance, the equation of motion of the blade in the rotor out-of-plane direction can be expressed by the following matrix formulation of the system of equations, each one referred to a node at a different radius (r) along the blade:

$$[m^R(r)]\{\ddot{u}^R(r,t)\} + [c^R(r)]\{\dot{u}^R(r,t)\} + [k^R(r)]\{u^R(r,t)\} = \{f^R(r,t)\} \tag{5.35}$$

where:
$\{u^R\}$ is the deformation vector in the out-of-plane direction,

$[m^R(r)]$ is the mass matrix per unit length,
$[c^R(r)]$ is the damping matrix (structural and aerodynamic contributions) per unit length,
$[k^R(r)]$ is the stiffness matrix per unit length,
$\{f^R(r,t)\}$ is the external force vector per unit length.

The mode-shapes and the natural frequencies for the undamped structure are obtained by solution of the following eigenvalue problem:

$$-\omega_n^2[m^R(r)]\{\varphi_n^R(r)\} + [k^R(r)]\{\varphi_n^R(r)\} = \{0\} \quad (5.36)$$

which is the homogeneous equation associated to the equation of motion of the blade, with the damping neglected and the deformation substituted by the harmonic solution:

$$\{u^R(r,t)\} = \{\varphi_n^R(r)\}\cos(\omega_n t) \quad (5.37)$$

The solution of the eigenvalue problem gives the modes-shapes , $\{\varphi_n^B\}$, and the natural frequencies ω_n of the structure.

For each mode (*n*) we can define the modal mass, the modal stiffness and the modal damping coefficient.

The modal mass is expressed as:

$$M_n = \int_0^R \{\varphi_n^R(r)\}^T [m^R(r)]\{\varphi_n^R(r)\}dr \quad (5.38)$$

The modal stiffness is expressed as:

$$K_n = \int_0^R \{\varphi_n^R(r)\}^T [k^R(r)]\{\varphi_n^R(r)\}dr \quad (5.39)$$

Since the mode-shapes are orthogonal with respect to the mass matrix and to the stiffness matrix, we have:

$$\int_0^R \{\varphi_m^R(r)\}^T [m^R(r)]\{\varphi_n^R(r)\}dr = \begin{cases} M_n \, for \; m = n \\ 0 \, for \; m \neq n \end{cases} \quad (5.40)$$

$$\int_0^R \{\varphi_m^R(r)\}^T [k^R(r)]\{\varphi_n^R(r)\}dr = \begin{cases} M_n\,\omega_n^2 & for\ m = n \\ 0 & for\ m \neq n \end{cases} \tag{5.41}$$

The modal damping coefficient is expressed as:

$$C_n = \int_0^R \{\varphi_n^R(r)\}^T [c^R(r)]\{\varphi_n^R(r)\}dr \tag{5.42}$$

that in a discrete formulation is :

$$C_n = \sum_{i=1}^M \{\varphi_{n,i}^R\}^T [c_i^R]\{\varphi_{n,i}^R\}\Delta r_i \tag{5.43}$$

where M is the number of sections of finite length along the blade, *i* refers to the radial element number *i,* and Δr_i is the length of the discrete element number *i.*

At the i-th station, the damping matrix $[c_i^R]$ is given by the combination of the local structural damping matrix and the local aerodynamic damping matrix obtained in the previous section:

$$[c_a^R] = \begin{bmatrix} c_{xx}^R & c_{xy}^R \\ c_{yx}^R & c_{yy}^R \end{bmatrix} = \begin{bmatrix} -\frac{\partial F_x^R}{\partial(r\Omega)} & \frac{\partial F_x^R}{\partial V} \\ -\frac{\partial F_y^R}{\partial(r\Omega)} & \frac{\partial F_y^R}{\partial V} \end{bmatrix} \tag{5.44}$$

Thus, the modal aerodynamic damping coefficient $C_{a,n}$ for the mode number *n* is given by:

$$C_{a,n} = \int_0^R \{\varphi_n^R(r)\}^T [c_a^R(r)]\{\varphi_n^R(r)\}^T\, dr \tag{5.45}$$

or, in a discrete formulation:

$$C_{a,n} = \sum_{i=1}^M \{\varphi_{n,i}^R\}^T [c_{a,i}^R]\{\varphi_{n,i}^R\}^T \tag{5.46}$$

The resolution of the deformation vector $\{u^R(r,t)\}$ in mode-shapes and normal coordinates will be given by:

$$\{u^R(r,t)\} = [\varphi^R(r)]\{q^R(t)\} \tag{5.47}$$

or alternatively by

$$\{u^R(r,t)\} = \sum_{n=1}^{N} \{\varphi_n^R(r)\} q_n^R(t) \tag{5.48}$$

In the first equation the mode-shapes are the columns of the matrix $[\varphi(r)]$ and $\{q^R(t)\}$ is the normal-coordinate vector, while in the second equation the matrix product is written as a sum.

5.2.2.2 Modal aerodynamic damping Flap-wise and edge-wise directions

The modal damping coefficients of the blade in the flap-wise and edge-wise directions for the mode number *n* have the following expressions:

$$c_{flap,n} = \int_{R_{hub}}^{R} c_{yy}^B \varphi_{flap,n}^2 \, dr \tag{5.49}$$

$$c_{edge,n} = \int_{R_{hub}}^{R} c_{xx}^B \varphi_{edge,n}^2 \, dr \tag{5.50}$$

where c_{yy}^B and c_{xx}^B are the local aerodynamic damping coefficients in the flap-wise and edge-wise directions respectively, as computed in the previous section.

5.2.2.3 Modal structural damping Flap-wise and edge-wise directions

The modal structural damping coefficient for the mode number *n* can be obtained by the expressions:

$$c_{flap,n-\,struct} = \zeta_{flap,n} \frac{(EI)_{flap,n}}{\pi f_{flap,n}} \tag{5.51}$$

$$c_{edge,n-\,struct} = \zeta_{edge,n} \frac{(EI)_{edge,n}}{\pi f_{edge,n}} \tag{5.52}$$

where:

$\zeta_{flap,n}$ is the damping ratio for the mode number n in the flap-wise direction,

$(EI)_{flap,n}$represents the modal stiffness for the mode n, defined as:

$$(\mathrm{EI})_{flap,n} = \int_{R_{hub}}^{R} EI(r)\left(\frac{d^2\varphi_{flap,n}}{d\eta^2}\frac{1}{(R-R_{hub})^2}\right)^2 dr\,,\ \ \eta = \frac{r}{R-R_{hub}} \tag{5.53}$$

and

$$f_{flap,n} = \frac{1}{2\pi}\sqrt{\frac{(\mathrm{EI})_{flap,n}}{m_{flap,n}}} \tag{5.54}$$

where:

$$m_{flap,n} = \int_{R_{hub}}^{R} \mu(r)\varphi^2 dr \tag{5.55}$$

with $\mu(r)$ which is the mass per unit length;

Analogous relations are valid for the edge-wise direction:

$\zeta_{edge,n}$ is the damping ratio for the mode number n in the edge-wise direction,

$$(\mathrm{EI})_{edge,n} = \int_{R_{hub}}^{R} EI(r)\left(\frac{d^2\varphi_{edge,n}}{d\eta^2}\frac{1}{(R-R_{hub})^2}\right)^2 dr\,,\ \ \eta = \frac{r}{R-R_{hub}} \tag{5.56}$$

and

$$f_{edge,n} = \frac{1}{2\pi}\sqrt{\frac{(\mathrm{EI})_{edge,n}}{m_{edge,n}}} \tag{5.57}$$

5.2.2.4 Simplified modal aerodynamic damping coefficient

In this work a simplified expression of the modal aerodynamic damping coefficient has been used during the preliminary design, as an index of the damping of the blade and, thus, of the amplitude of eventual stall induced vibrations.
First of all, the modal aerodynamic damping coefficient has been evaluated for both the flap-wise and edge-wise directions only for the first mode, thus the actual expressions are:

$$c_{flap,1} = \int_{R_{hub}}^{R} c_{yy}^{B} \varphi_{flap,1}^{2}\, dr \tag{5.58}$$

$$c_{edge,1} = \int_{R_{hub}}^{R} c_{xx}^{B} \varphi_{edge,1}^{2}\, dr \tag{5.59}$$

In addition, a mean wind speed value has been used to evaluate local aerodynamic damping coefficients, instead of the unsteady value of wind speed.
With this last assumption it is possible to evaluate a sort of mean value of the modal damping coefficient at each wind speed, making use of the only steady aerodynamic coefficients of the airfoils along the blade, which are parameters that can be known in a preliminary design phase.
This way, it is possible, already in an early phase of the design process, to have indications regarding the occurrence and amplitude of stall induced vibrations, without the need of any aeroelastic analysis.

5.2.2.5 Concluding considerations

From the expression of the local damping coefficient in the out-of-plane direction (that usually is very close to the flap - wise direction), it is possible to notice that a gentle stall of the airfoils along the blade (that means a low value of the absolute value $\left|\frac{dCl}{d\alpha}\right|$ beyond the stall) would be desirable to avoid the occurrence of stall induced vibrations.
The expression of modal damping coefficients (both in edge-wise and in flap-wise directions) furnishes another useful information for the optimization process.
For each direction and for each mode, the modal aerodynamic damping coefficient can be interpreted as a linear combination of the local damping coefficients of the different sections along the blade, each one multiplied by the local displacement related to the mode shape.

Looking at typical modes shapes of a wind turbine blade in the next figures , which can be considered essentially behaving as a cantilevered beam, it can be observed that the highest displacements always occur on the outer part of the blade.
This means that the highest contribution to the damping of the blade is given by the outer sections.
Thus, the blade optimization to avoid stall induced vibrations can be limited at this part of the blade.

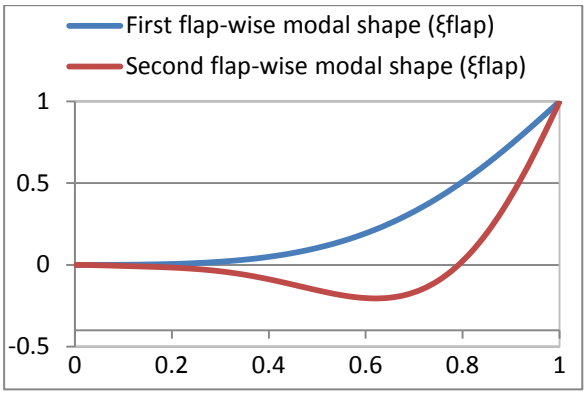

Figure 5.15: Flap-wise modal shapes (1st,2nd)

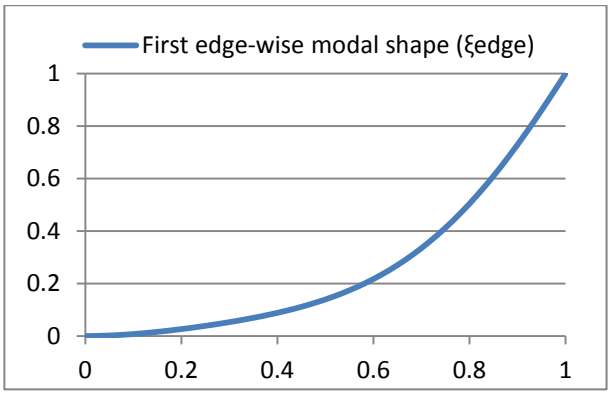

Figure 5.16: Edge-wise modal shape (1st)

5.2.3 Validation of the simplified modal aerodynamic damping coefficient

The simplified modal aerodynamic damping coefficient has been validated with several cases of wind turbines obtained during the optimization process, giving always results coherent with the behaviour of the blades evaluated by FAST_AD. An example is reported hereinafter.
The first case (V00_D) refers to the wind turbine analysed in Section 5.1, while the second one is the same wind turbine, but with different airfoils on the tip part of the blade (it will be presented in detail in Chapter 6).
For both the cases the minimum value on aerodynamic damping is achieved at about 11 m/s, according with the high stall induced vibrations observed in Section 5.1 at thie wind speed.
Furthermore, it can be noticed in the following figures that the lower minimum modal aerodynamic damping coefficient (DC) of the first wind turbine (V00_D) corresponds to an higher amplitude of stall induced vibrations with respect to the second turbine (V00_C).
This behaviour is shown for shaft bending moment, blade root bending moments (edge and flap wise direction) and power in the following figures.

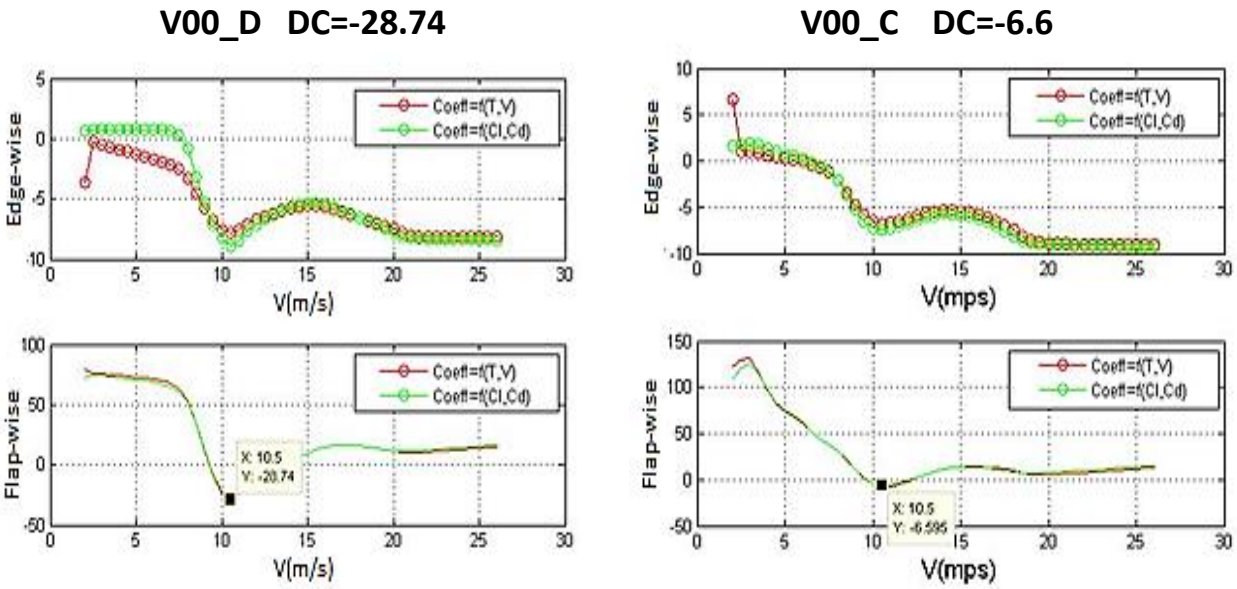

Figure 5.17: Simplified modal damping coefficient and minimum value (DC in the figures)

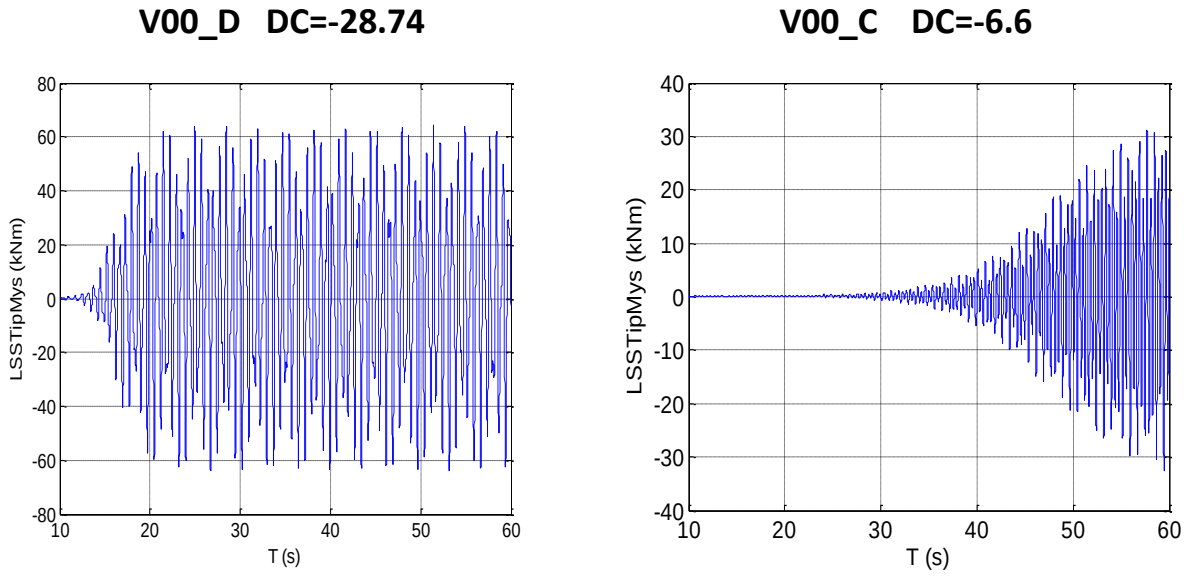

Figure 5.18: Shaft Bending Moment (t)

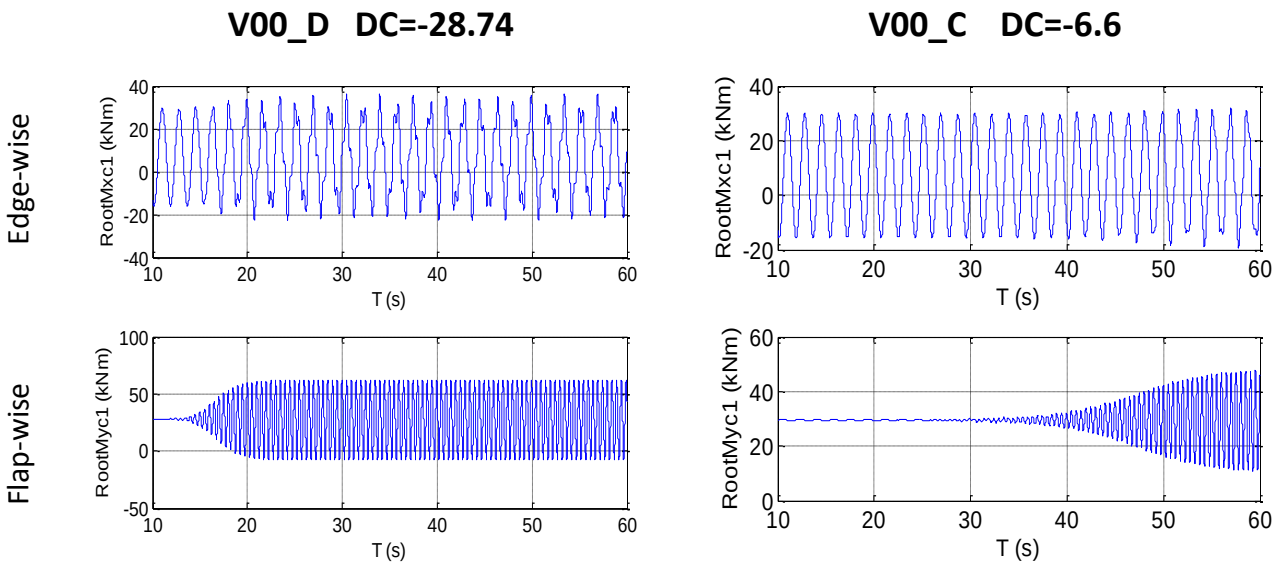

Figure 5.19: Blade Root Bending Moments (t)

(RootMxc1=Edge-wise direction; RootMyc1=Flap-wise direction)

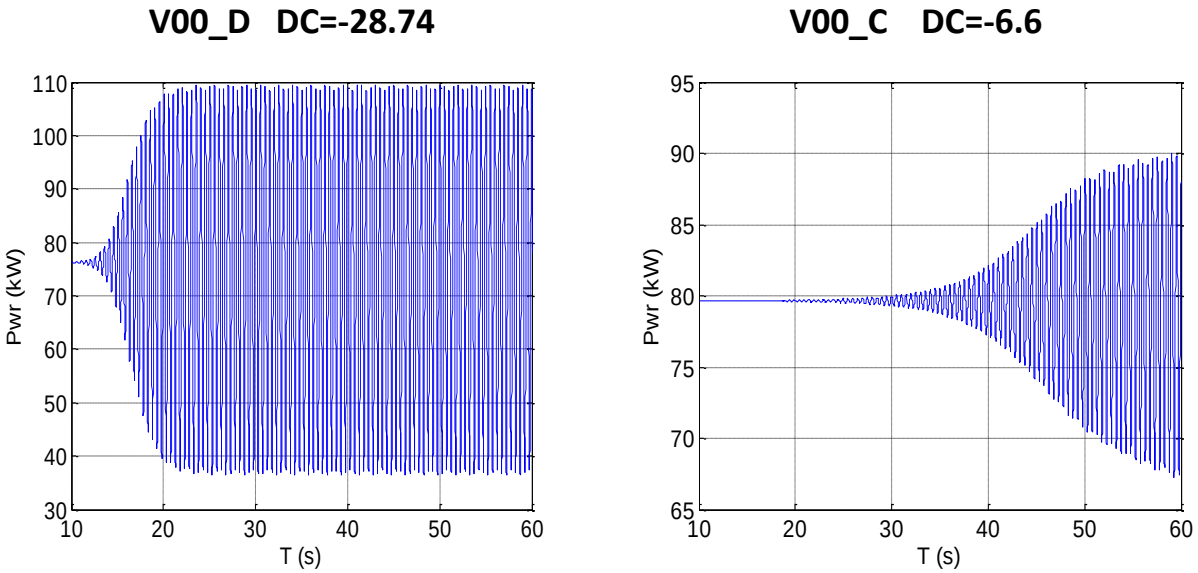

Figure 5.20: Power (t)

5.2.4 Investigation on parameters influencing aerodynamic damping

The following sections show several results of aeroelastic analyses performed to investigate the effect of changing different parameters of the wind turbine.
The wind turbine analysed is the one of the first example reported in this chapter.
The effect of changing tip airfoils, the effect on roughness, and the effect of dynamic stall are reported hereinafter.
The following settings in FAST_AD have been used for all the cases (which are the same imposed in the first example):

- Only the first mode in the flap-wise direction is enabled
- No modes in the edge-wise direction are enabled
- Structural damping (1st flap-wise mode): 0.5 %
- Tower shadow disabled
- Dynamic effects disabled (dynamic stall and dynamic inflow)
- Tilt=0 degrees (Tilt angle is intended as the angle between the rotor plane and a vertical plane)
- Yaw angle =0
- No wind shear
- Steady inflow conditions

5.2.4.1 Effect of tip airfoils

In this section, the effect of varying the slope of the lift curve beyond the stall for the outer airfoils of the blade (70%R-100%R) is analysed.
The first figure reports the analysis of shaft bending moment ('tilt' direction, Mys) in the time domain, for different values of slope of the lift curve beyond the stall. The slope after the maximum lift coefficient has been gradually increased, from zero to the actual value of the original tip airfoil (the airfoil 'D' in Section 5.1).
It can be noticed that significant vibrations already occur for an absolute value of the slope higher than 0.01 deg-1. Such a value of the slope can make the wind turbine design highly complex, since it can reduce the power control, as it will be shown in the next chapter.
Furthermore, vibrations occur for a range of wind speeds, between 11 m/s and 13 m/s, while in the original wind turbine these were significant at approximately one wind speed (11 m/s), that is congruent with the shape of the lift curve of the original airfoil (with a more localized abrupt stall).
To show this effect, and for completeness, analyses of shaft bending moment and root bending moments (flap-wise and edgewise) at both 11 m/s and 13 m/s are also reported.

dCl/dα=
0 deg-1

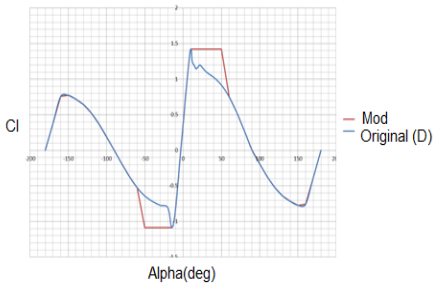

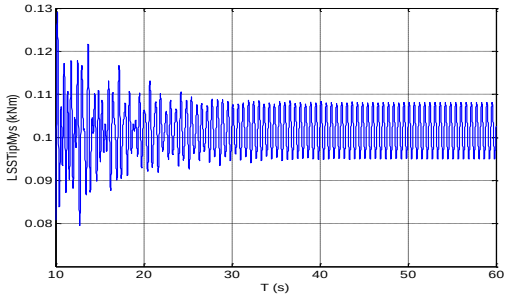

dCl/dα=
-0.005 deg-1

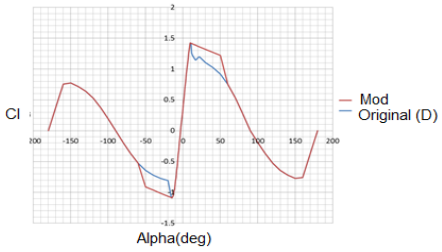

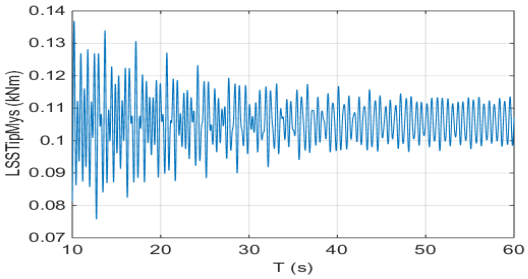

dCl/dα=
-0.015 deg-1

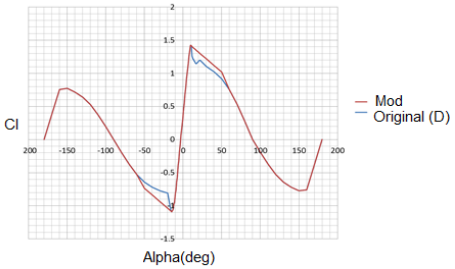

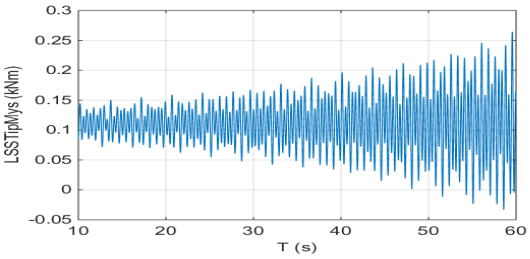

dCl/dα=
-0.01 deg-1

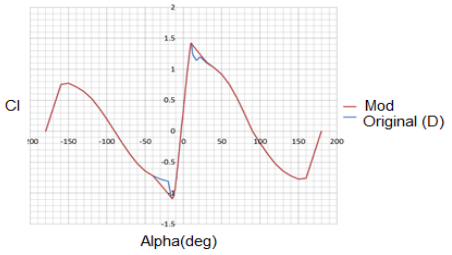

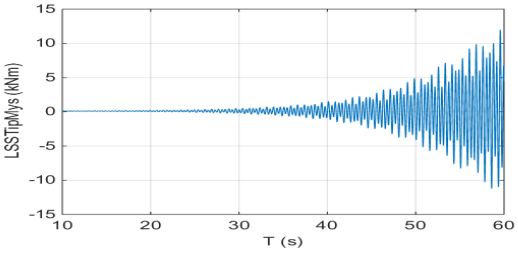

dCl/dα=
-0.02 deg-1

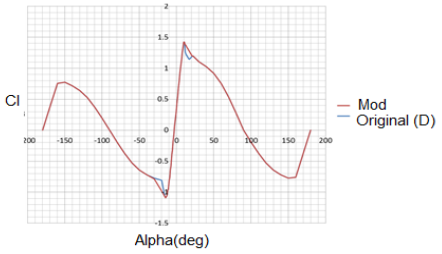

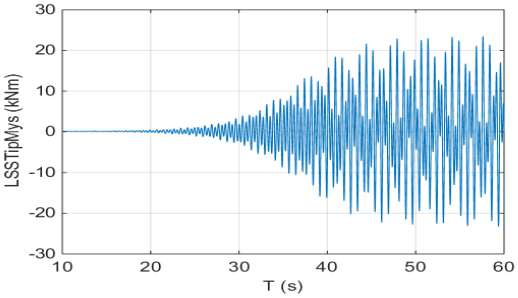

dCl/dα=
-0.025 deg-1

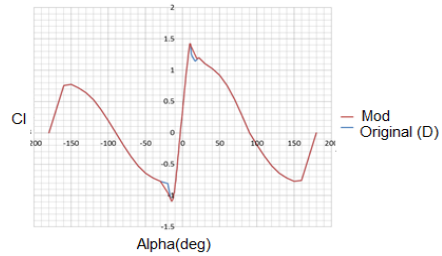

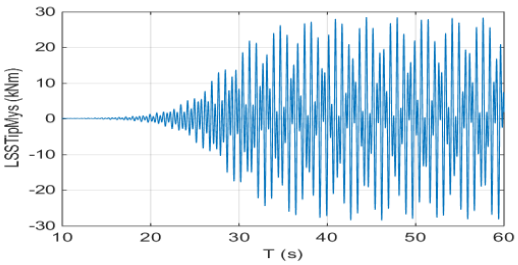

Figure 5.21: Effect of tip airfoils (70-100%R) on shaft bending moment – 11 m/s

Case 1: Post stall dCl/dα= 0 deg-1

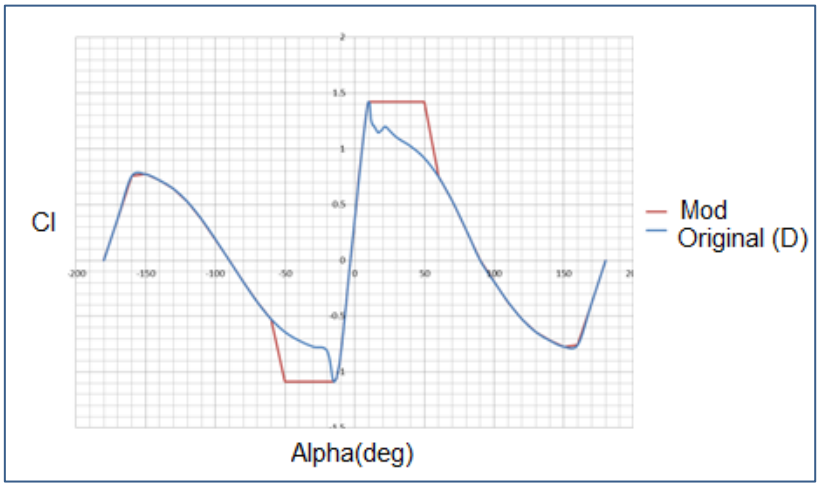

Figure 5.22: (Original airfoil - D) VS (Modified - dCl/dα=0) - Lift curves

11m/s

Original (V00_D)

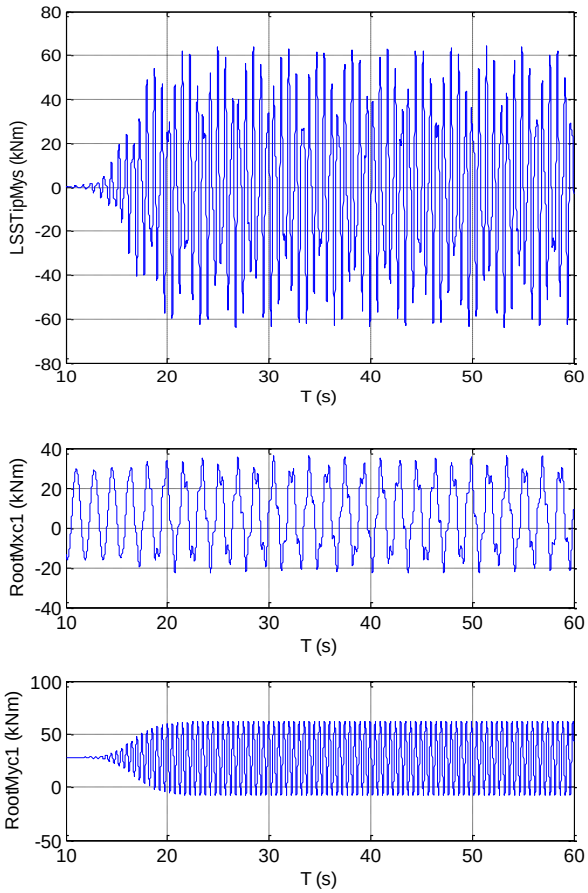

Tip airfoils modified - dCl/dα= 0 deg-1

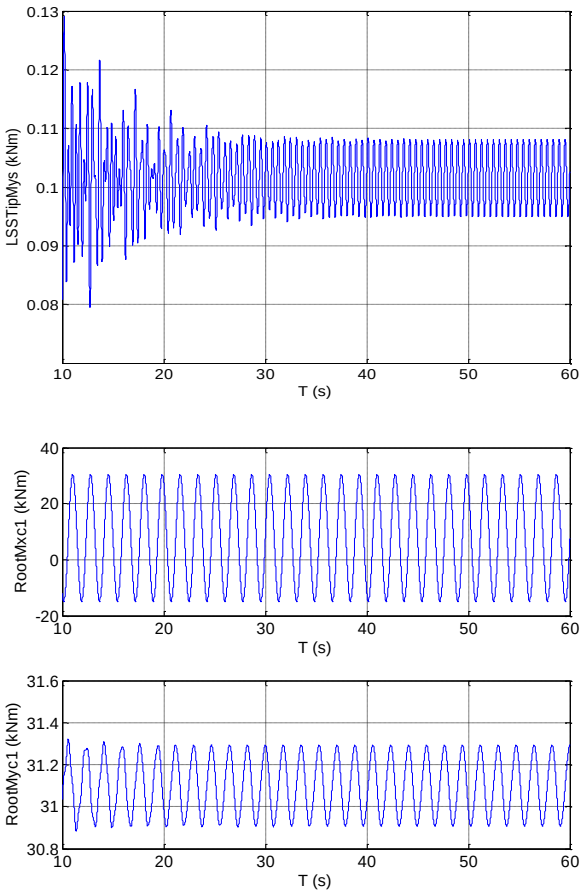

Figure 5.23: (Original airfoil - D) VS (Modified - dCl/dα=0) - Shaft (Mys) and blade root bending moments (Edge-wise (Mxc), Flap-wise (Myc))

V=11 m/s – dCl/dα= 0 deg-1

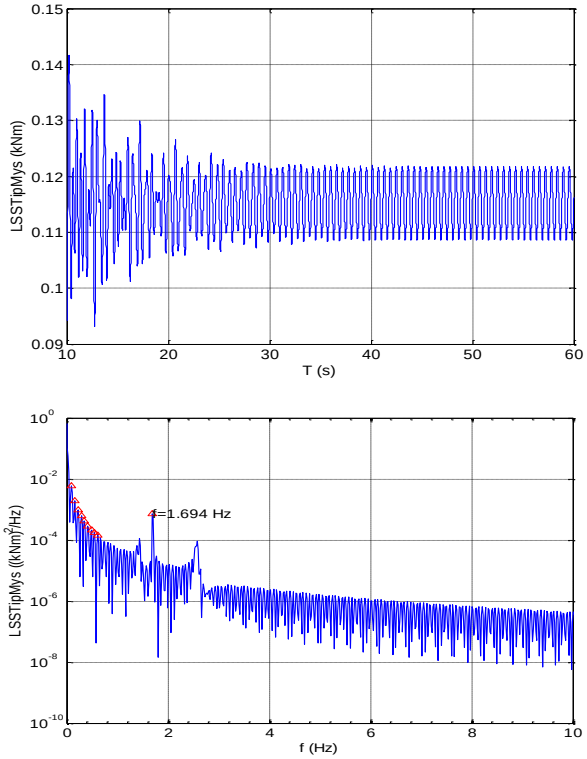

Figure 5.24: Shaft bending moment

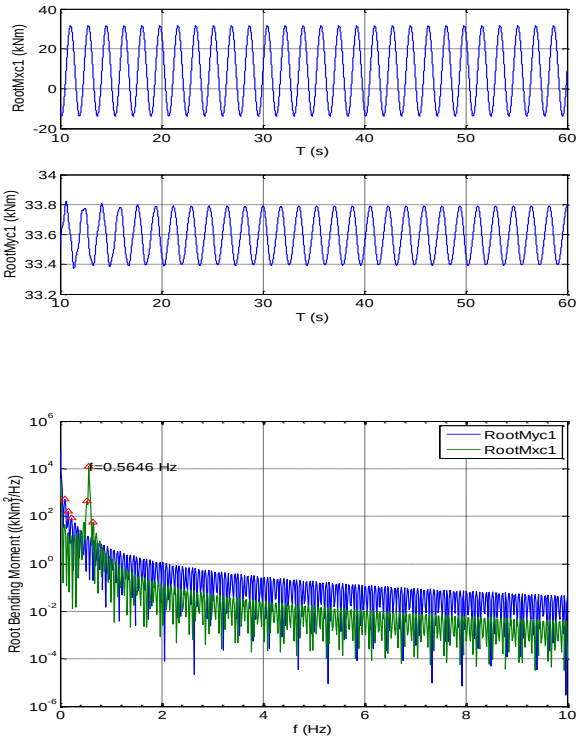

Figure 5.25: Blade root bending moments

V=13 m/s– dCl/dα= 0 deg^{-1}

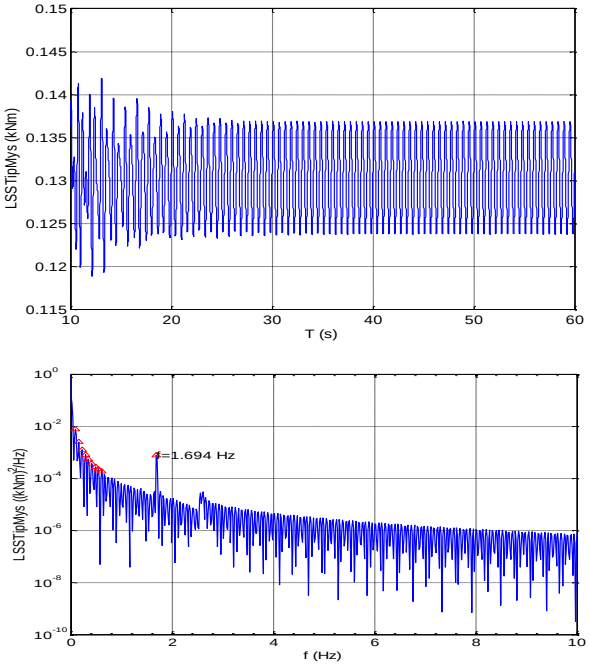

Figure 5.26: Shaft bending moment

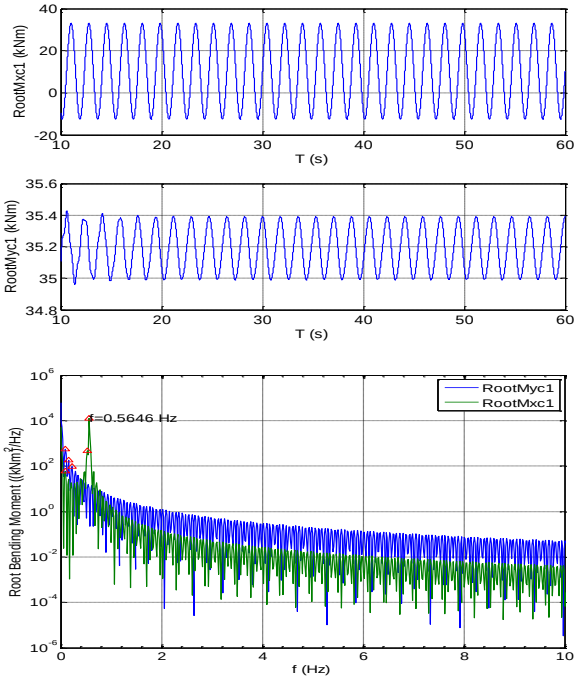

Figure 5.27: Blade root bending moments

Case 2: Post stall dCl/dα= -0.005 deg-1

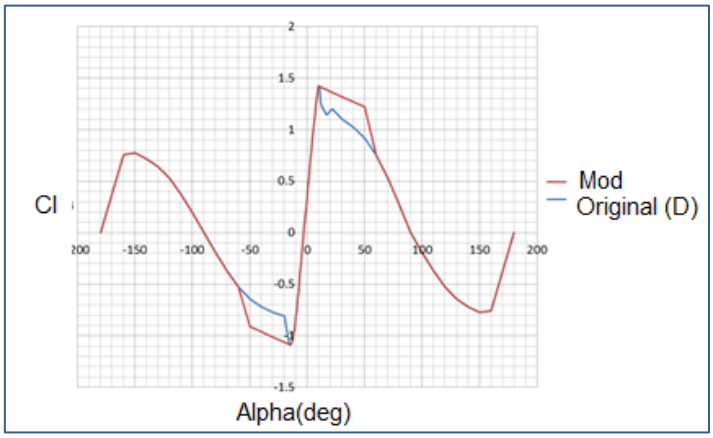

Figure 5.28: (Original airfoil - D) VS (Modified - dCl/dα=-0.005) - Lift curves

V=11 m/s

Original (V00_D)

Tip airfoils modified - dCl/dα= -0.005 deg-1

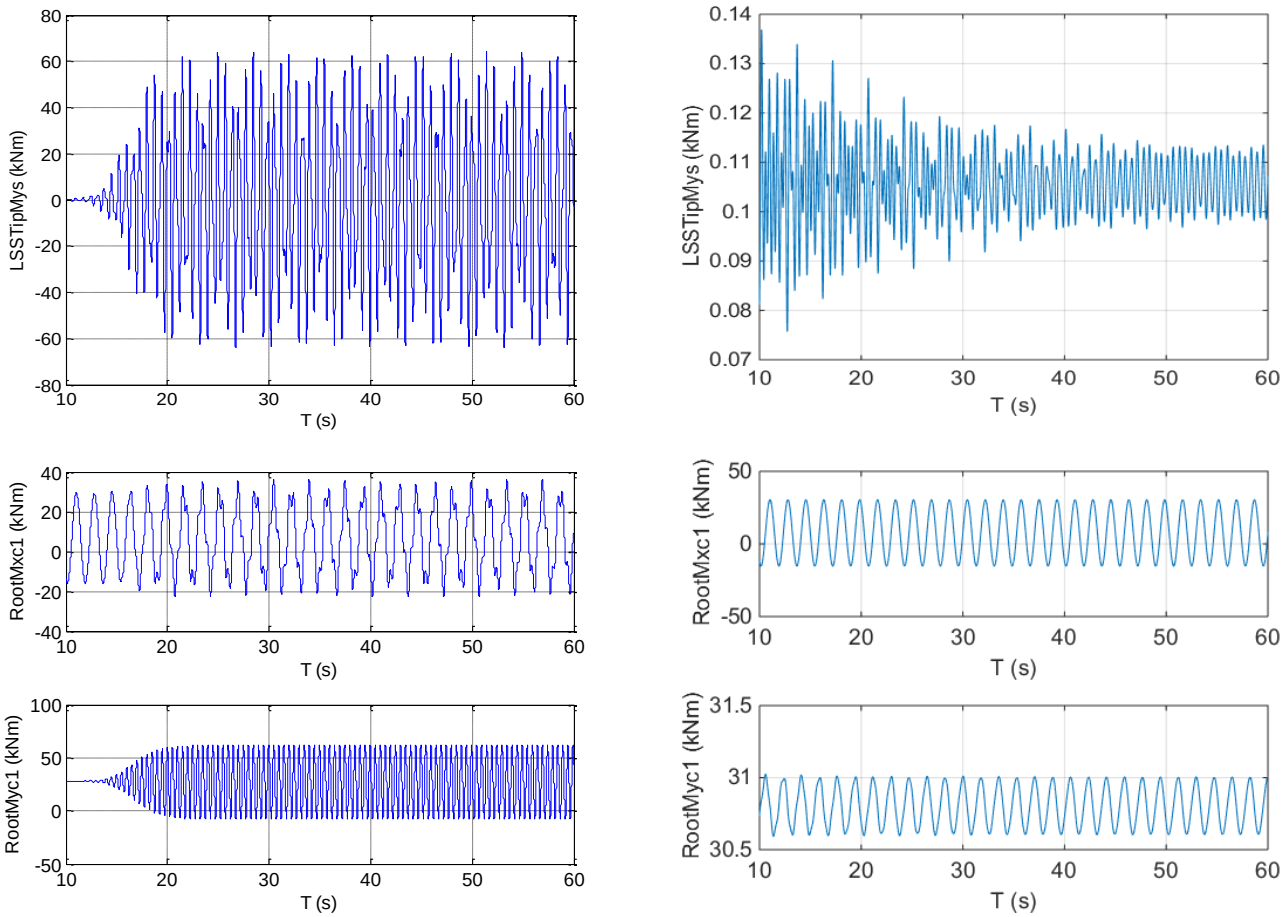

Figure 5.29: (Original airfoil - D) VS (Modified - dCl/dα=-0.005) - Shaft (Mys) and blade root bending moments (Edge-wise (Mxc), Flap-wise (Myc))

V=11 m/s – dCl/dα= = -0.005 deg-1

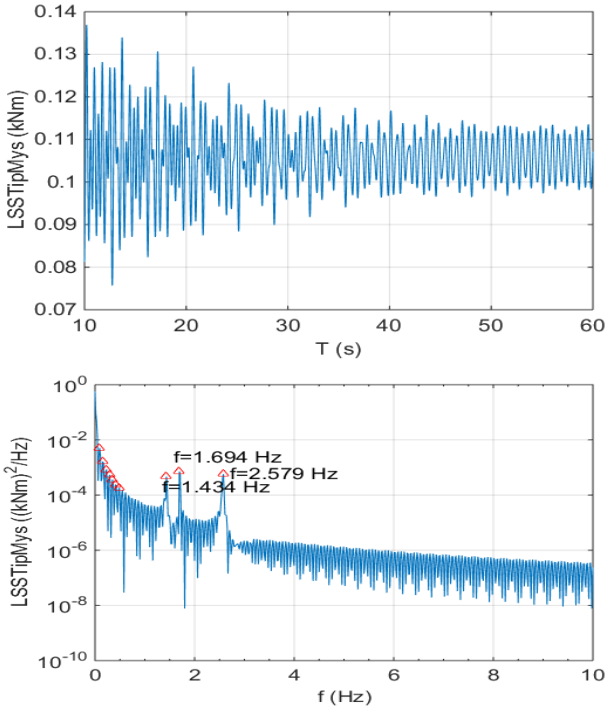

Figure 5.30: Shaft bending moment

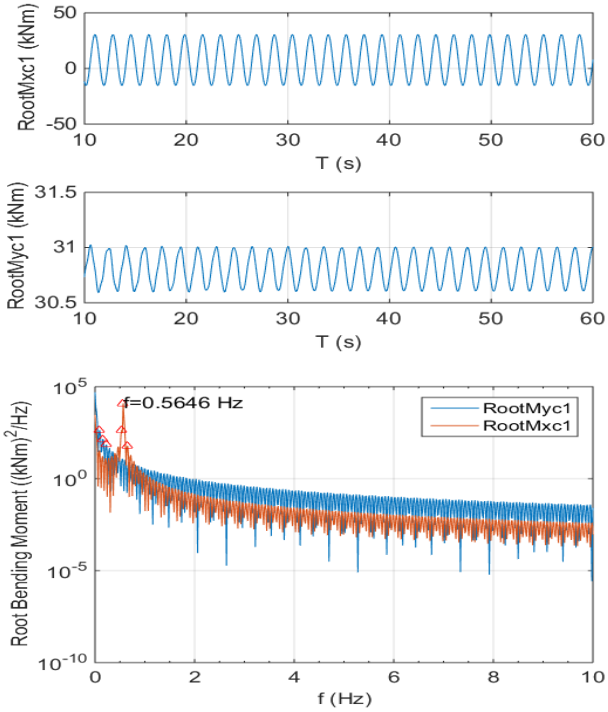

Figure 5.31: Blade root bending moments

V=13 m/s – dCl/dα= = -0.005 deg^{-1}

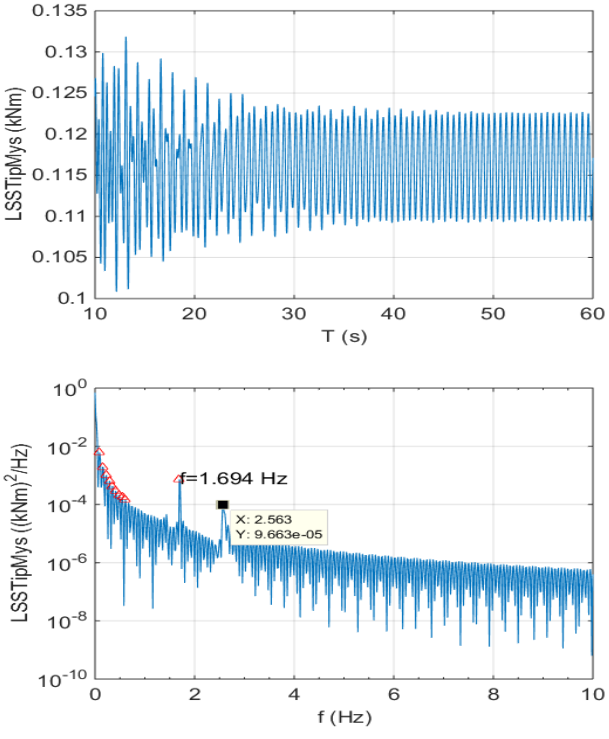

Figure 5.32:Shaft bending moments

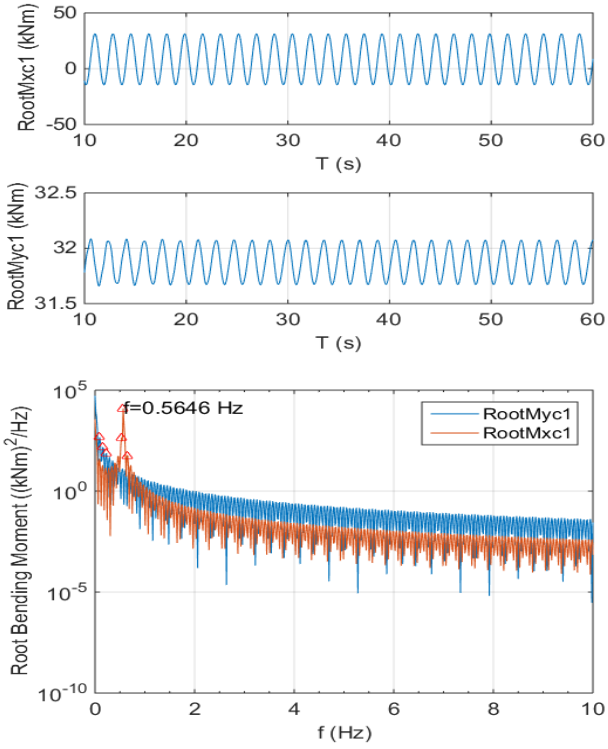

Figure 5.33: Blade root bending moments

Case 3: Post stall dCl/dα= -0.01 deg-1

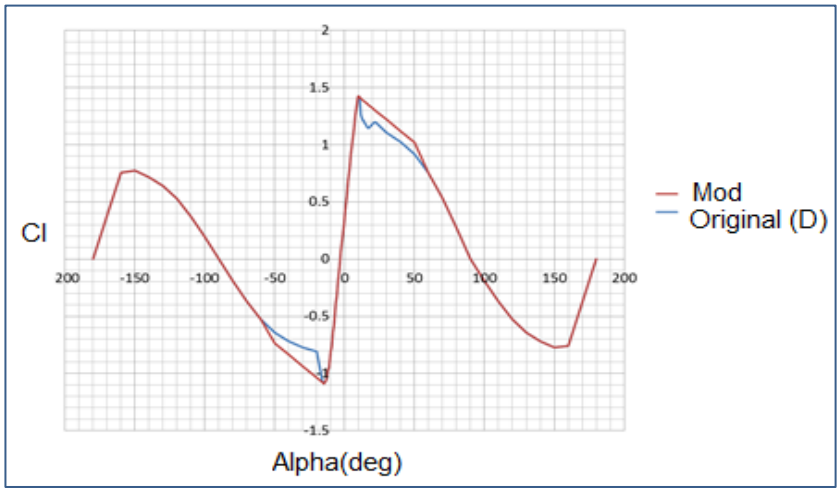

Figure 5.34: (Original airfoil - D) VS (Modified - dCl/dα=-0.01) - Lift curves

V=11 m/s

Original (V00_D)

Tip airfoils modified - dCl/dα= -0.01 deg-1

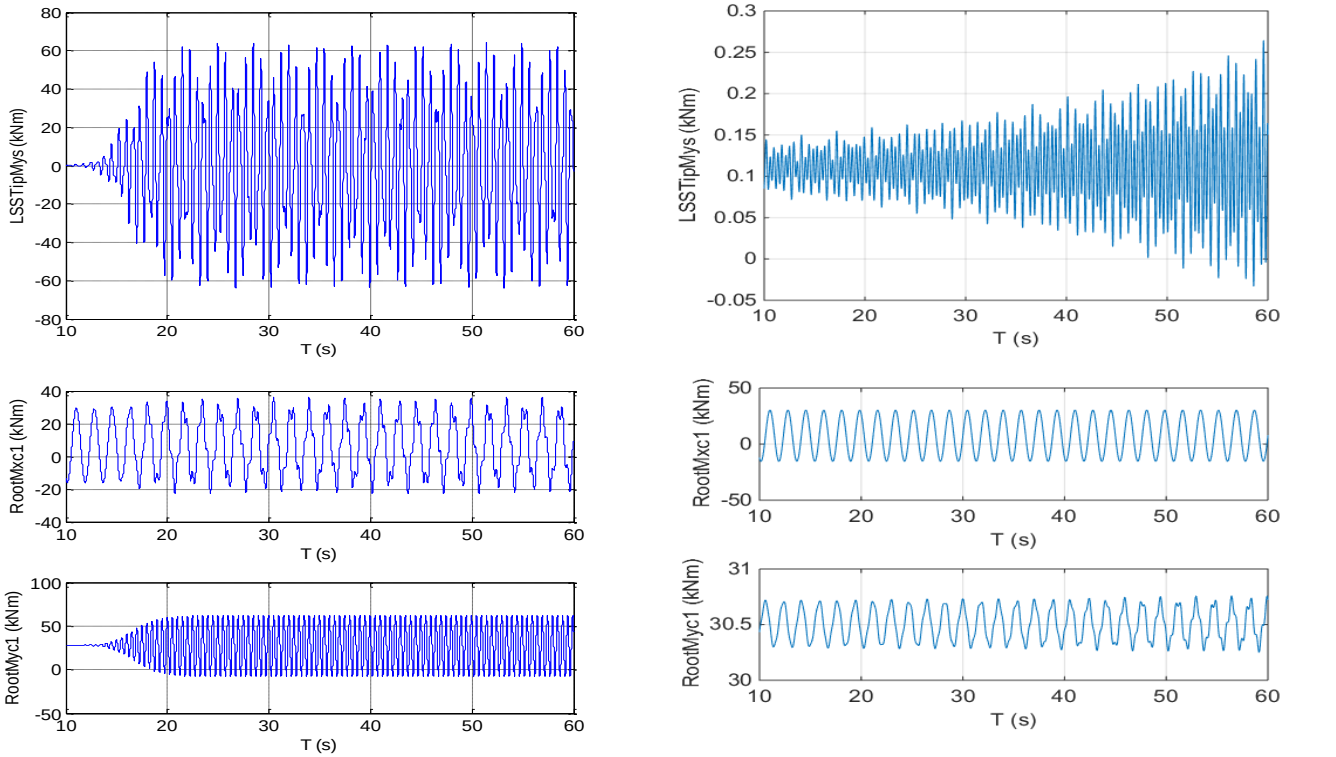

Figure 5.35: (Original airfoil - D) VS (Modified - dCl/dα=-0.01) - Shaft (Mys) and blade root bending moments (Edge-wise (Mxc), Flap-wise (Myc))

V=11 m/s – dCl/dα= = -0.01 deg-1

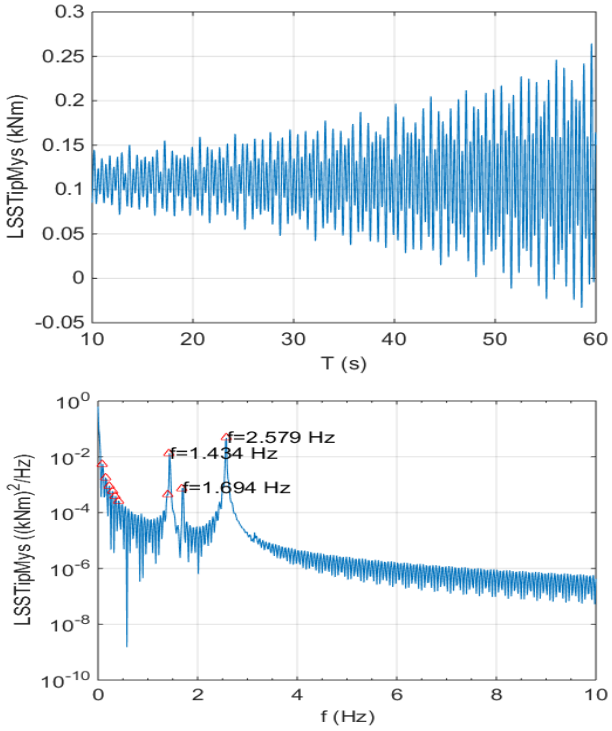

Figure 5.36: Shaft bending moment

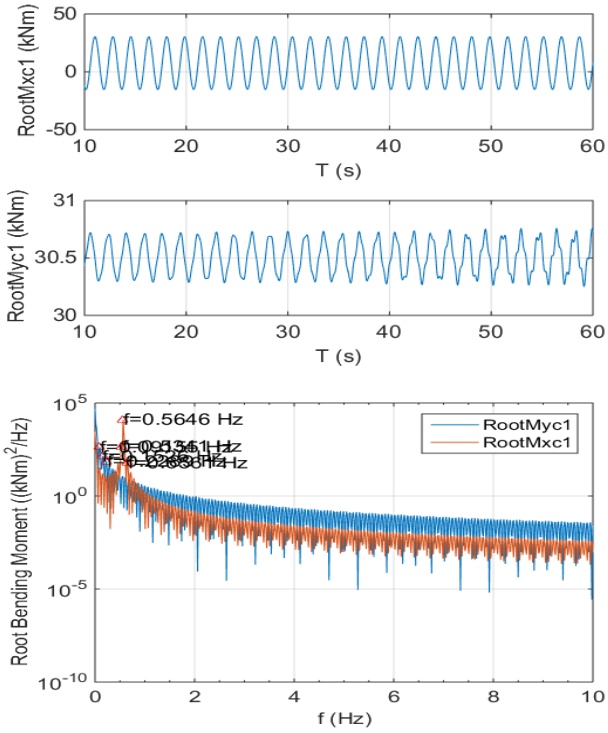

Figure 5.37: Blade root bending moments

V=13 m/s – dCl/dα= = -0.01 deg^{-1}

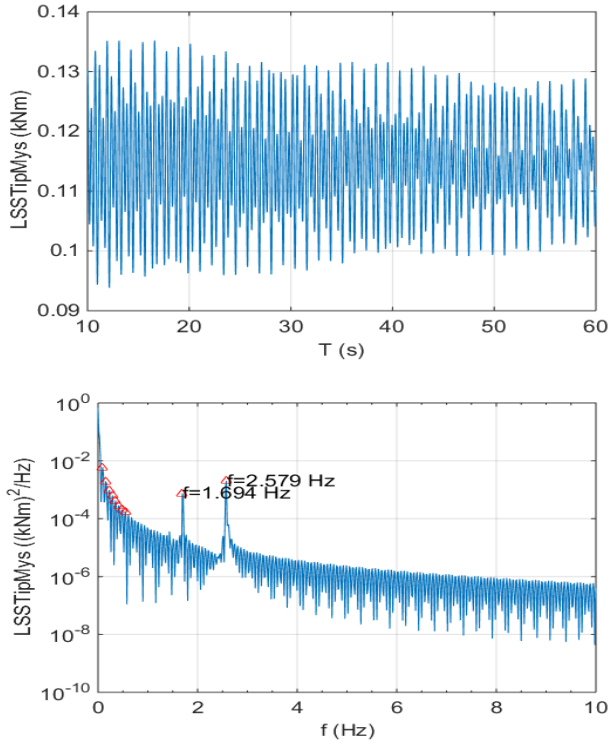

Figure 5.38: Shaft bending moment

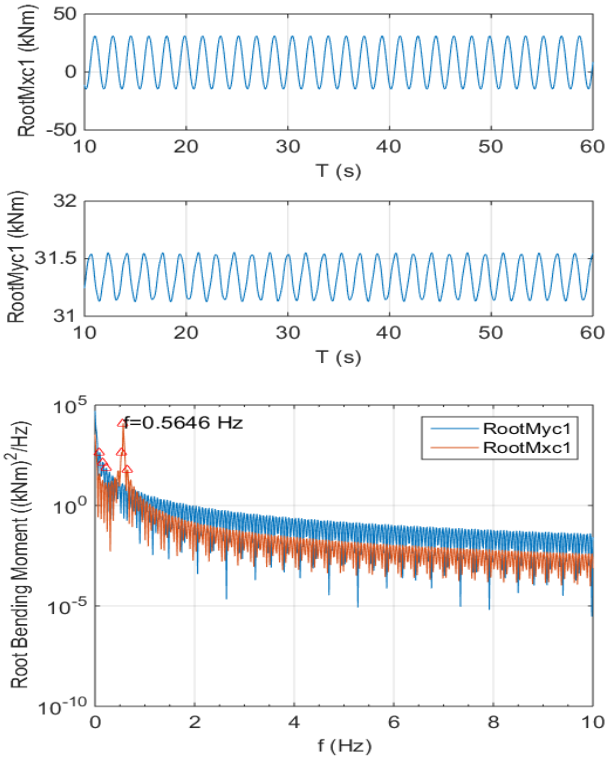

Figure 5.39: Blade root bending moments

Case 4: Post stall dCl/dα= -0.015 deg^{-1}

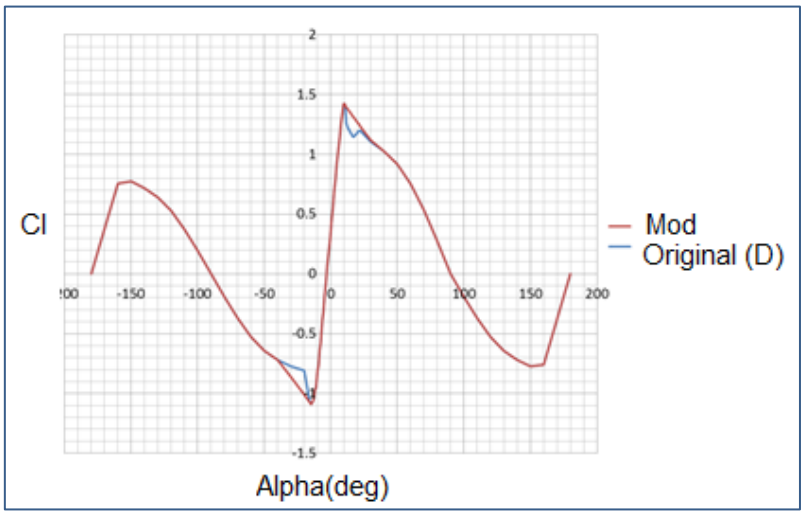

Figure 5.40: (Original airfoil - D) VS (Modified - dCl/dα=-0.015) - Lift curves

11 m/s

Original (V00_D)

Tip airfoils modified - dCl/dα= -0.015 deg^{-1}

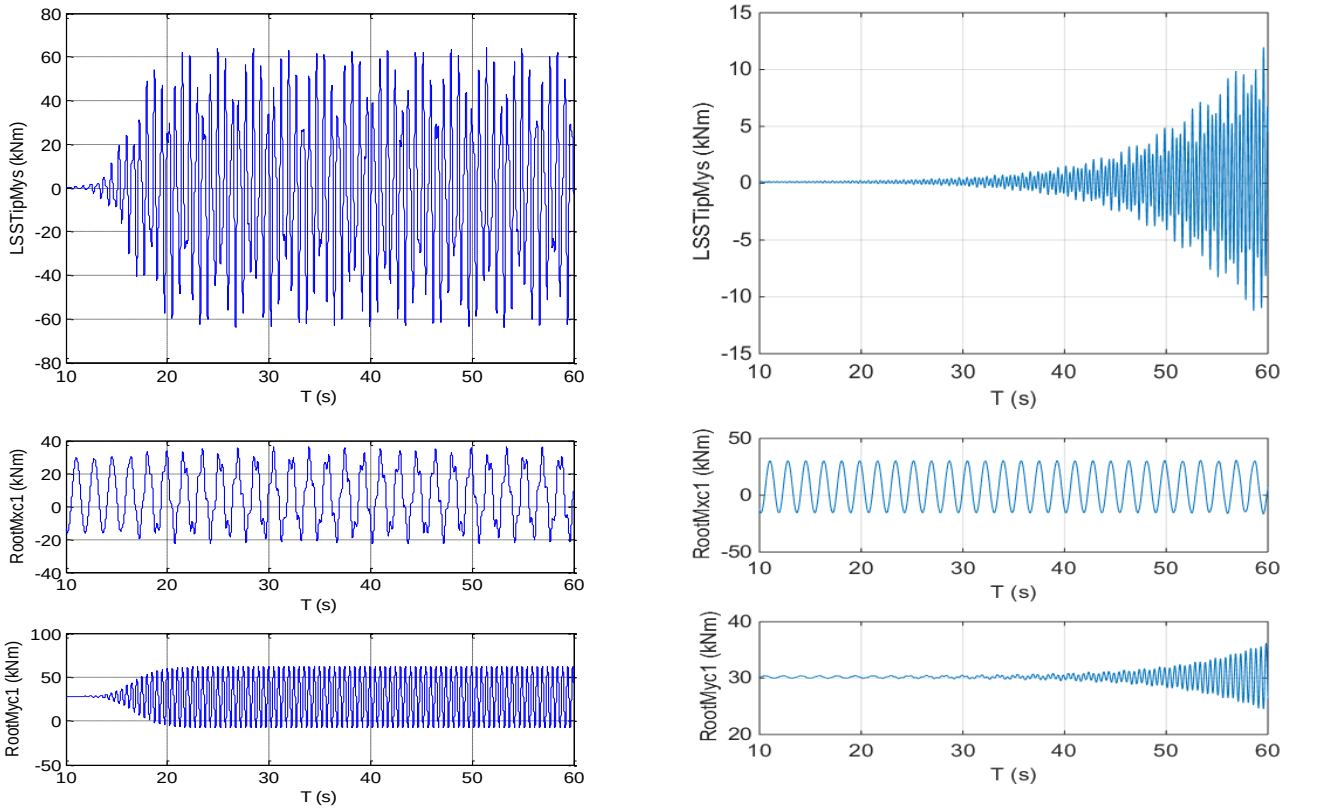

Figure 5.41: (Original airfoil - D) VS (Modified - dCl/dα=-0.015) - Shaft (Mys) and blade root bending moments (Edge-wise (Mxc), Flap-wise (Myc))

11 m/s– dCl/dα= = -0.015 deg^{-1}

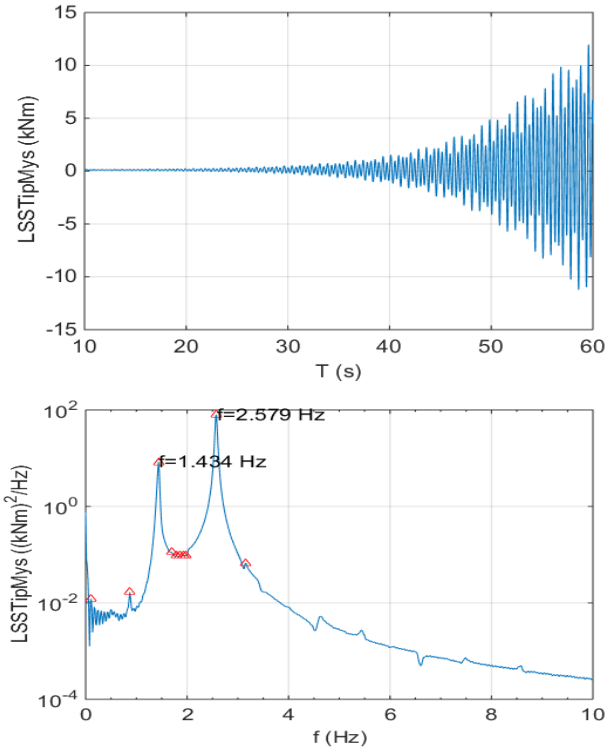

Figure 5.42: Shaft bending moment

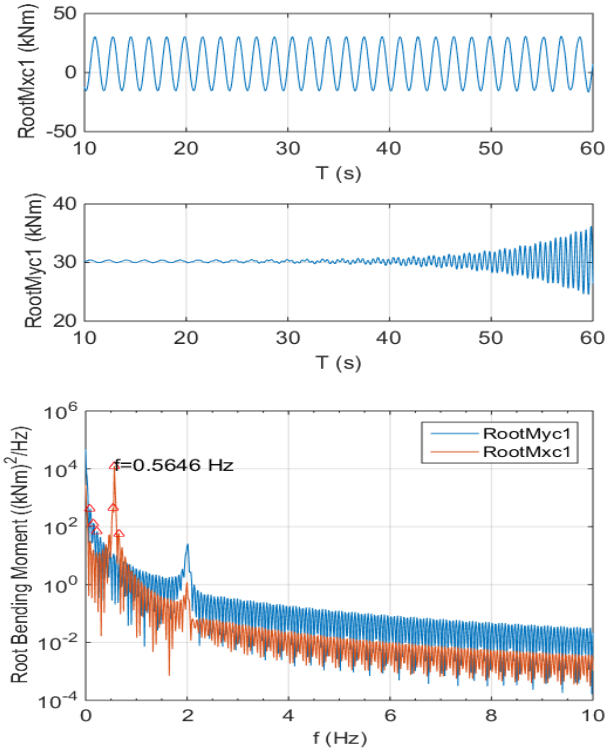

Figure 5.43: Blade root bending moments

13 m/s– dCl/dα= = -0.015 deg^{-1}

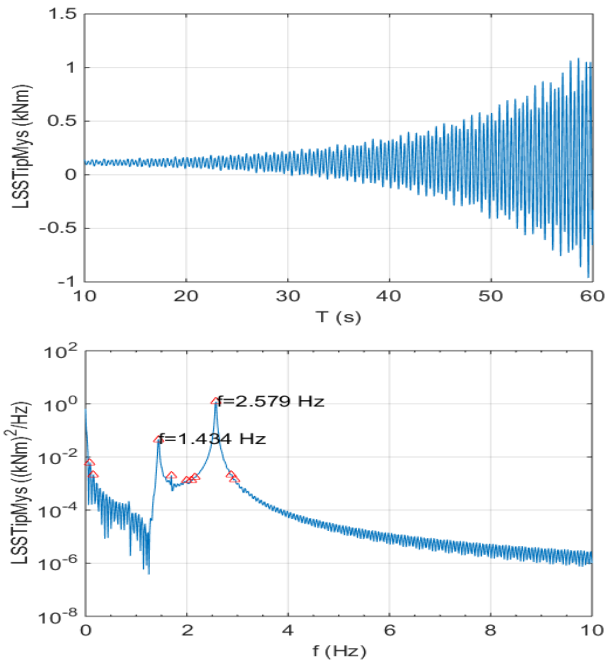

Figure 5.44: Shaft bending moment

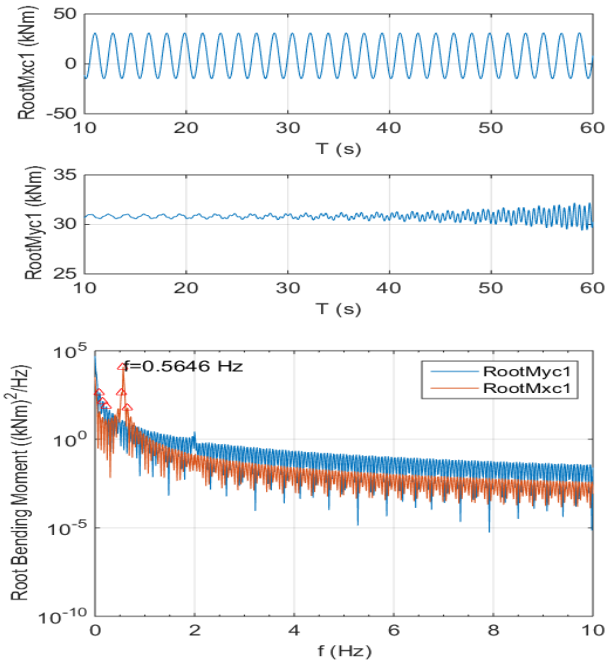

Figure 5.45: Blade root bending moments

Case 5: Post stall dCl/dα= -0.02 deg-1

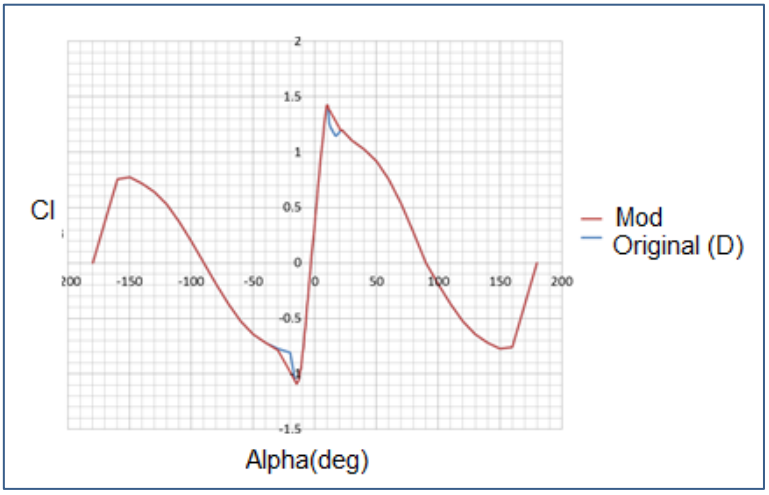

Figure 5.46: (Original airfoil - D) VS (Modified - dCl/dα=-0.02) - Lift curves

11 m/s

Original (V00_D)

Tip airfoils modified - dCl/dα= -0.02 deg-1

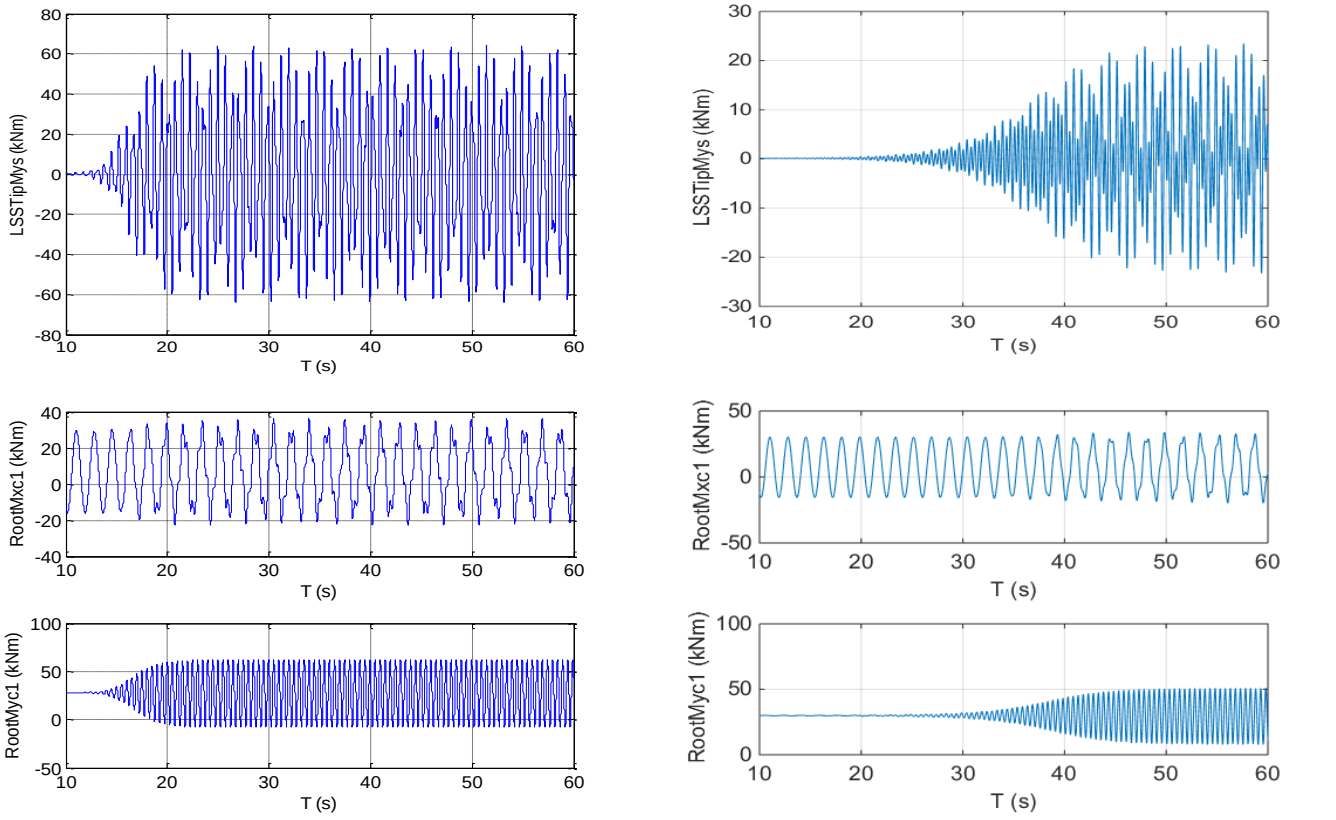

Figure 5.47: (Original airfoil - D) VS (Modified - dCl/dα=-0.02) - Shaft (Mys) and blade root bending moments (Edge-wise (Mxc), Flap-wise (Myc))

11 m/s– dCl/dα= = -0.02 deg^{-1}

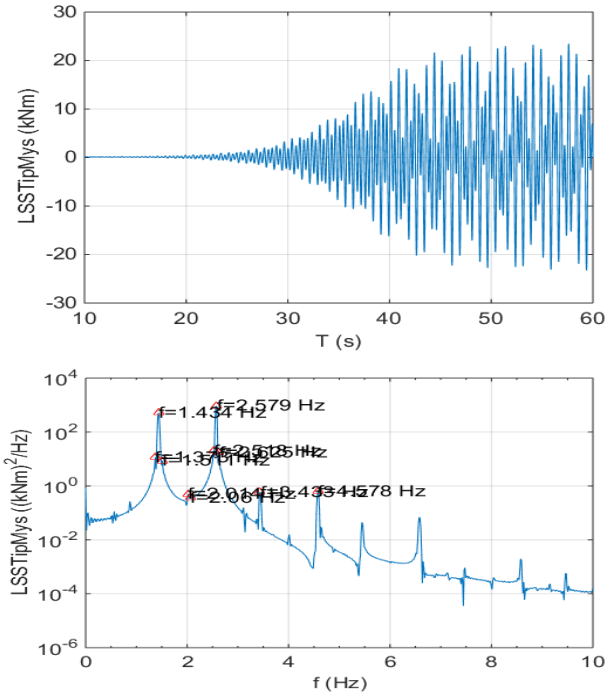

Figure 5.48: Shaft bending moment

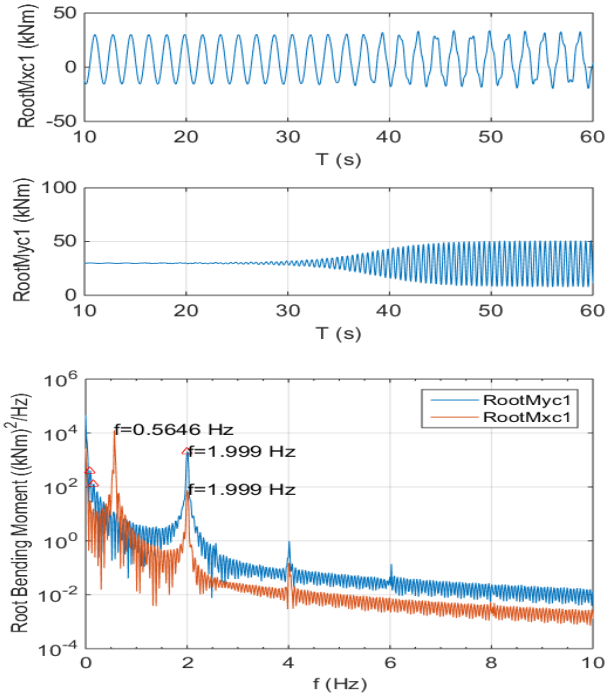

Figure 5.49: Blade root bending moments

13 m/s– dCl/dα= = -0.02 deg^{-1}

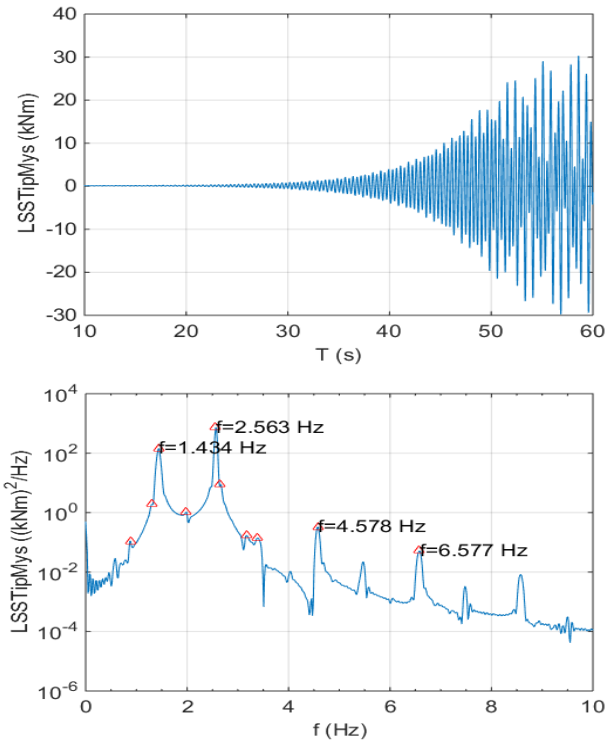

Figure 5.50: Shaft bending moment

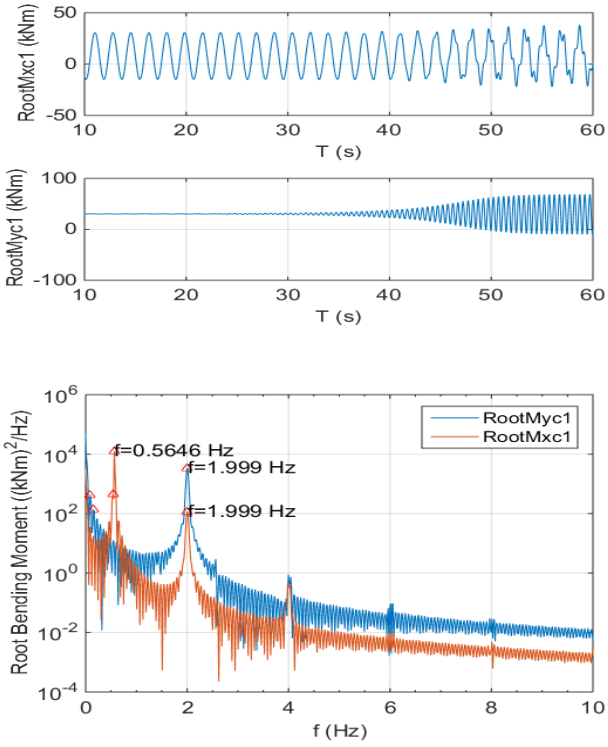

Figure 5.51: Blade root bending moments

Case 6: Post stall dCl/dα= -0.025 deg^{-1}

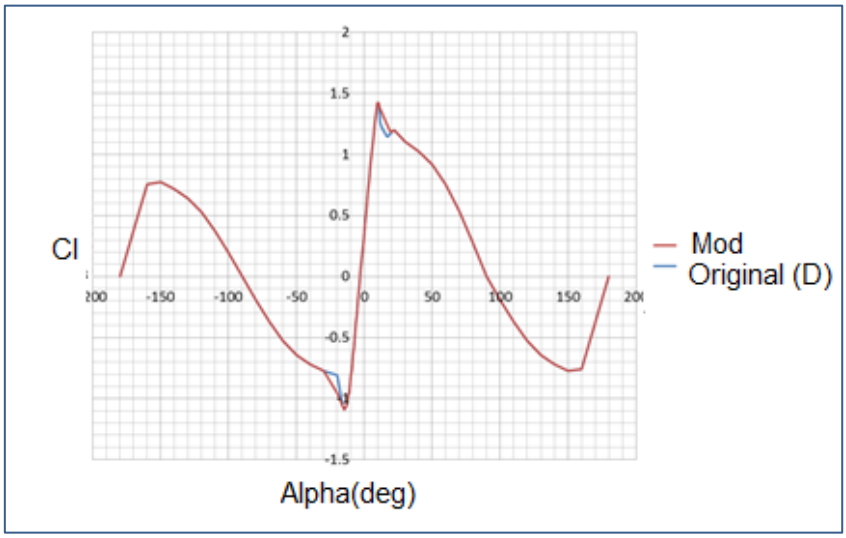

Figure 5.52: (Original airfoil - D) VS (Modified - dCl/dα=-0.025) - Lift curves

V=11m/s

Original (V00_D)

Tip airfoils modified - dCl/dα= -0.025 deg-1

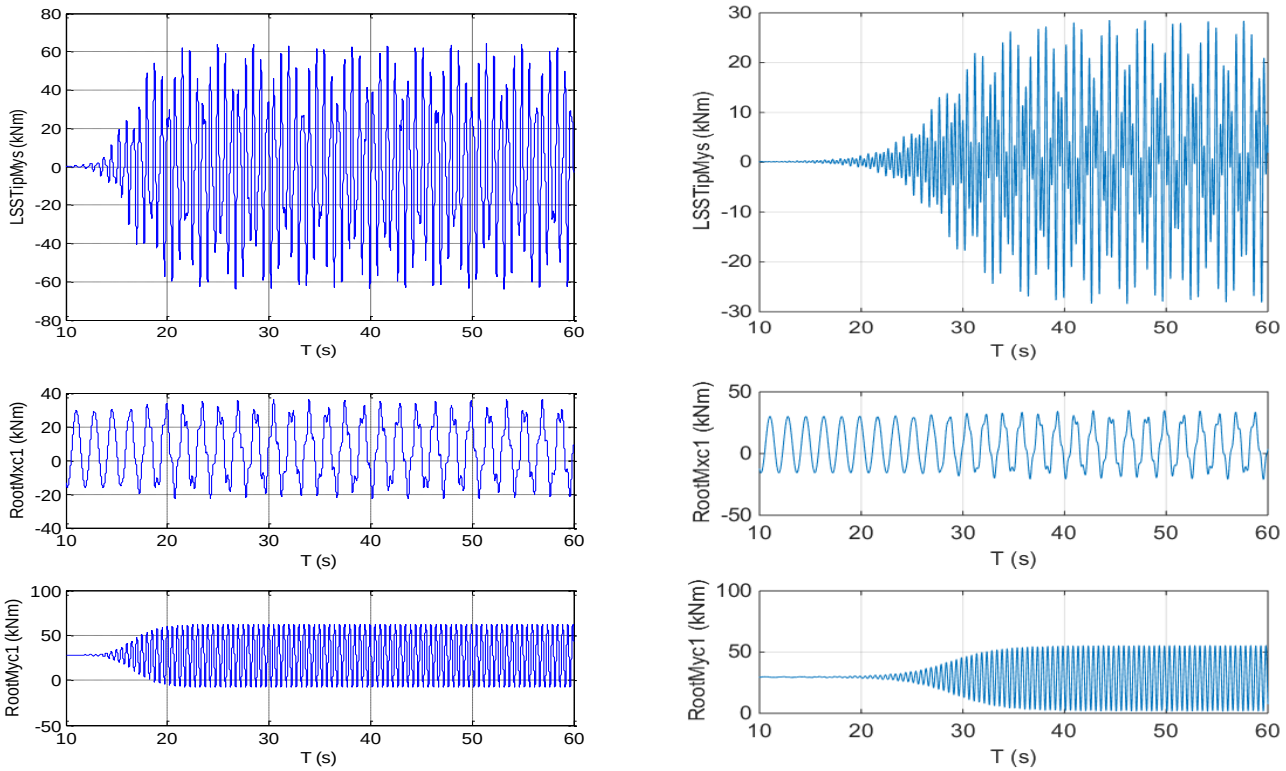

Figure 5.53: (Original airfoil - D) VS (Modified - dCl/dα=-0.025) - Shaft (Mys) and blade root bending moments (Edge-wise (Mxc), Flap-wise (Myc))

11 m/s– dCl/dα= = -0.025 deg^{-1}

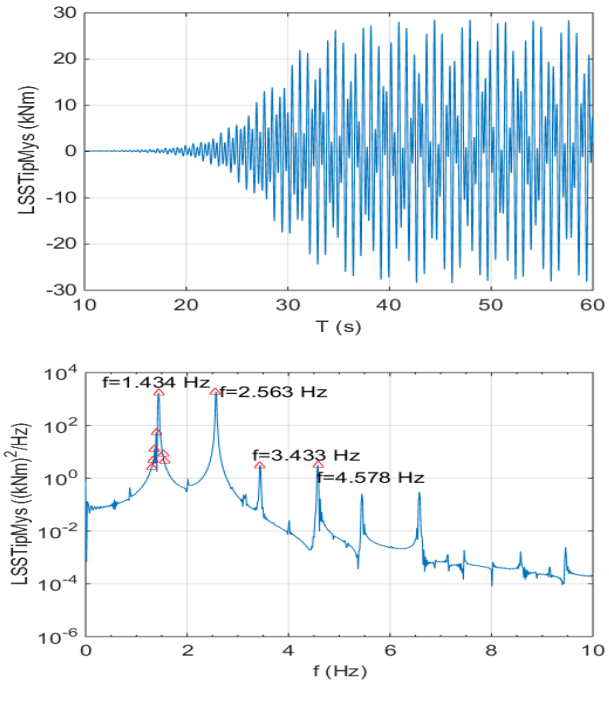

Figure 5.54: Shaft bending moment

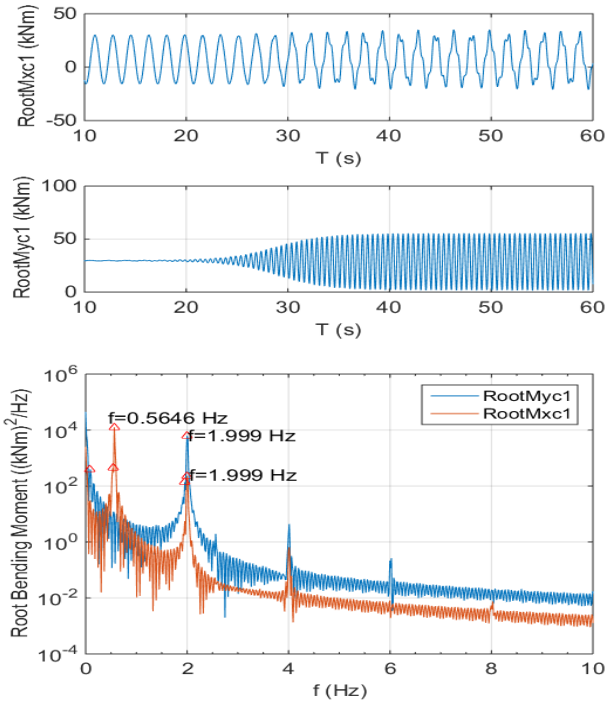

Figure 5.55: Blade root bending moments

13 m/s– dCl/dα= = -0.025 deg^{-1}

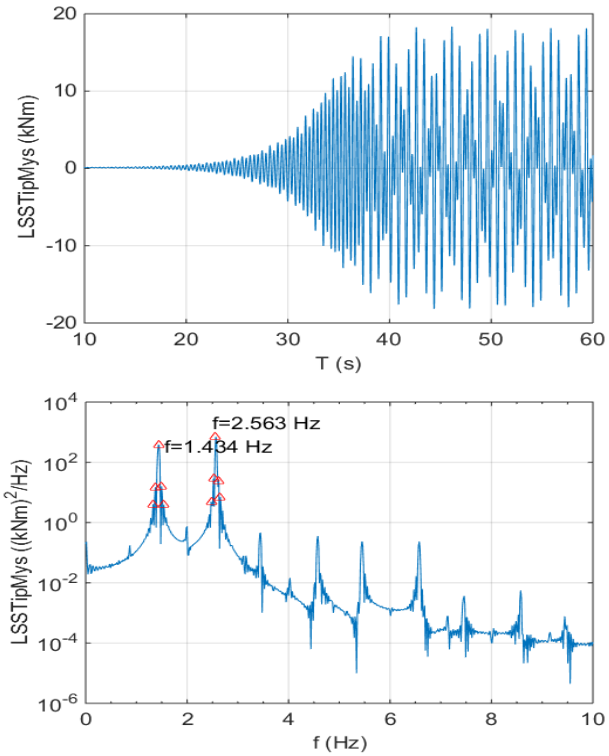

Figure 5.56: Shaft bending moment

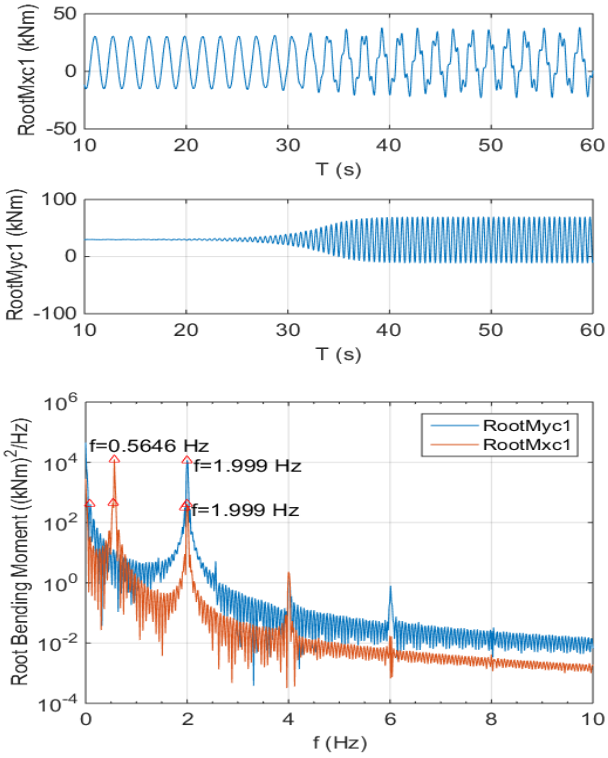

Figure 5.57: Blade root bending moments

5.2.4.2 Effect of structural damping

In the following figure the effect of changing the structural damping is reported.
It can be noticed that even doubling the damping ratio, stall induced vibrations show no sign of decreasing.

11 m/s

Damping ratio=0.5 % **Damping ratio=1.0 %**

Shaft bending moment (t)

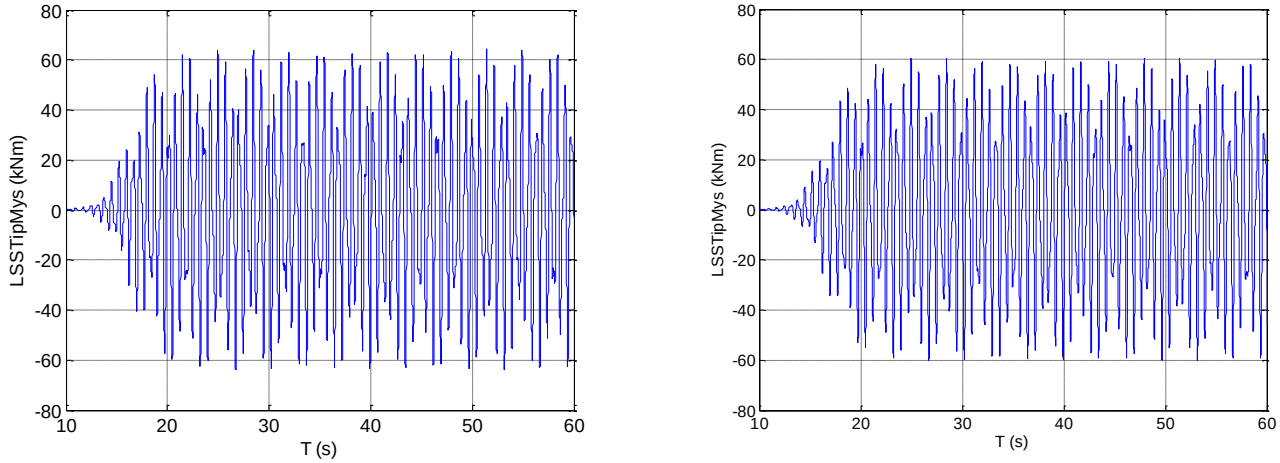

Root bending moments (t) (Edge-wise(Mxc), Flap-wise(Myc))

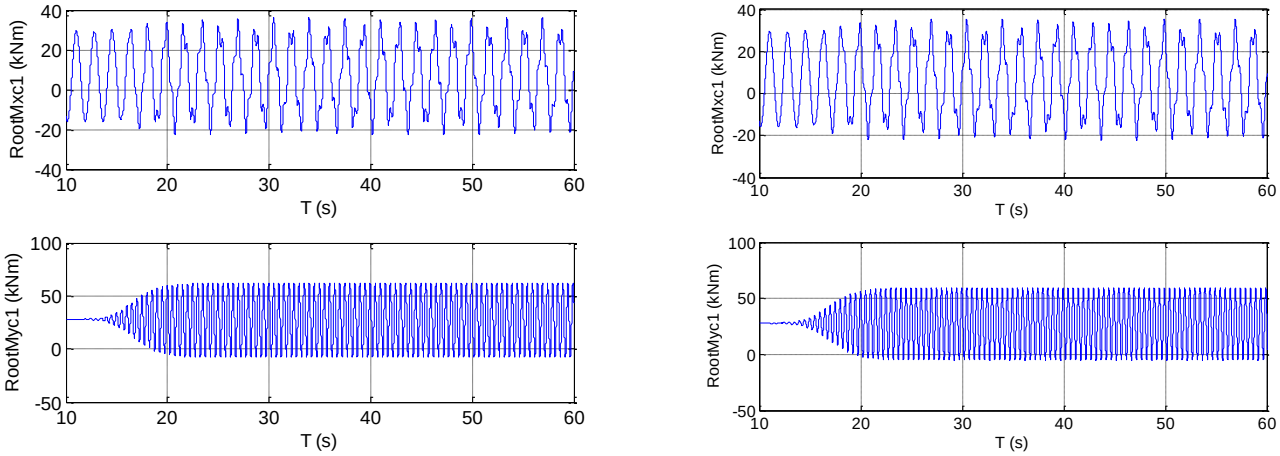

Figure 5.58: Effect of structural damping

5.2.4.3 Effect of structural stiffness

In the following figure the effect of changing the structural damping is reported.
As seen for structural damping, even doubling the stiffness, maximum values of vibration amplitude show no sign of decreasing.

11 m/s

Original **Original*2**

Shaft bending moment (t)

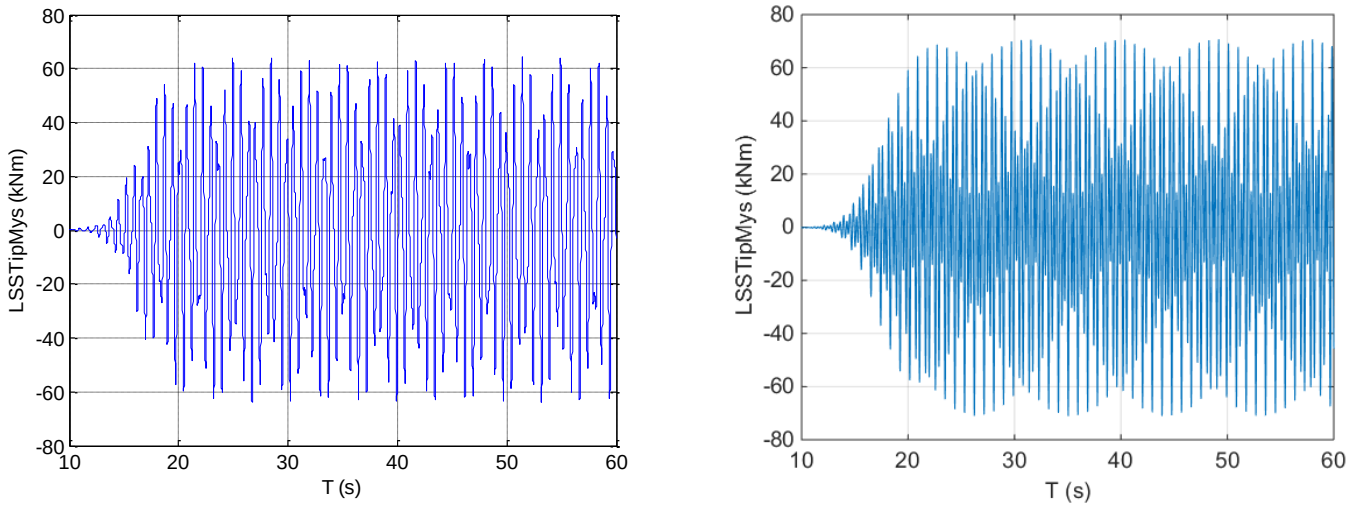

Figure 5.59: Effect of structural stiffness

5.2.4.4 Effect of roughness

In this section, the effect of roughness on the outer airfoils of the blade (65%R-100%R) is investigated. The presence of roughness is simulated in Rfoil by fixing the transition point at 0.01%c on the suction side of the airfoil and at 10%c on the pressure side.
Actually, one of the roughness effects on airfoils aerodynamic performances is the smoothing of the stall, thus roughness has always favourable effects with regard to stall induced vibrations.
For this reason, it is recommended to verify fatigue loads and lifetime of a wind turbine considering airfoils lift curves obtained in clean conditions.
The following figures show shaft bending moment, blade root bending moments and power in the time domain.

V=11 m/s

V00 - C_Clean **V00 - C_Rough**

Shaft bending moment (t)

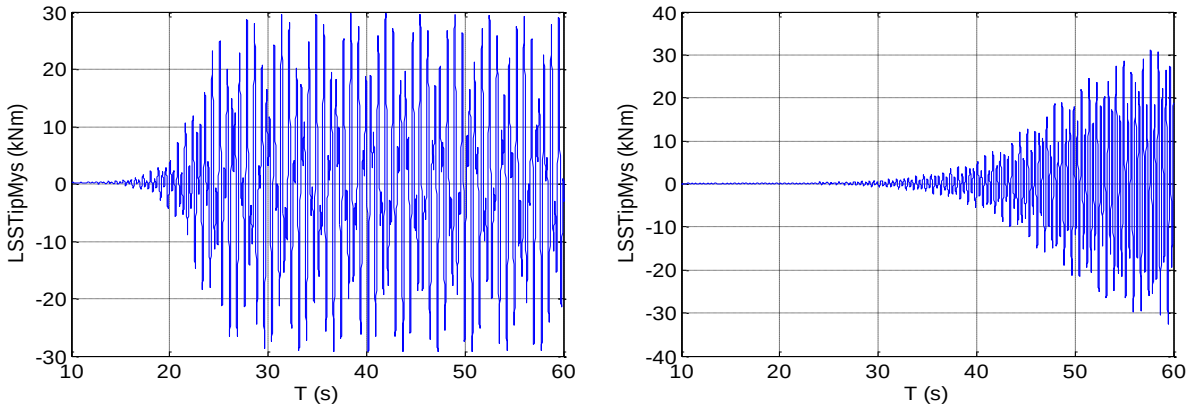

Root bending moments (t) (Edge-wise(Mxc), Flap-wise(Myc))

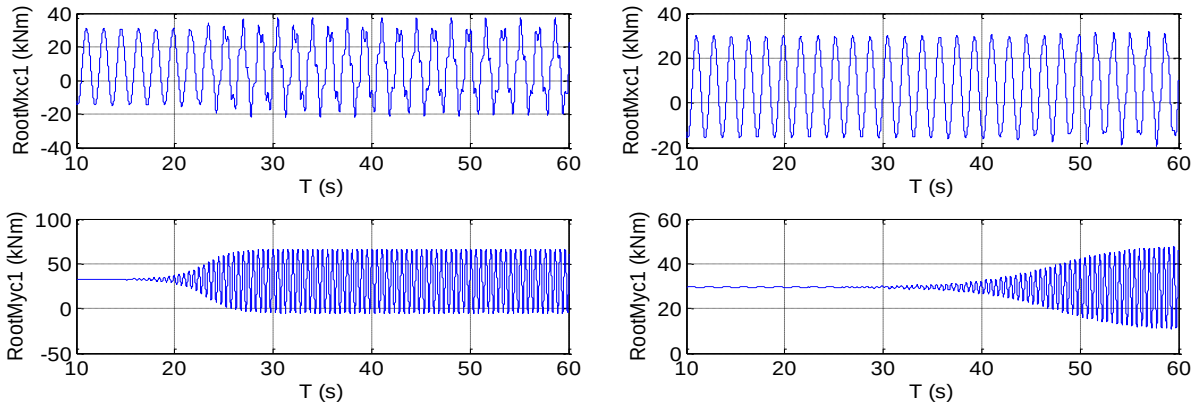

Power (t)

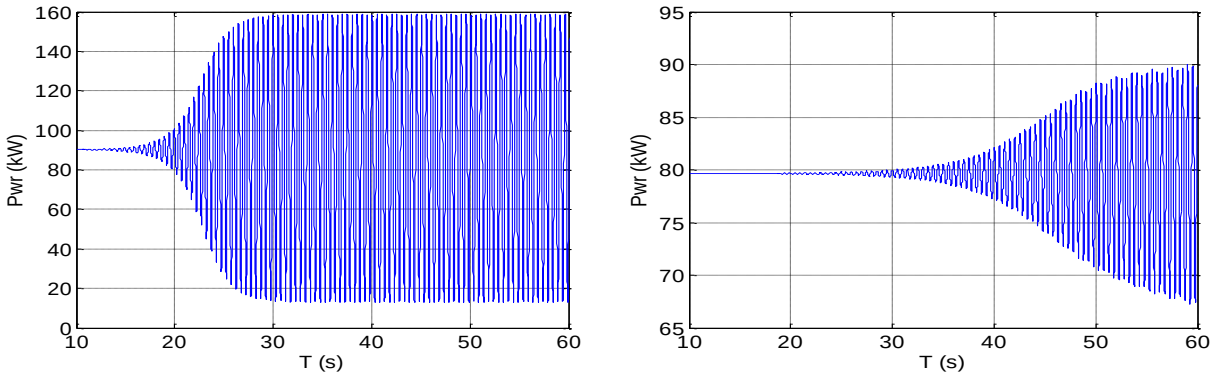

Figure 5.60: Effect of roughness

5.2.4.5 Effect of dynamic stall

The last analysis reported has been performed with dynamic stall enabled.
As it can be observed in the following figure it seems having a positive effect, reducing the amplitude of stall induced vibrations. This effect has not been further investigated. However, its effect is usually not capable to reduce stall induced vibrations to acceptable values.

V= 11 m/s

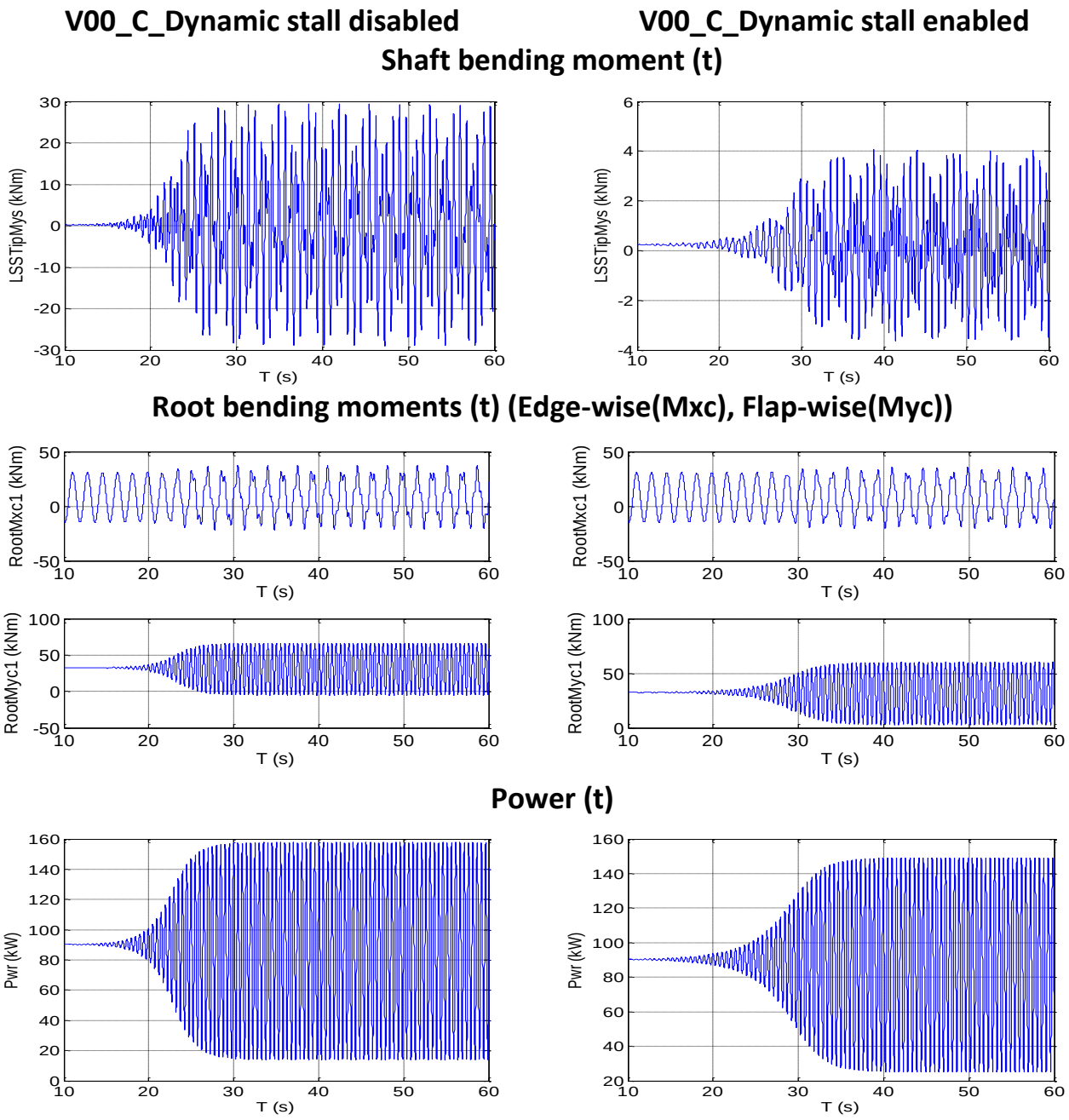

Figure 5.61: Effect of dynamic stall

Chapter 6
Blade design

The main objective of this work has been the application of the studies presented in the previous chapters to design the blades of an experimental, downwind stall regulated wind turbine for energy production at low wind speeds, which are slender and highly deformable, thus especially liable to experience stall induced vibrations.

A proper blade design should have the following objectives:

1) to maximize annual energy yield for a specified wind speed distribution;
2) to guarantee control of power output and loads at high wind speeds;
3) to design blades that resist extreme and fatigue loads;
4) to minimize weight and cost;
5) to minimize fatigue loads;
6) to avoid resonances.

The design of a stall regulated wind turbine still represents a challenging task, since it turns out to be a complex multi-objective optimization process, in which conflicting and highly interconnected aerodynamic and structural requirements need to be satisfied.
In particular, the aerodynamics of the blade has to be carefully treated, since it should ensure good power performances and it is also the only component to provide the machine control.
More specifically, the aerodynamics of the airfoils along the outer half of the blade plays a crucial role and, compared to pitch control wind turbines, more characteristics have to be considered and carefully treated, as explained in more detail in the following sections (and shown, for example, in the previous chapter regarding the stall induced vibrations).

In the first phase of this work, the main effort has been focused on maximizing the Annual Energy Production (AEP) and minimizing the rotor weight, not accounting for the dynamic behaviour of the blades.
Successively, a full aeroelastic analysis of the wind turbine optimized in the first phase – referred to as 'V00' – has been developed in unsteady conditions by using the aeroelastic code Fast_AD, to verify extreme loads, fatigue loads and thus the lifetime of the machine.

The results of this analysis have been shown in detail in the previous chapter, where the issue of stall induced vibrations has been addressed.
As shown, for the wind turbine 'V00' high vibrations occur beyond the power peak, leading to unacceptable fatigue loads and lifetime.
Thus, in the second phase of this work, this issue has been carefully addressed, in order to develop a new optimization process aiming at optimizing the annual energy production, the weight of the rotor and the dynamic behaviour of the blades at the same time.
More specifically, the studies presented in the previous chapter furnished several design suggestions which have been applied in the second phase of the optimization process to prevent the occurrence of stall induced vibrations.

6.1 AEP/Weight Optimization

The optimizations of Annual Energy Production (AEP) and rotor weight have been carried out making use of the code 'WTP_Tool' developed during this work, which aims to be a helpful aid during the preliminary design of both external and internal geometries of horizontal axis wind turbines blades.
In the following section a brief presentation of WTP_Tool is reported.
Then, the various steps of the design process developed in this work - with the related features included in WTP_Tool - are outlined.

6.1.1 WTP_Tool

WTP_Tool is a Matlab toolbox suitable for preliminary aerodynamic and structural design of horizontal-axis wind turbine (HAWT) blades, which is based on the use of the BEM code Wt_Perf (introduced in Chapter 4) for aerodynamic calculations.
It is provided of a simple and user-friendly graphic interface (GUI) which enables the designer to optimize the blade geometry step-by-step using interactive optimization tools with a few input parameters.

To start a new blade design, it is necessary to define:

- the main rotor parameters (hub radius, tip radius, number of blades, number of airfoils and the number of sections to discretize the blade)
- the airfoil at each blade section
- the main properties of the flow field
- design operating conditions

- the optimization algorithm settings

The tool is also provided with a database of airfoils which can be accessed to choose the airfoils for the different stations along the blade, and obtain their aerodynamic data and geometries.
The database contains more than 1700 airfoils and it is possible to choose between a search method by name or by different aerodynamic and geometrical properties of the airfoils.
It is also possible to add new airfoils data to the database, by computing them with Rfoil or Xfoil, or importing them from a text file.
Furthermore, WTP_Tool can interpolate airfoils data along the blade using the thickness as variable, evaluates rotational effects and extends the aerodynamic curves of the airfoils from -180 degrees to 180 degrees (using the Viterna-Corrigan method).

The code allows the user to perform the following tasks:

- to optimize annual energy production
- to perform a simplified structural pre-design of the blade to promptly give a rough estimation of the minimum rotor weight necessary to withstand maximum loads (as will be shown in the next section) and the maximum tip deflection of the blades;

and in addiction:

- to calculate the wind turbine aerodynamic performances in any off-design conditions, and for any combination of rotor speed, wind speed and pitch chosen by the user, through a post-processing module;
- to load an existing blade geometry and use this as a starting geometry for the optimization;
- to compare geometries and performances of two blades at a time;
- to modify the geometry by hand and promptly check the effects on the performance at any moment of the design process;
- to export the blade 3D coordinates to a text file compatible with a Macro which draws the geometry of the blade in SolidWorks. The user would then have the chance to do further analysis of the optimized blade, importing the CAD of the blade in a FEM or CFD program.

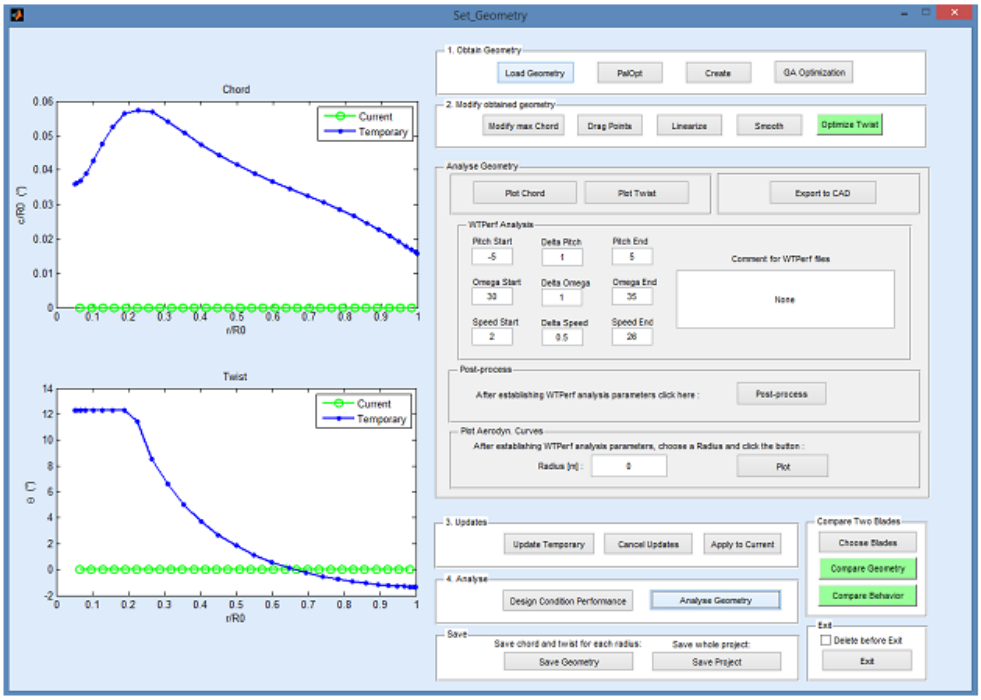

Figure 6.1: WTP_Tool graphic user interface (GUI)

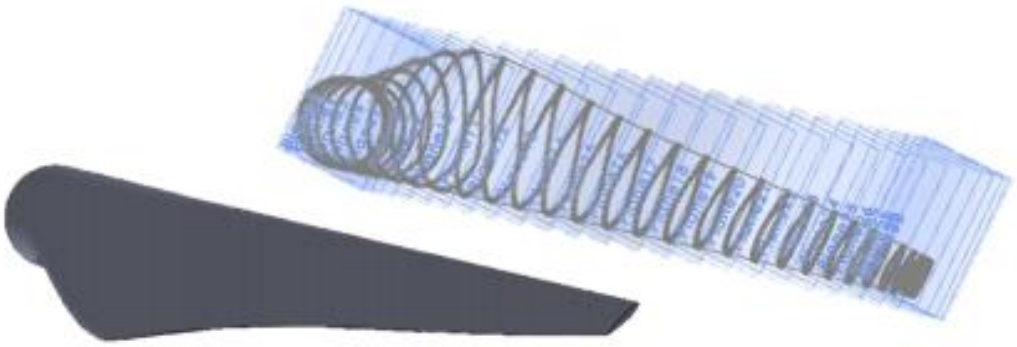

Figure 6.2: CAD obtained with an input file from WTP_Tool

6.1.2 Optimization of Annual Energy Production

The optimization of Annual Energy Production (AEP) essentially consists in the aerodynamic optimization of rotor blades external surface, which is defined by chord and twist distributions and by the airfoils geometries.

As previously said, the AEP optimization has been carried out by using the code WTP_Tool which provides the following options:

- to perform a blade geometry optimization based on Glauert's theory (through the Palopt algorithm), including Prandtl's approximation for hub and tip losses and a process of chord reduction and twist optimization, to obtaining a realistic blade geometry while keeping the power close to its ideal value;
- to perform a blade geometry optimization based on genetic algorithms (through the use of functions included in the HarpOpt code [71]);
- to modify the blade geometric parameters interactively, even acting on a single point of the geometry, and to perform the smoothing or even the linearization of the geometry;
- to choose the type of distribution for both chord and twist : linear, parabolic, manual (the points will be interpolated by cubic spline);
- to drag points and manually modify the geometry by shifting the points one by one along the vertical axis (if the user wants to apply significant and localized modifications to chord or twist distributions);
- to perform the optimization of the twist angle for the whole length of the blade, after chord modifications.

For the Glauert analytical optimization of chord and twist distributions, the tool implements the code Palopt, which is a code developed by the research group ADAG of the Department of Industrial Engineering (DII) of the University of Naples "Federico II".
With the Glauert analytical solution, the ideal chord length would be excessively large close to the root since relative wind velocity is very low here and the design method tends to produce a blade with equally distributed tangential forces. Thus, specific tools have been developed for interactively reducing the ideal chord length in the inner part of the blade and to optimize the twist angle, in order to compensate for the decreased aerodynamic torque involved by said chord modification.
With this procedure the blade is optimized for a single operating condition, thus it is not the best choice for stall regulated wind turbines, which work in totally different conditions depending on the wind speed, as shown in the first chapter.

For stall regulated machines a multi-point optimization of the blade turns out to be necessary, which can be better performed with the use of Genetic Algorithms (GA).
For the optimization based on Genetic Algorithms, the algorithm implemented in WTP_Tool is the one provided by Matlab, and its implementation is based on the procedure used by the open source code HARPOpt [71] developed at NREL.
The objective function of the genetic algorithm is the Annual Energy Production (AEP).
The algorithm aims to obtain a power curve as close as possible to the ideal curve (defined as shown in the first chapter of this work), that means to minimize the coloured area in the next figure.

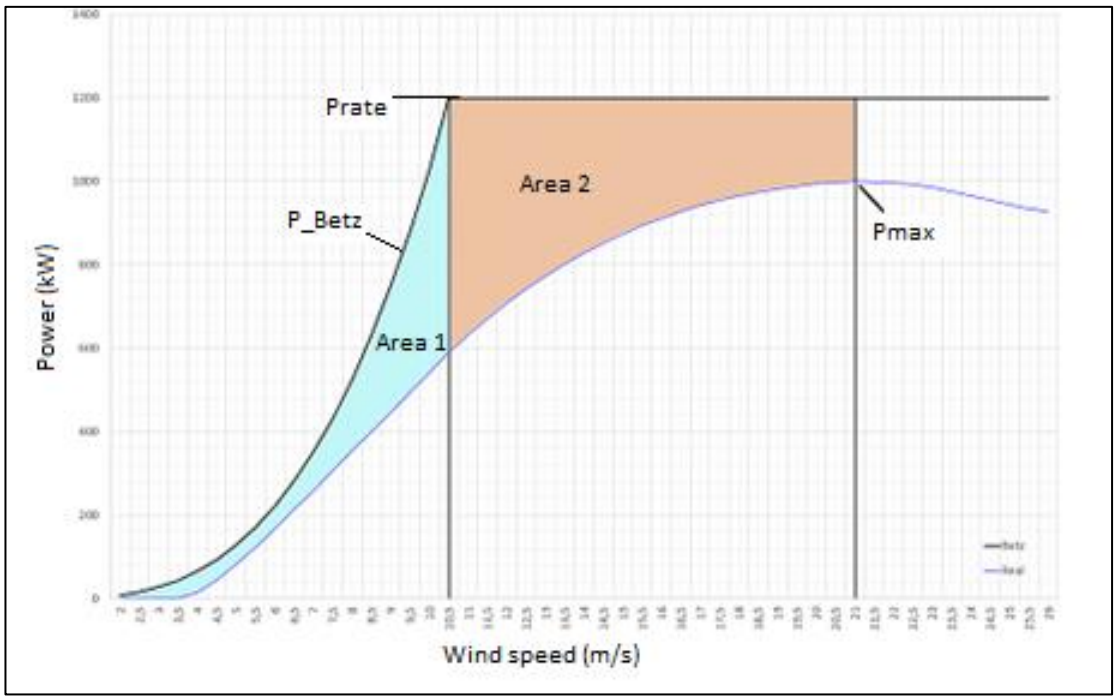

Figure 6.3: Ideal and real power curve, divided in regions used for the computation of the Fitness Function.

The boundary constraints for the GA are, basically, set on the chord, twist and thickness distributions along the blade, which must be monotonically decreasing for the blade to be structurally feasible.

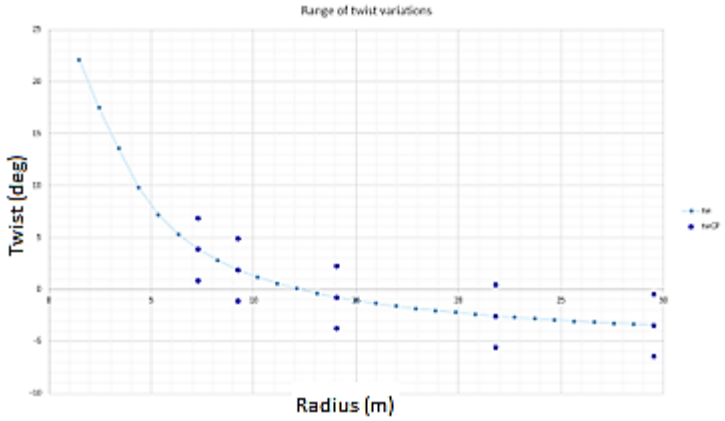

Figure 6.4: Lower and upper bounds of twist

Most of the bounds that the GA uses for the generation of the first population as well as the evolution of the next generations are chosen in the GUI by the user.

Some functions of HarpOpt have been modified to improve optimization results. In particular, new constraints have been applied for the evaluation of the Fitness Function (that means terms subtracted in the Fitness Function when the constraints are not respected).

Only one of the new constraints gave noticeable improvements with respect to HarpOpt.

This constraint forces the power peak not to exceed the rated power (Prated) (an input parameter defined by the user). As a generator for a stall-regulated wind turbine operates at its maximum capacity when the rated power is reached, it is very important that the wind turbine never gives a power higher than Prated.

One of the problems encountered while using HarpOpt has been the occurrence of power peak higher than the Prated. As shown in the next figure, this problem would seem to be solved, as shown in the following figure.

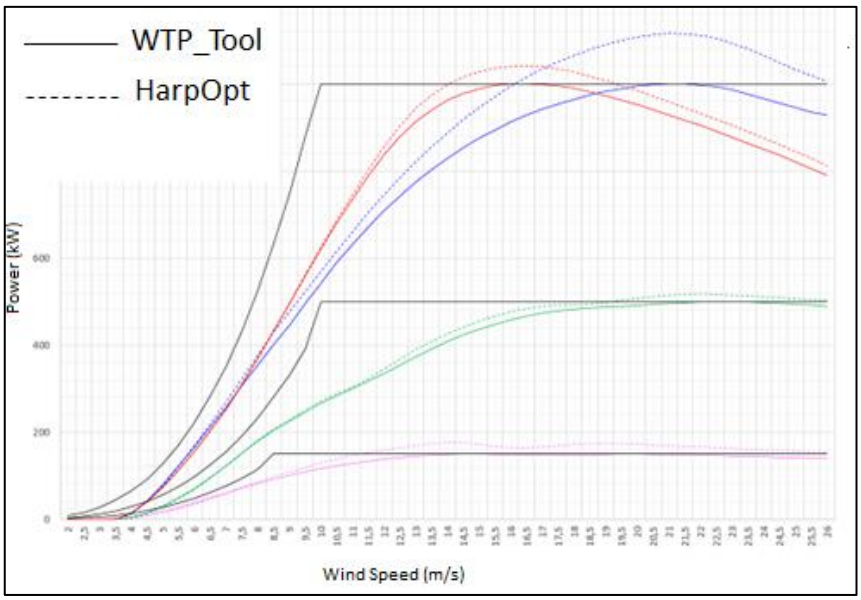

Figure 6.5: Comparison between optimization results of HarpOpt and WTP_Tool

The resulting fitness function has the following expression:

$$F = -AEP + 0.2 \cdot AEP \cdot \frac{AEP1_{Betz} - AEP1}{AEP1_{Betz}} + 0.2 \cdot AEP \cdot \frac{AEP2_{Prated} - AEP2}{AEP2_{Prated}} + 0.5 \cdot AEP \cdot \frac{P_{rated} - P_{max}}{P_{max}} \quad (6.1)$$

Another of the possible improvements suggested by HARP Opt developers is the generation of the initial population with analytical optimum blades for improving its performance, apart from the randomly created shapes that Harp Opt currently uses.

Thus, the possibility of creating the first population from an user defined blade shape (or a shape obtained with the Glauert analytical optimization) has also been included in WTP_Tool.

6.1.2.1 Selection/design of proper airfoils for AEP optimization

As shown in the previous chapters, aerodynamics of the airfoils along the blade plays a crucial role in the case of stall regulated wind turbines and, compared to pitch control wind turbines, more characteristics have to be considered and carefully treated.

Regarding the AEP maximization, a single point optimization can be sufficient for pitch controlled wind turbines, that means optimization of the aerodynamic efficiency of the airfoils.

Whereas for stall regulated machines a multi-point optimization of the blade and of the airfoils turns out to be necessary, since these work in a quite wide range of angles of attack depending on the wind speed, as shown in the following figures.

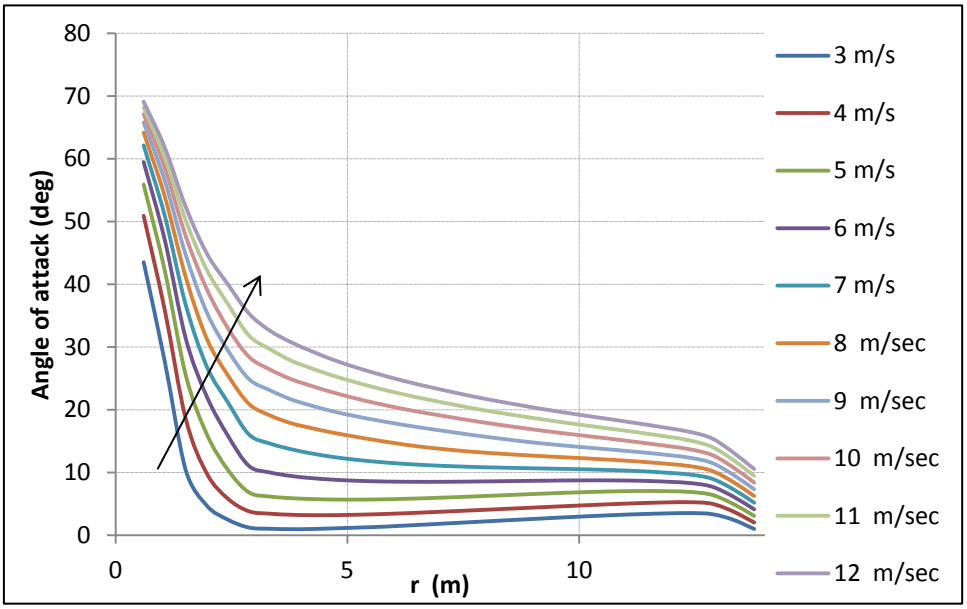

Figure 6.6: Angle of attack along the blade of a stall regulated wind turbine

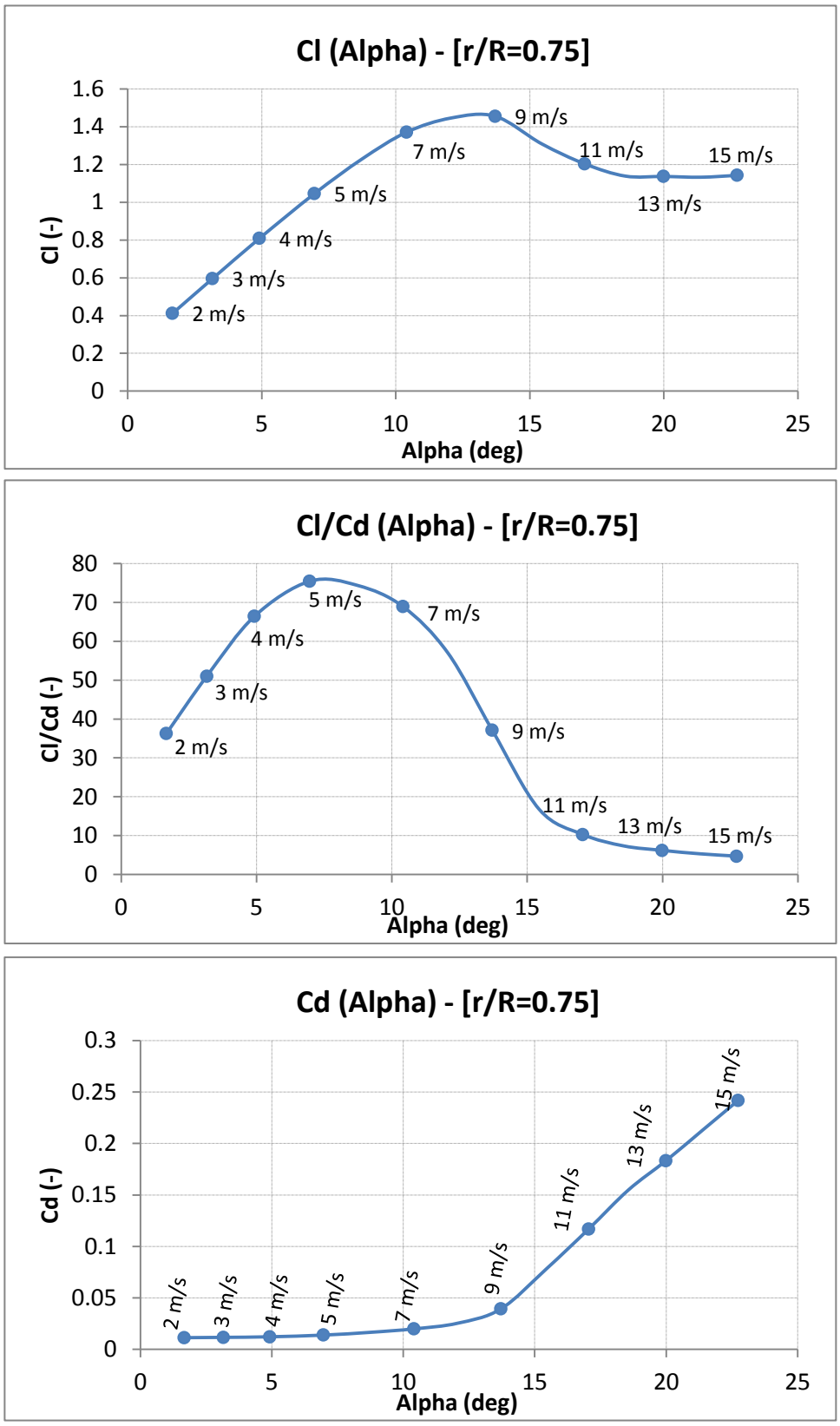

Figure 6.7: Lift, efficiency and drag curve of the airfoil at the station r=75%R and working points at different wind speeds

For these reasons, the selection/design of the airfoils and the blade shape design are more delicate than in the case of pitch-regulated turbines.
In particular, the airfoils should guarantee high wind turbine performances at each wind speed, and also the needed machine control capabilities.

Depending on the area of the blade, the requirements change quite a lot.
In fact, as shown in the following figures, the outer sections give higher contribution to the power output, thus they have to be optimized to produce high performances, while the inner sections have to be designed to provide essentially low-weight and structural integrity to the blade (as will be discussed in the next section).

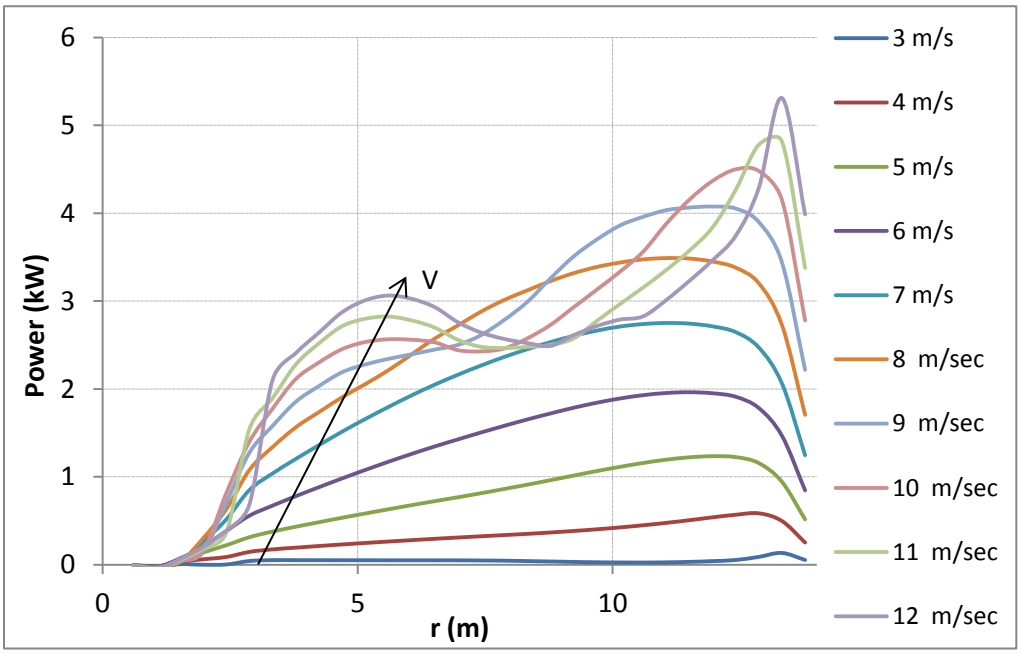

Figure 6.8: Power distribution along the blade

The primary parameters that increase the Annual Energy Production of the rotor are the aerodynamic efficiency (Cl/Cd) and the lift coefficient (Cl) of the airfoils, as can be noticed looking at the expression of the local torque along the blade provided by the Blade Element Theory:

$$dQ = B\frac{1}{2}\rho V_{total}^2 (Cl \cdot sin\varphi - Cd \cdot cos\varphi) crdr \qquad (6.2)$$

that can also be written as:

$$dQ = B\frac{1}{2}\rho V_{total}^2 Cl\left(sin\varphi - \frac{1}{(\frac{Cl}{Cd})}cos\varphi\right) crdr \qquad (6.3)$$

As previously said, for stall regulated wind turbines these high performances should be guaranteed for a range of angles of attack as large as possible. More specifically, a “large” aerodynamic efficiency curve would be desirable.

To complete the challenging scenario, the impact of roughness on the rotor performance should be also addressed when the airfoil is designed/selected.
Normally, the annual production decreases when the blade is contaminated by dirtiness (e.g. mosquitos), damages (e.g. erosion) or imperfections. Designing an airfoil that is robust (or less sensitive) to roughness would contribute to maintain a stable performance on the long run.
Thus, it is important to have airfoils with low losses of maximum lift coefficient and aerodynamic efficiency in ‘rough’ conditions, and also low variation of angles of attack at which these are obtained.
Special attention should be put also to avoid a significant change of stall and post-stall behaviour of the airfoils, to not influence wind turbine performances nearby the power peak and at higher wind speeds.
Finally, it should be kept in mind that a higher value of AEP can be obtained not only with a higher maximum efficiency of the airfoils, but also with a lower power peak wind speed, that means with a stall angle of attack (α_Clmax) closer to the maximum efficiency angle of attack (α_Emax).
Unfortunately, it is difficult to find airfoils satisfying all the desired requirements, and, usually, a compromise has to be found.

As an instance, the aerodynamic characteristics of the two airfoils that have given the best power curves among all the attempts made in this work are reported in the following figures.
The first one (‘Riso’) belongs to the airfoil family ‘Riso’, the second one (S821’) is part of the NREL's S-Series airfoil family.
The aerodynamic characteristics are reported for both clean (‘free’ in the figures) and rough (‘fix’ in the figures) conditions and have been obtained by using Rfoil. To simulate the rough condition the transition point (from laminar to turbulent flow) is fixed at x/c=0.01 on the suction side of the airfoils and at x/c=0.1 on the pressure side.
The airfoil ‘Riso’ represents an optimum solution for the optimization in clean conditions but it presents a high alteration of performances in presence of roughness, while the airfoil ‘S821’ is characterized by lower performances but presents very low alteration of performances in rough conditions.

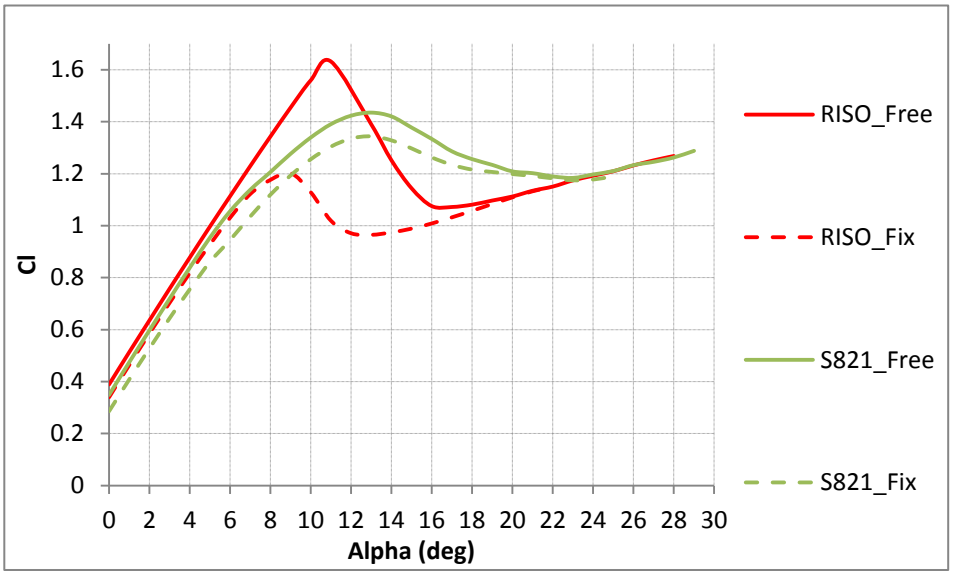

Figure 6.9: Airfoil 'Riso' and airfoil 'S821' - Lift coefficient

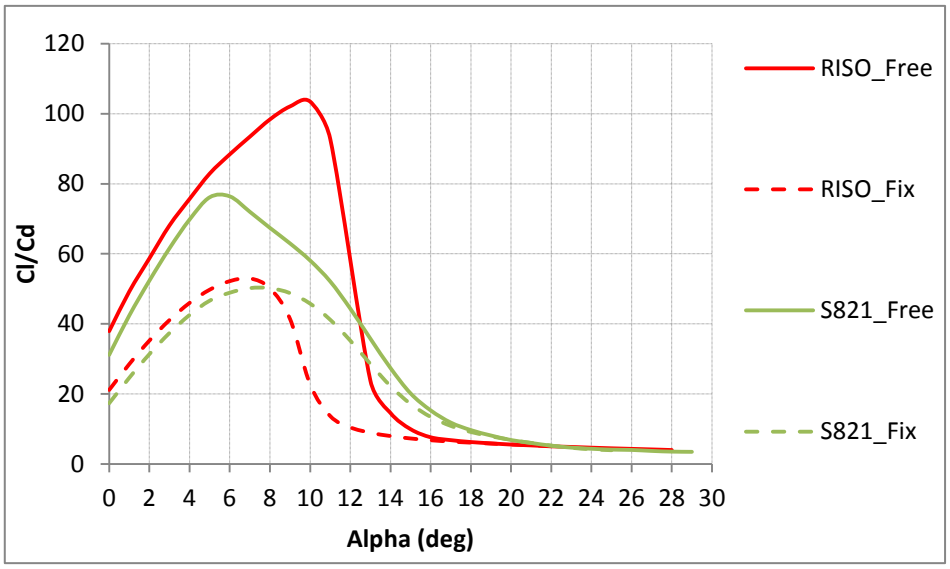

Figure 6.10: Airfoil 'Riso' and airfoil 'S821' - Aerodynamic efficiency

In these figures, it can also be observed that the stall in rough conditions is typically smoother than in clean conditions. This causes, in most of the cases, a lower power control in rough conditions and higher stall induced vibrations in clean conditions.

Normalized power curves of the wind turbines optimized with these two airfoils on the outer half of the blade are reported in the next figure, to show the effect of the airfoils on the overall performances of the wind turbine. All the considerations done for the airfoils can be confirmed looking at the related power curves.

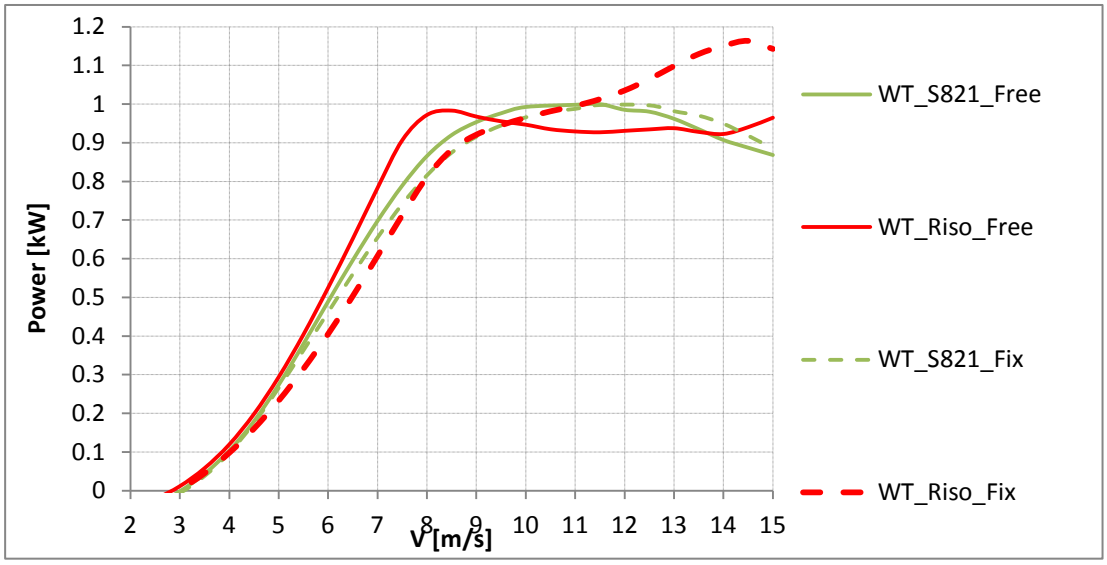

Figure 6.11: Wind turbines optimized with airfoil 'Riso' and airfoil 'S821' - Power curve

Since a wind turbine could work both in clean and rough conditions during its lifetime, in this work both the cases have been considered within the optimization process, thus a range of possible performances between the 'clean' and 'rough' power curves is always taken into account.

The 'rough' power curve is considered because it is the most conservative in terms of overall performances and power control (as shown in the previous figures).

The 'clean' power curve is considered because it is the most conservative for extreme and fatigue loads (due to higher stall induced vibrations due to a more abrupt stall).

In addition, the possibility of varying the pitch of the blades after a first field test is provided, to compensate the loss of performances due to eventual geometry imperfections.

6.1.3 Weight optimization

Structural design consists in blade material selection and the determination of structural cross sections along the blade.

A proper structural design should guarantee that all the sections withstand extreme and fatigue loads and, at the same time, it should minimize the weight of the blades with the related costs of production.

Inevitably there is interaction between the AEP optimization and the weight minimization stages, as the blade thickness needs to be large enough to accommodate a spar which is

structurally efficient and to have a higher moment of inertia of the section but, at the same time, higher thickness implies higher drag, thus low performances of the airfoil.
To minimize the rotor weight, in this work the code WTP_Tool has been used during the preliminary design phase of the wind turbine.
The code can perform a simplified structural design of the blade, promptly giving a rough estimation of the minimum rotor weight necessary to withstand maximum loads and an indicative value of the maximum tip deflection of the blades.
Then, a further structural optimization of the cross sections has been performed at the end of the preliminary design phase, verifying the strength of the blade through aeroelastic analyses and FEM analyses.

Geometries of cross sections of a blade can be quite complex because of the presence of spars, ribs, panels and other structural members. Thus, WTP_Tool is based on the assumption of a simplified geometry that is completely defined by the main geometrical properties of the airfoil, as reported by Selig in [72] and shown in the next figure. This simplified geometry is used to evaluate an approximate value of the moment of inertia about the axis coincident with the airfoil chord, which is needed to evaluate minimum skin thickness, as explained below.

Figure 6.12: Typical actual cross section of a blade

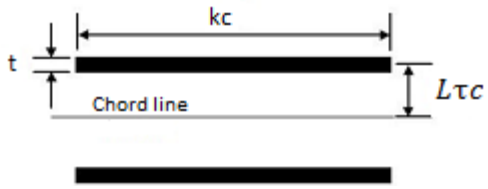

Figure 6.13: Schematic representation on the cross section.
Adapted from [72]

The basic properties of the composite material can be defined by the user, that means to define a basic laminate: number of plies and thickness, density, orientation of fibres and mechanic properties for each layer. Once the properties of each layer have been defined, global properties of the basic laminate - such as its overall Young modulus, shear modulus, total thickness and allowable stress (σ_{adm}) - are estimated.

The load condition considered to size the skin thickness of the thin-walled airfoil is the one producing the maximum bending moment at the root section of the blade, multiplied by a

factor of 2.6. This value has been individuated as a proper safety factor to account for extreme loads occurring in unsteady operating conditions, on the basis of several comparisons performed between steady results of WTPerf and results of unsteady aeroelastic analyses performed with FAST_AD. In particular, extreme loads usually occur for the Design Load Case DLC 1.4 of the IEC standards, which is the load case for which an extreme coherent gust with direction change of the wind occurs while the wind turbine is producing power nearby the rated power wind speed.

Given the external surface of a blade, the basic laminate of the composite material and the maximum loads computed by WTPerf along the blade, WTP_Tool computes the minimum thickness of the airfoil skin - and thus the number of basic laminates - necessary to withstand local stresses at each station using the following expression:

$$t_{dim} = \frac{M \cdot Y_{max}}{I \cdot \sigma_{adm}} \tag{6.5}$$

where:
M is the local flapping moment;
Y_{max} is half of the maximum thickness of the airfoil;
σ_{adm} is the allowable stress, which depends on the basic laminate,
I is the airfoil's moment of inertia about the axis coincident with the chord and intended per unit thickness of the skin.
The moment of inertia $(I \cdot t)$ is computed modelling the airfoil as in Figure 6.13, reported again for clarity

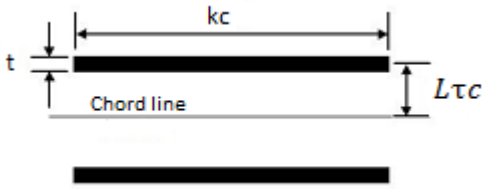

Figure 6.14: Schematic representation on the cross section. Adapted from [72]

where:
c is the chord length,
t is the thickness of the skin panel,
τ is the maximum ratio between thickness and chord of the airfoil,
k and L are two dimensionless coefficients.
Thus, $(I \cdot t)$ is computed with the following expression.

$$I \cdot t = 2\left(\frac{kct^3}{12} + (ktc)(L\tau c)^2\right) \tag{6.6}$$

Neglecting the first term in the bracket we obtain (with a good approximation, being the skin panel usually very thin):

$$I \cdot t = 2(ktc)(L\tau c)^2 \tag{6.7}$$

and, finally:

$$I = 2k(L\tau)^2 c^3 \tag{6.8}$$

Selig in [72] used the following values for the coefficients k and L:
K=0.4
L=0.5*0.9
These coefficients lead to good results for a small thickness ratio τ (up to 25%c) of the airfoil, while they commit a substantial error for higher values of τ.
The following figure shows the comparison between the value of I obtained implementing this method and the I computed by XFOIL ("True" in figure) for a generic airfoil, as function of maximum thickness ratio (τ) (this is modified varying the thickness of the same airfoil in Xfoil). It can be seen that the more is τ the more is the error committed.

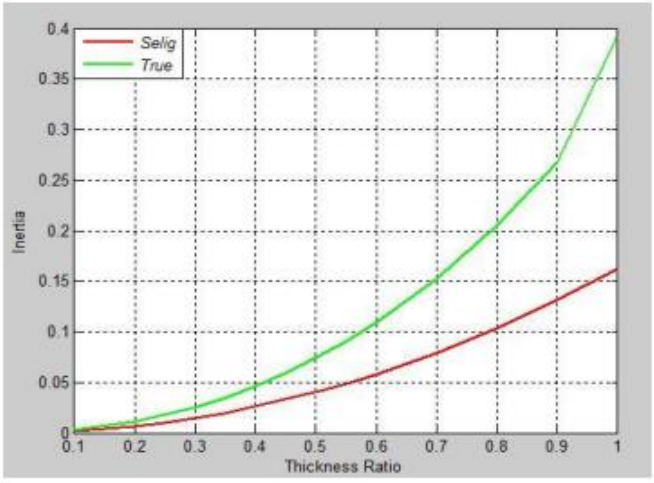

Figure 6.15: Comparison between inertia per unit thickness computed by Selig and by Xfoil, as function of maximum airfoil thickness

Since very large airfoils must be adopted close to the hub, this error is unacceptable and it is necessary to use coefficients (k,L) varying with the thickness ratio of the airfoil. Same considerations can be applied as the chord of the airfoil changes, because the more is the chord the more is the physical thickness of the section and the error committed. Furthermore, it is necessary to account for the twist angle θ of the airfoil because we are considering the bending moment in the out-of-plane direction (close to the flap-wise direction).

To correct the errors committed with the variation of these three parameters (τ, c, θ) the coefficient M is used, which is defined as:

$$M = k_\tau(\tau) \cdot k_c(c) \cdot k_\theta(\theta) \tag{6.9}$$

Thus, we have:

$$I = 2\tau^2 c^3 M \tag{6.10}$$

where the coefficients $k_\tau(\tau)$, $k_c(c)$ and $k_\theta(\theta)$ are functions of τ, c and θ, respectively.
The values of $k_\tau(\tau)$, $k_c(c)$ and $k_\theta(\theta)$ have been obtained through a parametric study for a range of τ, c and θ.
In the next figure the moment of inertia per unit thickness (I) computed with this method is compared to the one obtained with Xfoil, at each station of a twisted and tapered blade.
The curve indicated as 'Ia-Ncoeff' is obtained with kc, kτ and kθ computed for the actual values of τ, c and θ at each station of the blade.
The curve indicated as 'Ia-1coeff' is obtained with kc, kτ and kθ computed as average values of all those obtained in the parametric study.
The curve indicated as 'Ia-rangecoeff' is obtained with three values for each of kc, kτ and kθ, computed as average values of those obtained for three ranges of τ, c and θ, respectively.
The error committed is very small whatever method is used and is practically irrelevant in the case 'Ia-Ncoeff', except for the zone adjacent to the hub (where the moment of inertia can be analytically computed, the blade having circular sections at the root) which is not reported in the graph.

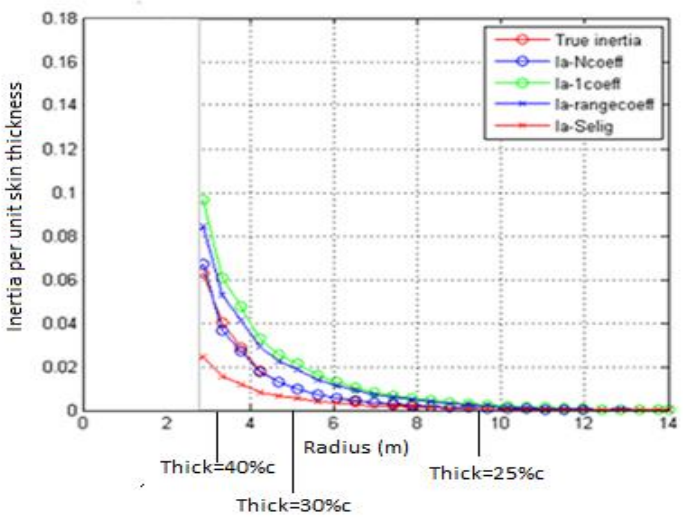

Figure 6.16: Inertia per unit thickness computed by WTP_Tool compared to the correct value.

6.1.3.1 Selection of proper airfoils for weight optimization

Regarding the choice of airfoils to adopt to minimize the weight, they should have a thickness as large as possible (compatibly with performances) to maximize the moment of inertia, especially on the inner part of the blade, which is the part that takes up all the forces put upon the entire blade length. Usually the blade needs a very thick root section (t/c≈ 0.4), which is not positive aerodynamically. However, this part gives a low contribute to the power output and structural requirements are predominant.

6.2 First phase of the optimization-Wind turbine 'V00'

The result of the first phase of the optimization process developed in this work is the wind turbine "V00" analysed in the previous chapter regarding the stall induced vibrations.
Blade geometry has been obtained by using genetic algorithms and a further step-by-step optimization procedure of both annual energy and weight, by using WTP_tool.
The principal objectives of the optimization have been:

- minimizing the cut-in wind speed;
- minimizing the rated power wind speed;
- maximizing the annual energy for a mean wind speed of 4 m/s;
- defining a twist distribution ensuring the rotor blades stall gradually rather than abruptly when the wind speed reaches its critical value, but also ensuring a good control of power and loads at high wind speeds;
- minimizing the rotor weight.

First of all, the values of rotor radius (R=14m) and rotational speed (RPM=34) have been fixed.
For the maximum chord region ($r = 20 \div 25\%R$) an airfoil of the DU airfoil family, widely used in wind energy applications, has been adopted. This airfoil has been chosen because it presents a quite high maximum thickness (τ_max=30%) and quite low post-stall values of lift coefficient, useful to compensate lift augmentation due to stall delay. It is referred to as airfoil 'D30' in this work.
For the middle part of the blade ($r = 35 \div 60\%R$) a specifically designed airfoil 'G25b' has been used.
The airfoil has been designed by using the airfoil optimization code 'Optfoil' developed at the Department of Industrial Engineering of the University of Naples "Federico II" by F. Grasso [73], which applies a gradient-based method to find the optimal solution,
This airfoil has been designed to have good aerodynamic performances (high maximum lift coefficient and high aerodynamic efficiency) both in clean and rough conditions, low

variation of stall angle of attack between clean and rough conditions, and also a quite high maximum thickness (τ_max=25%).

For the outer part of the blade (70-100%R) another airfoil of the DU airfoil family has been used. It presents a τ_max=25% and is referred to as airfoil 'D' in this work. This airfoil has similar characteristics respect to the airfoil 'G25b' but an higher loss of efficiency in rough conditions and a lower value of maximum lift coefficient, useful to improve power control at high wind speeds and to limit the bending moment along the blade.

The geometries are interpolated in the transition sections of the blade (between two airfoils).

In the next figures, the aerodynamic performances of the airfoils are reported,in clean (free)and rough (fixed) conditions.

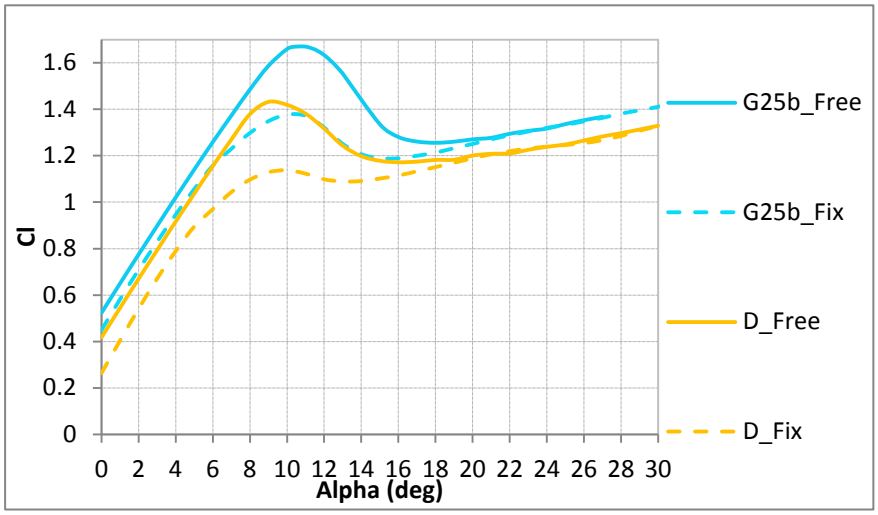

Figure 6.17: Lift coefficent of outer airfoils of the wind turbine 'V00' Clean and rough conditions

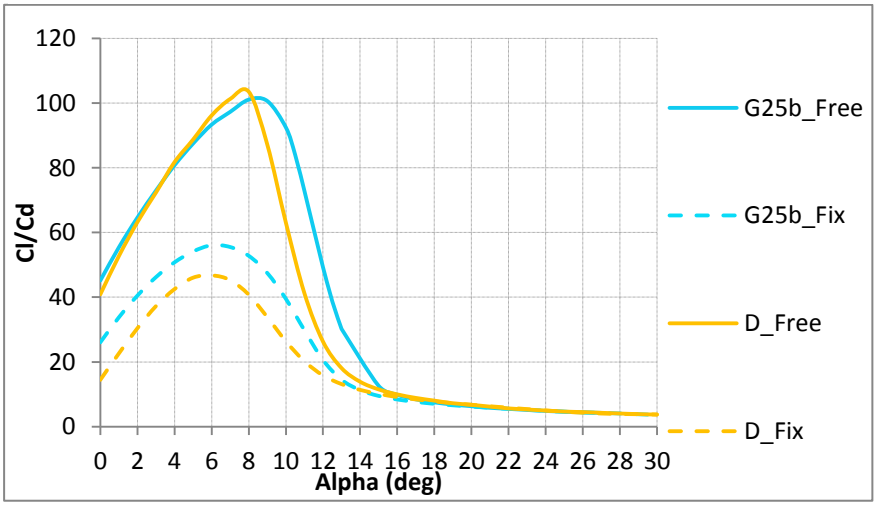

Figure 6.18: Aerodynamic efficiency of outer airfoils of the wind turbine 'V00' Clean and rough conditions

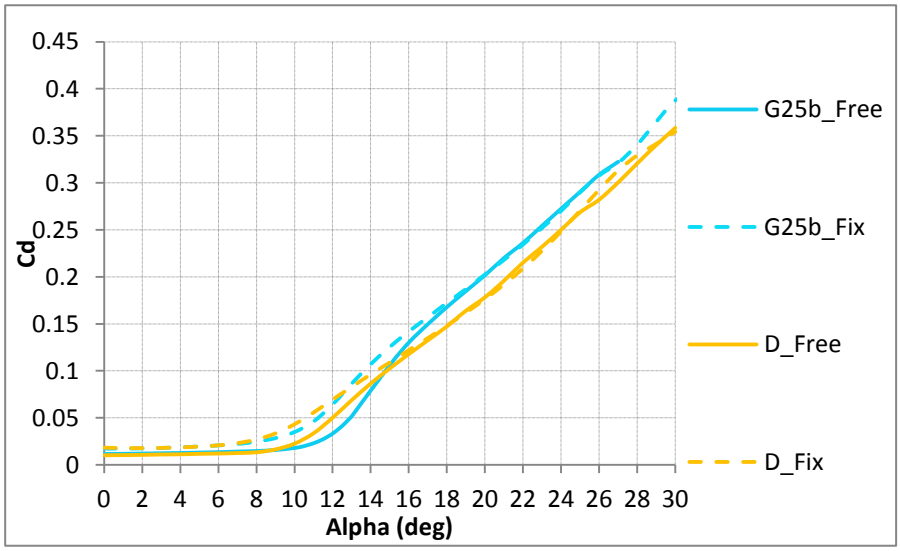

Figure 6.19: Drag coefficient of outer airfoils of the wind turbine 'V00' Clean and rough conditions

Finally, the power curve of the optimized wind turbine is shown in the next figure, for both clean ('free' in the figure) and rough ('fix' in the figure) conditions.
In the same graph it is also reported the power curve in rough conditions at a pitch value that would guarantee the best performance of the wind turbine.

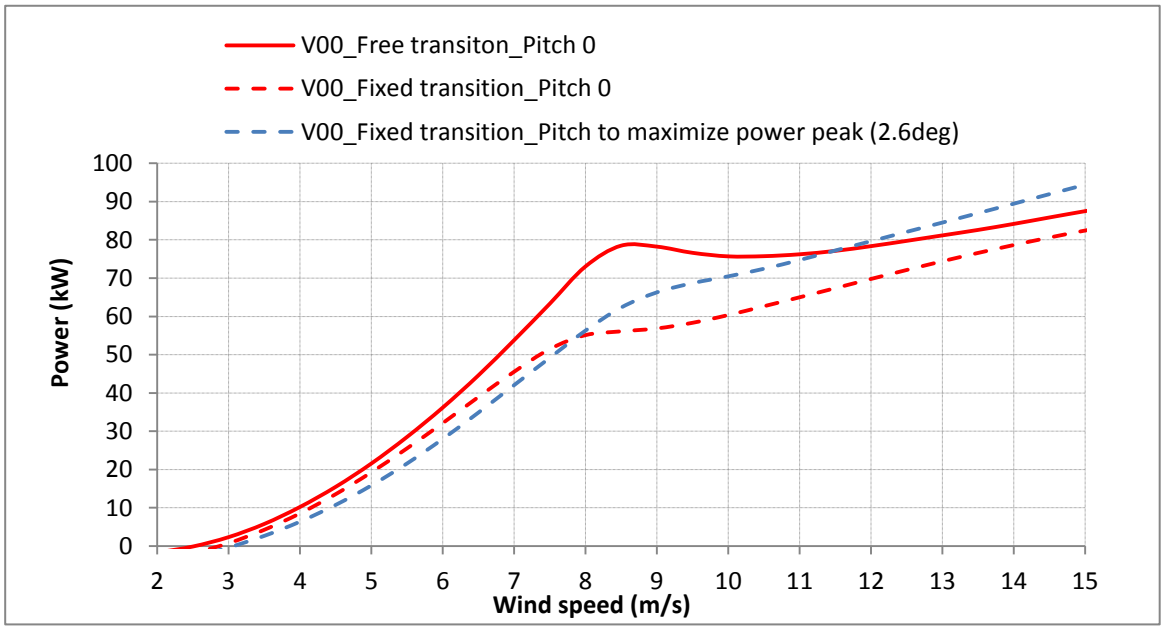

Figure 6.20: Wind turbine V00 – Power curve in clean (free) and rough (fixed) conditions

It has to be highlighted that in the first phase of the optimization process, the increasing power beyond the power peak, observable in the figure, has been considered acceptable, based on the BEM power overestimation beyond the stall. One of the objectives of the second phase of the optimization has been achieving a higher power control than the wind turbine 'V00' to have a higher safety margin.

As shown in the previous chapter, a full aeroelastic analysis of the optimized wind turbine (V00) showed high vibrations at some wind speeds beyond the power peak, leading to unacceptable fatigue loads and lifetime.
Thus, in the second phase of this work, a new optimization process has been developed, aiming at optimizing the annual energy production, the power control and the dynamic behaviour of the wind turbine, preventing the occurrence of vibrations.

6.3 Second phase of the optimization – Wind turbine 'WT_G25x'

6.3.1 Optimization of the dynamic behaviour of the blade

The main purpose of the second phase of the optimization has been the blade modification of the wind turbine V00 to avoid the occurrence of high stall induced vibrations beyond the power peak.
On the basis of the investigations presented in the previous chapter, two strategies have been adopted, which can be applied also in the preliminary aerodynamic design of a wind turbine and don't need additional devices on the blade (as, for example, vortex generators in the inner part of the blade, as suggested by Petersen et. al. [1].
The first one consists in modifying the airfoils of the tip part of the blade (≈75%-100%R depending on each case), while the second one modifies the twist distribution of the tip part of the blade. Both of them are discussed in the following sections.

6.3.1.1 Modification of tip airfoils

As shown in Chapter 5, local damping of single sections of the blade highly depends on the stall behaviour of the airfoils. More specifically, damping coefficient increases with the slope of the airfoil lift curve beyond the stall.
Furthermore, it has been seen that tip airfoils are the main responsible of the whole damping of the blade.

Looking at the lift curve of the tip airfoil 'D' on the wind turbine 'V00', it is possible to observe that it shows an abrupt stall, which is the main responsible of stall induced vibrations, as shown in the previous chapter. In particular it has been seen that, the highest vibrations occur exactly when the representative tip airfoil (the middle one of the tip airfoils, at r≈85%R) reaches the angle with maximum absolute value of the negative slope of the lift curve.

Thus, as a first attempt, different airfoils with smoother stall than the original one have been tried on the tip part of the blade (75%-100%R).
For all the attempts made in this work, the effect has always been a reduction of the absolute value of the simplified modal damping coefficient (with the related stall induced vibrations) and less power control at high wind speeds.
The loss of power control is due to higher lift coefficients in the post-stall regime, caused by the smoother stall of the airfoils.

An example is reported in the following figures, to show the typical effect of using an airfoil with a smoother stall in the tip region, in terms of power curve, simplified modal damping coefficient and its minimum value (reported as 'DC').
The new airfoil is denominated 'C' in the figures, while the original one 'D'. 'V00_D' is the original wind turbine and 'V00_C' is the blade with the new airfoil.

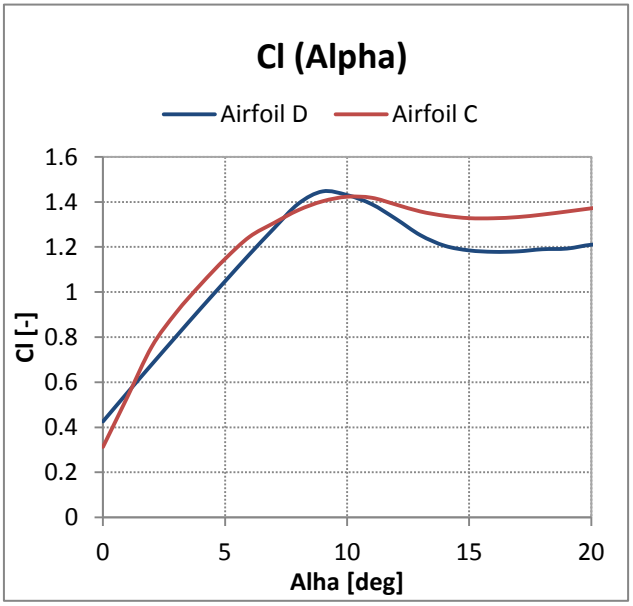

Figure 6.21: Lift curve of original airfoil (D) and new airfoil

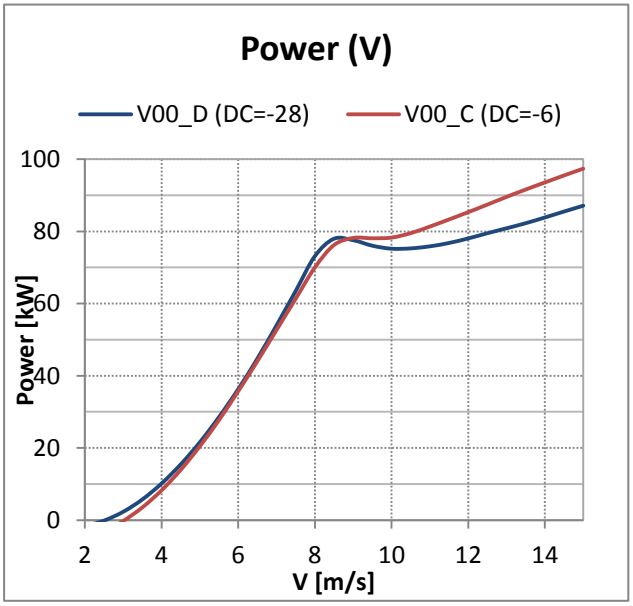

Figure 6.22: Effect of new tip airfoils (smoother stall) on the power curve

Original tip airfoil
DC=-28.74

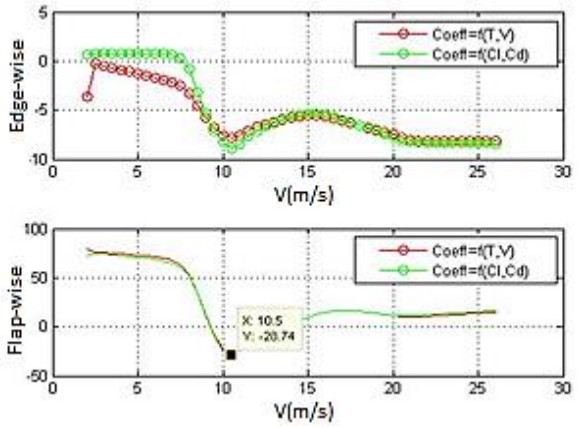

Figure 6.23: Original turbine - Simplified modal damping coefficient Minimum value: DC=-28.74)

Original tip airfoil
DC=-6.6

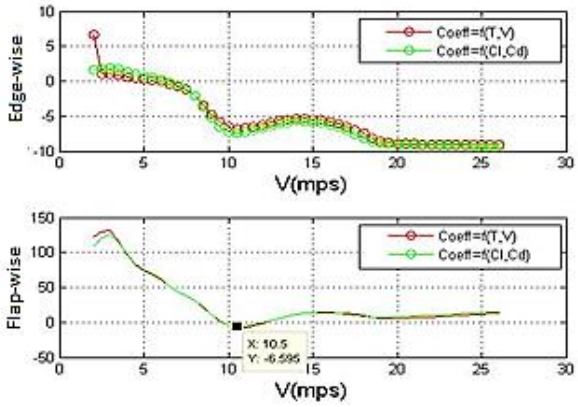

Figure 6.24: Turbine with modified tip airfoils - Simplified modal damping coefficient Minimum value: DC=-6.6

6.3.1.2 Back-twist

Petersen et al. [1] performed several parametric studies to investigate the influence of different blade design parameters (such as airfoil types, blade twist, structural pitch, and stiffness) on aerodynamic damping and power production.

On the basis of these studies they provided several design suggestions to prevent stall induced vibrations on stall regulated wind turbines.

In this work one of these suggestions has been adopted, which consists in a positive change of tip twist, such that the trailing edge of the tip airfoils move in downwind direction.

The result is that, at each wind speed, these airfoils work at a lower angle of attack.

This positive twist of the tip elements is also referred to as “back-twist”.

Ideally, the back-twist of the blade can be tuned such that the tip airfoils, the higher responsible of stall induced vibrations, can work at angles of attack where the flow is still attached up to the cut-out wind speed. Thus, it is possible to avoid these airfoils working in

the post stall region, where the slope of the lift curve becomes negative and leads to negative values of aerodynamic damping coefficient.
In other words, if a given blade has a minimum negative aerodynamic damping at a certain wind speed, the back-twist can shift this minimum towards the cut-out wind speed.
Actually, with the only back-twist is not always possible to achieve a positive damping coefficient without a noticeable alteration of the power curve, as shown in the next figures.
In the these figures, the effects of back twist on the wind turbine 'V00' are shown in terms of: geometry of the blade, power curve and working point of a representative tip airfoil (r≈85%R) at the wind speed of minimum modal aerodynamic damping coefficient (≈11 m/s).
Furthermore, the minimum value of simplified modal aerodynamic damping coefficient (DC) is reported for the original blade and the blade modified with back-twist.

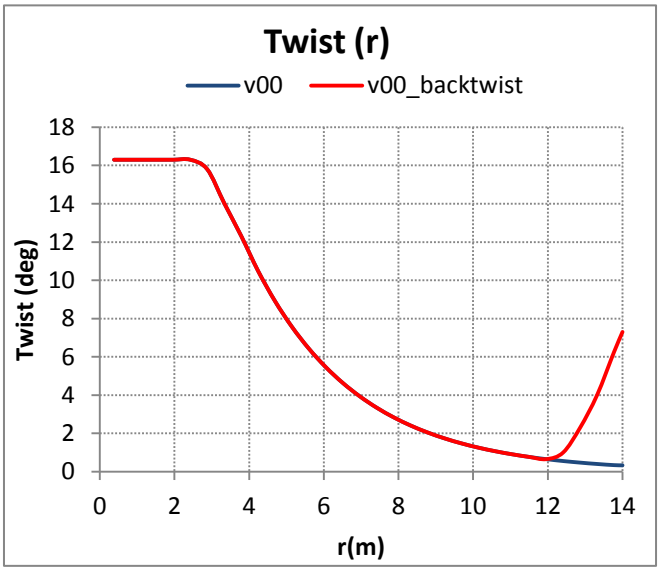

Figure 6.26: Effect of back-twist on geometry

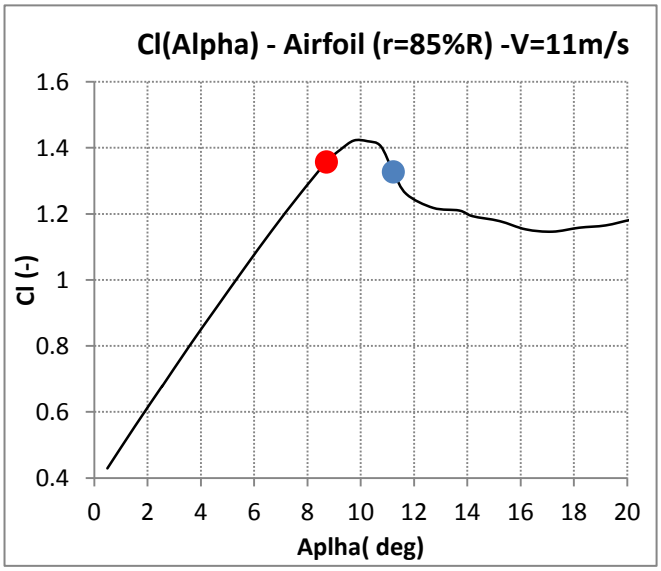

Figure 6.25: Effect of back-twist on the working point of airfoil at r=85%R

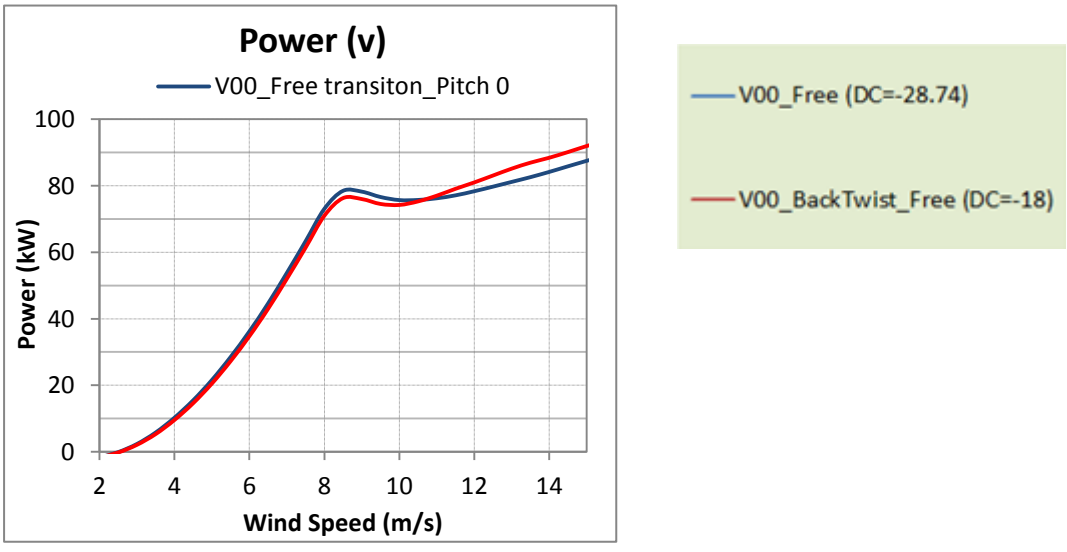

Figure 6.27: Effect of back-twist on power curve and minimum modal aerodynamic damping coefficient (DC)

For all the attempts done in this work, the effect of back-twist has always been a reduction of the damping coefficient and stall induced vibrations, a little reduction of power peak and less control at high wind speeds, as it can be noticed in the figure.
The loss of power control is caused by tip airfoils working at lower angles of attack and in post stall regime at wind speeds beyond the power peak; thus, for the same wind speed, they will have higher lift coefficients with respect to the blade without back-twist.

On the basis of different attempts made to validate the simplified modal aerodynamic damping coefficient (DC) introduced in the previous chapter, it has been concluded that a value of DC higher than about DC=-5 is necessary to have an acceptable reduction of stall induced vibrations.
To achieve this value, it has always been necessary to use a combination of back-twist and airfoils with smoother stall than the original airfoil "D" near the tip.

Finally, it has to be noticed that the curves reported until now have been obtained using aerodynamic coefficients of the airfoils computed by Rfoil not considering rotational effects.
In the following figure, the curves of the last example are compared to those obtained by using airfoils coefficients computed by Rfoil with rotational effects, and the power curve computed with a CFD run, to show that the loss of power control is, actually, even worse.

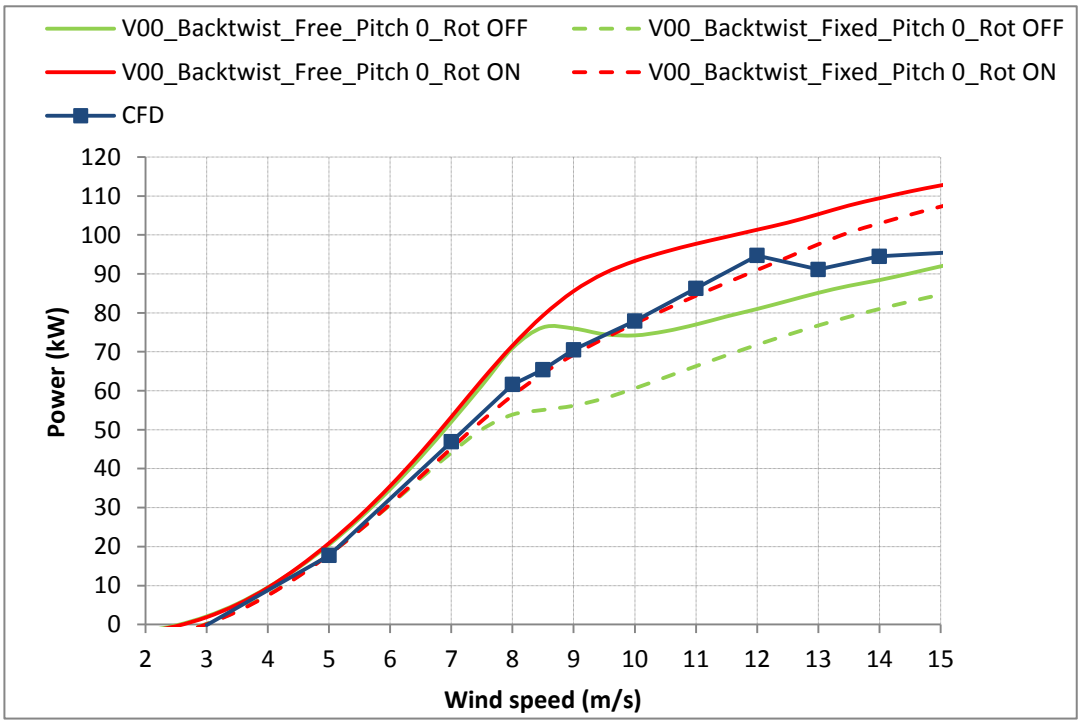

Figure 6.28: Wind turbine 'V00_Backtwist' – Power curve computed by CFD and Wtperf+Rfoil, with and without taking into account rotational effects – Clean (free) and rough (fixed) conditions

This comparison had already been reported in Chapter 3, to show the rotational effects on power curves, and to show that CFD approximately gives the same results given by Rfoil in rough conditions and considering rotational effects.

Since both the back-twist and the airfoil variation cause less power control, actually the need of low stall induced vibrations and power control represent two conflicting requirements that make the design of a stall regulated wind turbine an highly complex challenge.
Finding a good compromise between these two aspects has been one of the main efforts in this work.
More specifically, it has been necessary adopt the back-twist solution and to find an airfoil for the outer part of the blade, capable to guarantee power control and a good dynamic behaviour of the blade at the same time.

6.3.2 The new airfoil 'G25x'

Several existing airfoils has been tested for the tip part of the blade (together with back-twist) adapting twist distribution for each one of them.
As shown in the next figure, these exhibit a huge variety of lift curves and aerodynamic efficiency curves.

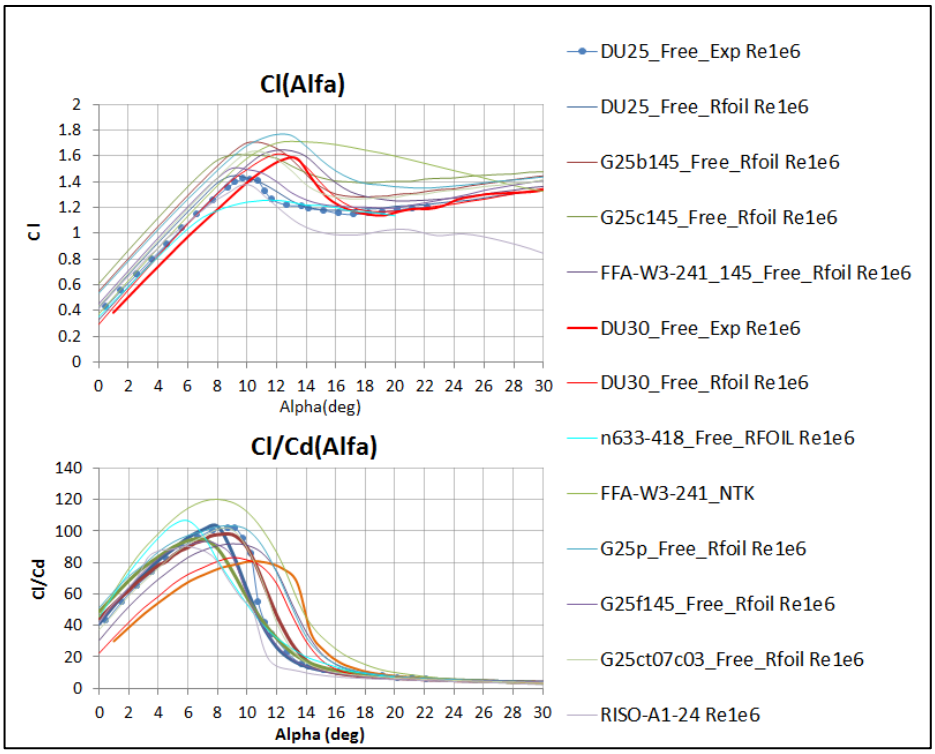

Figure 6.29: Lift and aerodynamic efficiency curves of several airfoils tested in this work

Nevertheless, with no one of these airfoils it has been possible to satisfy all the requirements at the same time: good performances, power control and absence of stall induced vibrations.
Thus, a new airfoil has been designed to achieve the desired results.
The new airfoil 'G25x' has been obtained through the use of the airfoil optimization code 'Optfoil' [73], the same code used to obtain the airfoil 'G25b' for the previous wind turbine.
The optimization process had the purpose to obtain an airfoil exhibiting all the desirable characteristics individuated during this work, for airfoils specifically suited to stall regulated wind turbines, for both the middle and tip regions of the blade.

These characteristics can be summarized as follows:

- airfoil characteristics to maximize Annual Energy Production
  - high aerodynamic efficiency (E=Cl/Cd) in a range of angles of attack as large as possible
  - high maximum lift coefficient (Cl_max)
  - α_Emax as close as possible to α_Clmax

- low sensitivity to roughness
  - low reduction of aerodynamic efficiency (E)
  - low reduction of maximum lift coefficient (Clmax)
  - low variation of α_Emax
  - low variation of α_Clmax
  - similar post stall dCl/dα in free and fixed conditions (for power control)

- airfoil characteristics to prevent stall induced vibrations
  - good stall behaviour (gentle stall)

- airfoil characteristics to guarantee power control
  - low lift coefficient and aerodynamic efficiency beyond the stall

The maximum thickness of the airfoil has been fixed at a value of 25% of the chord in the optimization and it has been adopted for the outer half of the blade.
The result of the optimization is an airfoil with aerodynamic characteristics that turn out to be a compromise between the characteristics of the airfoils 'Riso' and 'S821', each one of them representing the 'optimum' in respect to some aspects of the optimization, but not for other ones.
In particular, as previously said, the airfoil 'Riso' would represent an optimum solution for the optimization of stall regulated wind turbines in clean conditions but it presents high

alteration of performances in presence of roughness, while the airfoil 'S821' is characterized by lower performances but it presents negligible performances alteration in rough conditions.

Furthermore, the airfoil 'S821' represents the 'optimum' in respect to aerodynamic damping and stall induced vibrations, thanks to a gentle stall, while the airfoil 'Riso' leads to pronounced stall induced vibrations.

In the next figure, the aerodynamic performances of the three airfoils are compared in clean (free) and rough (fixed) conditions.

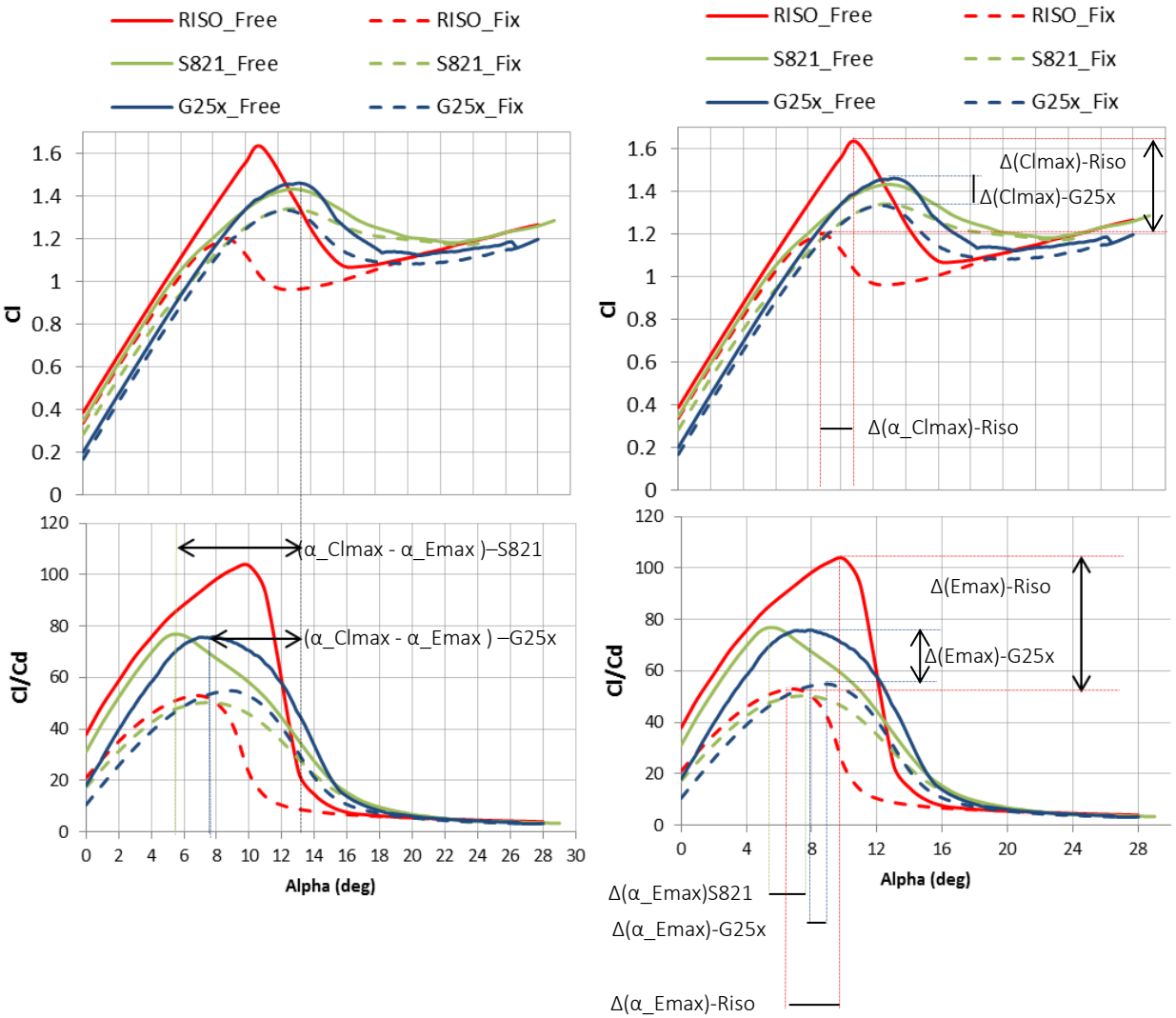

Figure 6.30: Comparison between airfoil G25x, S821 and Riso
Lift and aerodynamic efficiency curves

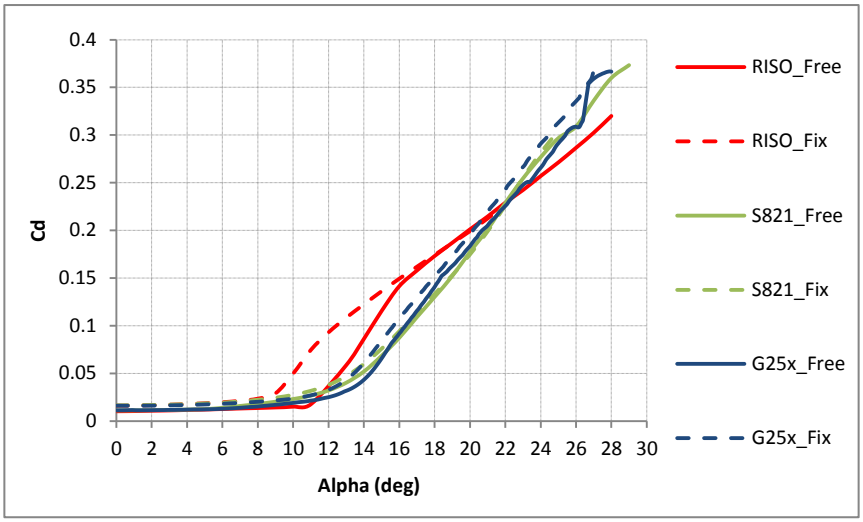

Figure 6.31: Comparison between airfoil G25x, S821 and Riso Drag curves

6.3.3 Final result – Wind turbine WT_G25x

The following figure shows the power curves (obtained using WtPerf) of the wind turbines optimized with the three airfoils presented in the previous section, with the related values of Annual Energy production (AEP) (for a mean wind speed of 4 m/s) and the simplified modal aerodynamic damping coefficient (DC).
It can be noticed that the airfoil G25x allows to obtain:

- low alteration of the power curve in rough conditions; in particular: lower alteration with respect to the case 'Riso', and comparable alteration with respect to the case 'S821';
- an intermediate power peak wind speed with respect to the other airfoils
- an intermediate AEP with respect to the other airfoils
- an intermediate value of damping coefficient with respect to the other airfoils

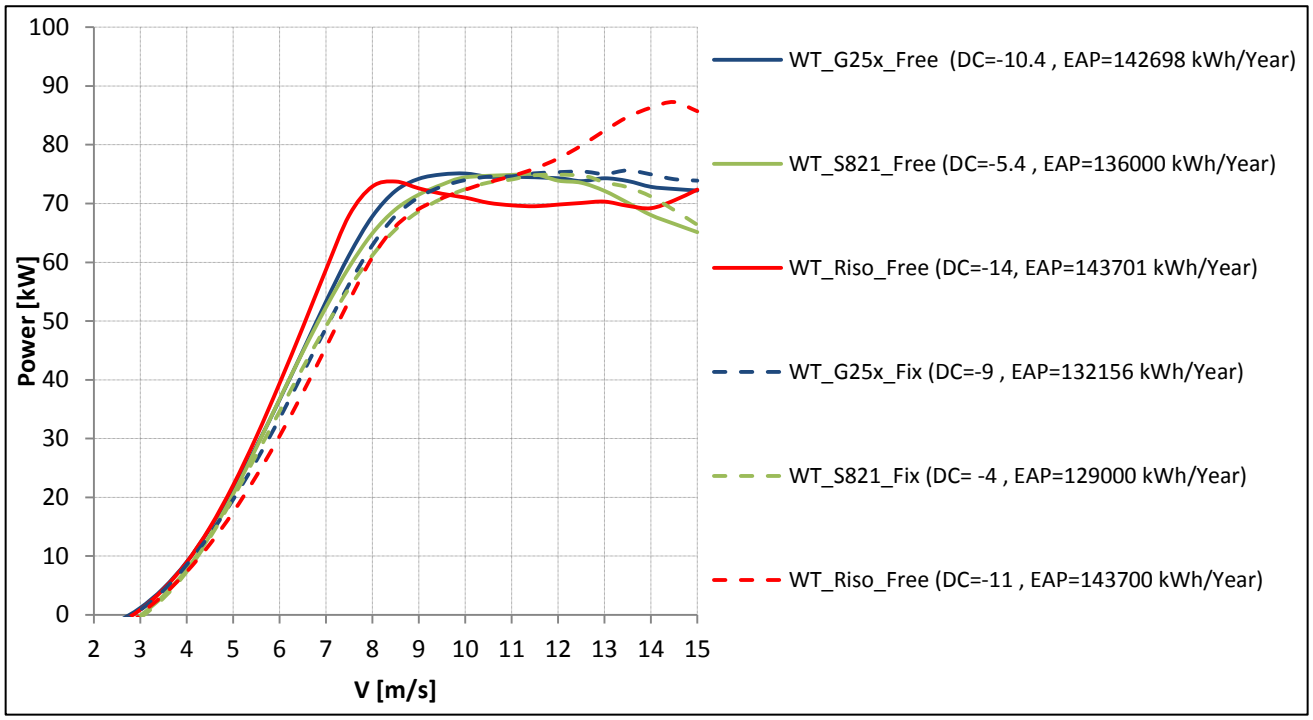

Figure 6.32: Power curve of final wind turbine ('WT_G25x') compared to wind turbines 'WT_Riso' and 'WT_S821'

In the following table the values of AEP for the wind turbines 'WT_G25x' and 'WT_S821' in clean conditions (free) are compared to the AEP of 'WT_Riso' in clean conditions, which represents the best result in terms of AEP; while in Table 2 the ratio between the AEP in clean and rough conditions for each wind turbine is reported.

Table 1: AEP of 'WT_G25x' and 'WT_S821' respect to AEP of 'WT_Riso'

(AEP_G25x_Free)/(AEP_Riso_Free)	0.99
(AEP_S821_Free)/(AEP_Riso_Free)	0.95

Table 2: AEP in rough conditions (fixed) compared to AEP in clean conditions (free)

(AEP_G25x_Fix)/(AEP_G25x_Free)	0.93
(AEP_S821_Fix)/(AEP_S821_Free)	0.95
(AEP_Riso_Fix)/(AEP_Riso_Free)	0.81

Looking at these results, it can be concluded that 'WT_G25x' represents an optimum compromise between the other two wind turbines, also considering the value of damping coefficient reported in the previous figure.

In all the cases, the airfoil mentioned is used for the outer half of the blade (50%-100%R), while the airfoil D30 is used for the maximum chord section (r≈20%R).
The geometries of airfoils between the station r=20%R and r=50% R have been obtained by interpolating the shape of the airfoil D30 and the shape of the outer airfoil in each case.
Regarding the method used to compute the power curves, it has to be reminded that, as shown in Chapter 3 and Chapter 4, it is possible to have a good prediction of the power curve (that means accounting for rotational effects, hub losses and tip losses) using a BEM code if:

- 2-dimensional aerodynamic coefficients are considered for the airfoils of the outer half of the blade;
- 3-dimensional aerodynamic coefficients are considered for the airfoils of the inner half of the blade.

Thus, to account for rotational effects (hub and tip losses are taken into account by the BEM code), the following procedure has been adopted to compute the aerodynamic coefficients for the different sections of the blade:

- r=20%R
  Since the section of the blade between the blade root and the station r=20%R has not been altered during the optimization process, the aerodynamic coefficients of the airfoil D30 (at the r=20%R station) have been extracted by the CFD run performed for the wind turbine V00_backtwist (as shown in Chapter 3).

- r=50%R-100%R
  2D aerodynamic coefficients

- r=20%R-50%R
  Aerodynamic coefficients interpolated between the coefficients at r=20%R and r=50%R.

The power curves of the final wind turbine and the wind turbine V00 with back-twist (V00_backtwist obtained by CFD calculations) are finally compared in the next figure to show the effect of the new airfoil 'G25x'.
The values of the simplified modal aerodynamic damping coefficient (DC) and the Annual Energy Production (AEP) are also reported.

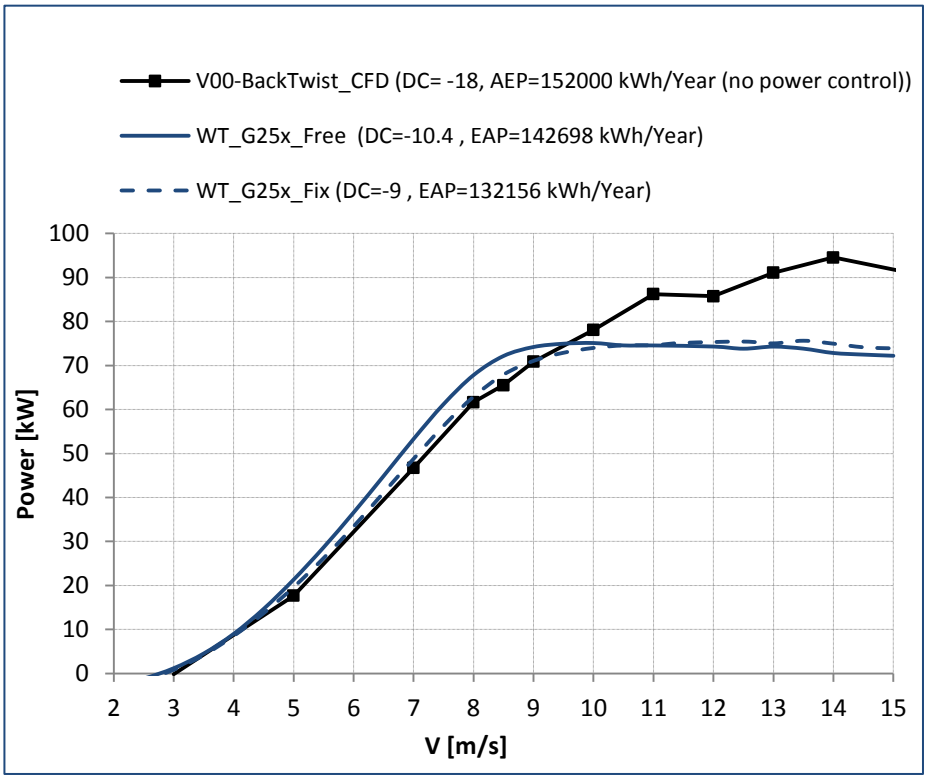

Figure 6.33: Final result (WT_G25x) of the work compared to the result of the first phase of optimization (V00) modified only with back-twist.

This last comparison shows that - for a stall regulated wind turbine - good performances (in clean and rough conditions), power control and low stall induced vibrations have been obtained only with the use of a specifically suited airfoil on the outer part of the blade.

Conclusions

In this work the design of an horizontal axis, stall regulated wind turbine has been addressed. The main effort has been focused on defining fast and accurate methodologies of preliminary design, capable of taking into account all the issues related to the aerodynamic behaviour of the blades in stall and post stall regimes, where stall regulated wind turbines reach the maximum power output, and where the aerodynamics of the blades has to ensure power and loads control.

In particular, regarding performance prediction of wind turbines in a preliminary design, advantages and shortcomings of BEM theory have been highlighted and the validation of a BEM code has been performed comparing its results in steady operating conditions with results obtained with a steady CFD simulation and those obtained with a BEM based aeroelastic code in unsteady conditions.

It has been demonstrated that BEM theory can provide results as accurate as those obtained with CFD in steady operating conditions if a correct modelling of airfoil performances along the blade is implemented.

Furthermore, it has been seen that BEM steady results are almost identical to the average of those obtained with an aeroelastic analysis in unsteady conditions.

Thus, with a correct modelling of airfoil performances, BEM based codes can be used with quite confidence in a preliminary design phase.

The issues of modelling airfoils performances on a rotating blade have been investigated and the use of the panel code Rfoil (which is able to account for rotational effects) has been validated through the comparison of the airfoil aerodynamic curves obtained with this code and those extracted from a 3D CFD simulation of a rotating rotor, for different stations along the blade. It has been seen that lift curves of the airfoils predicted by Rfoil are almost matching the CFD curves at all the stations along the blade; while drag coefficient is underestimated by Rfoil with respect to CFD results, for angles of attack beyond the stall.

Furthermore, the dynamic behaviour of the blades has been analysed; in particular, the phenomenon of stall induced vibrations has been addressed and some design solutions have been tested.

Finally, on the basis of these preliminary studies, the aerodynamic design of an experimental stall regulated wind turbine has been performed, and desirable characteristics of airfoils suited to this kind of machines have been identified.

The wind turbine obtained as final result of this work reaches all the main objectives of the design process: satisfying power performances in clean and rough conditions, good dynamic behaviour and power control.

References

[1] J.T.Petersen, H.A.Madsen, A.Björck, P.Enevoldsen, S. Øye, H.Ganander, “Prediction of Dynamics Loads and Induced Vibrations in Stall,” 1998.

[2] P. J. Moriarty, “AeroDyn Theory Manual” , 2005.

[3] *Glauert,H. “Airplane Propellers“. Form Div. L, Aerodynamic Theory, ed. W.F.Durand. Berlin: Springer Verlag, 1935. (Reprinted by Peter Smith, Glouster, Mass.,1976)*.

[4] Wilson, R.E.; Lissaman, P.B.S.; ‘Applied Aerodynamics of Wind Power Machines’; Oregon State University, USA, 1974.

[5] Burton, T., et al.; Wind Energy Handbook ; John Wiley & Sons, UK, 2001.

[6] Hansen, M.O.L.; Aerodynamics of Wind Turbines ; Second Edition, Earthscan, London, UK, 2008.

[7] J. M. Jonkman, “Modeling of the UAE Wind Turbine for Refinement of FAST _ AD” , 2003.

[8] J. G. Schepers, D. Foussekis, S. Øye, and R. R. Smith, “Verification of European Wind Turbine Design Codes , VEWTDC ; Final report,” *Ecn-01-055*, no. May, pp. 1–26, 2002.

[9] D. Simms, S. Schreck, M. Hand, and L. J. Fingersh, “NREL Unsteady Aerodynamics Experiment in the NASA-Ames Wind Tunnel : A Comparison of Predictions to Measurements,Technical Report NREL/TP-500-29494,” *Natl. Renew. Energy Lab.*, 2001.

[10] Van Rooij R.PJ.O.M., 1997, Modification of the boundary layer calculations in RFOIL for improved airfoil stall prediction, Delft University of Technology, Report IW-96087R.

[11] B. O. G. Montgomerie (ECN), A. J. Brand (ECN), J. Bosschiers (NLR), and R. P. J. O. M. Van Rooij (TUD), “THREE-DIMENSIONAL EFFECTS IN STALL,” 1997.

[12] M. Drela (MIT), “Drela M., 1989, X.FOIL: An analysis and design system for low Reynolds number airfoils, In: Lecture Notes in Engineering 54, Springer Ve,” pp. 1–32.

[13] Bosschers,J., 1995, Influence of blade rotation on the sectional aerodynamics of a wind turbine blade, National Aerospace Laboratory NLR, Report NLR CR 95290 L.

[14] M. M. Hand, D. a Simms, L. J. Fingersh, D. W. Jager, J. R. Cotrell, S. Schreck, and S. M. Larwood, “Unsteady Aerodynamics Experiment Phase VI : Wind Tunnel Test Configurations and Available Data Campaigns” 2001.

[15] L.A. Viterna and R.D. Corrigan, 1981, Fixed-pitch rotor performance of large horizontal axis wind turbines, In: Proc. Workshop on Large Horizontal Axis Wind Turbines, Report NASA CP-2230.

[16] “Tangler, J.L.; Insight into Wind Turbines Stall and Post-Stall Aerodynamics"; Wind Energy (2004) 247-260.”

[17] McCroskey, W.; Yaggy, P. Laminar boundary layers on helicopter rotors in forward flight. AIAA J. 1968, 6, 1919–1926.

[18] Robinson, M.; Hand, M.; Simms, S.; Schreck, S. Horizontal axis wind turbine aerodynamics: Three-dimensional, unsteady, and separated flow influences. In Proceedings of the FEDSM99, San Francisco, CA, USA, 18–23 July 1999; Number FEDSM99-S295-01.

[19] Corten, G. Flow Separation on Wind Turbine Blades. Ph.D. Thesis, University of Utrecht, Utrecht, The Netherlands, 2001.

[20] Sørensen, N.N.; Michelsen, J.A.; Schreck, S. Navier-Stokes predictions of the NREL phase VI rotor in the NASA Ames 80 ft _ 120 ft wind tunnel. Wind Energy 2002, 5, 151–169.

[21] Schreck, S.J.; Sørensen, N.N.; Robinson, M.C. Aerodynamic structures and processes in rotationally augmented flow fields. Wind Energy 2007, 10, 159–178.

[22] Dumitrescu,H., M Alexandrescu, N Alexandrescu: Boundary layer state and flow field structure on wind turbine blades. Proceedings ofthe Romanian Academy 2005, Series A, 6(3), pp 219-228.

[23] Lindenburg, C. Investigation into Rotor Blade Aerodynamics; Technical Report ECN-C03-025; ECN: Petten, The Netherlands, 2003.

[24] H. Himmelskamp, Profile Investigations on a Rotating Airscrew, Reports and Translations / MAP Völenrode (MAP, 1947).

[25] Banks, W.; Gadd, G. Delaying effect of rotation on laminar separation. AIAA J. 1963, 1, 941–942.

[26] Klimas, Paul C. (Sandia, Albuquerque, NM87185); 'Three-dimensional stall effects'. 1-st IEA Symposium on the Aerodynamics of Wind Turbines, London, 1986, pp.80-101.

[27] Schreck, S.; Robinson, M. Rotational augmentation of horizontal axis wind turbine blade aerodynamic response. Wind Energy 2002, 5, 133–150.

[28] Tangler, J.L. Insight into wind turbine stall and post-stall aerodynamics. Wind Energy 2004, 7, 247–260.

[29] Wood, D. A three-dimensional analysis of stall-delay on a horizontal-axis wind turbine. J. Wind Eng. Ind. Aerodyn. 1991, 37, 1–14.

[30] H. Snel, R. Houwink and J. Bosschers, 1994, Sectionalprediction of lift coefficients on rotating wind turbine blades in stall, ECN - Renewable Energy, Report ECN-C--93-052.

[31] I. Herráez, B. Stoevesandt, and J. Peinke, "Insight into Rotational Effects on a Wind Turbine Blade Using Navier–Stokes Computations",Energies 2014, 7, 6798-6822; doi:10.3390/en7106798;ISSN 1996-1073.

[32] J. G. Schepers, K. Boorsma, A. Bon, C. Kim, and T. Cho, "Results from Mexnext " pp. 14–17, 2011.

[33] Snel, H. (ECN), Houwink, R. (NLR), and Bosschers, J. (NLR) ; 'SECTIONAL PREDICTION OF LIFT COEFFICIENTS ON ROT A TING WIND TURBINE BLADES IN ST ALL '. ECN-C--93-052, Petten, December 1994.

[34] Z. Du and M. Selig, 'The effect of rotation on the boundary layer of a wind turbine blade,' Renewable Energy 20, 167–181 (2000).http://dx.doi.org/10.1016/S0960-1481(99)00109-3.

[35] Z. Du and M. Selig, A 3-D stall-delay model for horizontal axis wind turbine performance prediction, AIAA Paper No. 85-21, 1998.

[36] Chaviaropoulos, P.K. (CRES) and Hansen, M.O.L. (Risø); 'Investigating three-dimensional and rotational effects on wind turbine blades by means of a quasi-3D Navier-Stokes solver '. Journal of Fluids Engineering, Vol.22, No.2, 2000, pp.330-336.

[37] C. Lindenburg, "MODELLING OF ROTATIONAL AUGMENTATION BASED ON ENGINEERING CONSIDERATIONS AND MEASUREMENTS,European Wind Energy Conference, London, 22- 25 November, 2004," 2004.

[38] Corten, G.P. (PhD, University of Utrecht); 'Flow Separation on Wind Turbine Blades'. ISBN 90-393-2582-0, NUGI 837, January 2001.

[39] Corrigan, J.J. and Schillings, J.J. (Bell Helicopter T extron Inc, Fort Worth, T exas); 'Empirical Model for Stall Delay due to Rotation'. American Helicopter Society Aeromechanics Specialists conf, San Francisco CA, Jan. 1994.

[40] T angler, J.L. (NREL) and Selig, Michael S. (Univ . of Illinois, Urbana); 'An evaluation of an empirical model for stall delay due to rotation for HA WTs'. In Proceedings Windpower '97, Austin TX, pp.87-96.

[41] Breton, S.P.; Coton, F.N.; Moe, G. A study on rotational effects and different stall delay models using a prescribed wake vortex scheme and NREL phase VI experiment data. Wind Energy 2008, 11, 459–482.

[42] Guntur, S.; Bak, C.; Sørensen, N. Analysis of 3D stall models for wind turbine blades using data from the MEXICO experiment. In Proceedings of the 13th International Conference on Wind Engineering, Amsterdam, The Netherlands, 10–15 July 2011.

[43] K. Boorsma, J. G. Schepers, H. A. Madsen, N. Sørensen, W. Z. Shen, C. Schulz, and S. Schreck, "Mexnext-II : The Latest Results on Experimental Wind Turbine Aerodynamics 3 Influence of blade shape de- In a first phase of Mexnext several comparisons.

[44] N. N. Guntur, S., & Sørensen, "A Detailed Study of the Rotational Augmentation and Dynamic Stall Phenomena for Wind Turbines. DTU Wind Energy. (DTU Wind Energy PhD; No. 0022(EN)),," 2013.

[45] *Ervin Burton, Tony; Sharpe, David; Jenkins, Nick; Bossanyi. Wind Energy Handbook. John Wiley & Sons, LTD, 1947.* .

[46] C. Lindenburg, "Investigation into Rotor Blade Aerodynamics Analysis of the stationary measurements on the UAE phase-VI rotor in the NASA-Ames wind tunnel," *Ecnnl*, no. July, p. 114, 2003.

[47] Snel H., R. Houwink and J. Bosschers, 1994, Sectionalprediction of lift coefficients on rotating wind turbine blades in stall, ECN - Renewable Energy, Report ECN-C--93-052.

[48] J. Bosschers, 1996,Modelling of rotational effects with a 2D viscous-inviscid interaction code, National Aerospace Laboratory NLR, Report NLR CR 96521 C.

[49] G. Ronsten, 1994, Geometry and installation in wind tunnels of a Stork 5.0 WPX wind turbine blade equipped with pressure raps, Aeronautical Research Institute of Sweden FFA, Report FFAP-A 100.

[50] G. Ronsten e.a., 1989,Pressure measurements on a 5.35 m HA WT in CARDC 12x16 m2 wind tunnel compared to theoretical pressure distributions, Aeronautical Research Institute of Sweden FFA, Report FFA TN 1989-.

[51] A.J. Brand, J,W.M. Dekker, C.M. de Groot and M. Spfith, 1996, Overview of aerodynamic measurements on an Aerpac 25WPX wind turbine blade at the HAT25 experimental wind turbine - Fourth Quarter 1995, ECN - Renewable Energy, Report ECN-DE Memo-96-14.

[52] A. D. Platt, "WT _ Perf User Guide for Version 3 . 05 . 00," no. November, 2012.

[53] S Guntur, N N Sørensen , An evaluation of several methods of determining the local angle of attack on wind turbine blades, 2014 J. Phys.: Conf. Ser. 555 012045.

[54] D. C. Maniaci, "An Investigation of WT _ Perf Convergence Issues,49th AIAA Aerospace Sciences Meeting including the New Horizons Forum and Aerospace Exposition, 4 - 7 January 2011, Orlando, Florida.

[55] Buhl, M.L., Jr.; Wright, A.D.; Tangler, J.L. (December 1997). Wind Turbine Design Codes: A Preliminary Comparison of the Aerodynamics. NREL/CP-500-23975. Golden, CO: National Renewable Energy Laboratory.

[56] J. M. Jonkman and M. L. B. Jr, "FAST User ' s Guide," 2005.

[57] Wilson, Robert E.; Lissaman, Peter B.S.; Walker, Stel N.; Aerodynamic Performance of Wind Turbines. Corvallis, Oregon: Oregon State University, June 1976.

[58] Hibbs, B., Radkey, R. L. 1 98 1 . Small wind energy conversion systems rotor performance model comparison study. Rockwell Int., Rocky Flats Plant, RFP-4074/1 3470/3633 1 /8 1-0.

[59] Wilson, Robert E.; Walker, Stel N. Performance Analysis of Horizontal Axis Wind Turbines. Corvallis, OR: Oregon State University, September 1984. Prepared for the National Aeronautics and Space Administration Lewis Research Center under Grant NAG-3-278.

[60] Van Grol, H.J.; Snel, H.; Schepers, J.G. Wind Turbine Benchmark Exercise on Mechanical Loads: A state of the Art Report Volume 1 (Part A) Main Body of the Report. ECN-C--91-030. Petten, The Netherlands: Netherlands Energy Research Foundation ECN, January .

[61] Buhl, M.L., Jr. 2004. A New Empirical Relationship between Thrust Coefficient and Induction Factor for the Turbulent Windmill State. NREL/TP-500-36834. Golden, CO: National Renewable Energy Laboratory, September.

[62] Leishman, J. G., Beddoes, T. S., 1989. A Semi-Empirical Model for Dynamic Stall. Journal of the American Helicopter Society. 34(3): 3-17.

[63] Gormont, R. E. (1973)A Mathematical Model of Unsteady Aerodynamics and Radial Flow for Application to Helicopter Rotors. US Army Air Mobility Research and Development Laboratory, Technical Report, 76–67.

[64] Snel, H. and Schepers, J. G. (1991) Engineering models for dynamic inflow phenomena.Proc. 1991 European Wind Energy Conference, Amsterdam, pp. 390–396.

[65] Pitt, D. M. and Peters, D. A. (1981) Theoretical predictions of dynamic inflow derivatives.Vertica, 5(1), 21–34.

[66] Suzuki, A. and Hansen, A.C. 'Dynamic Inflow Model for YawDyn,' Proceedings of the 1998 AWEA Windpower Conference, Bakersfield, CA: pp. 233–240, 1998.

[67] Manjock, A. 'Evaluation Report: Design Codes FAST and ADAMS ® for Load Calculations of Onshore Wind Turbines.' Report No. 72042. Humburg Germany: Germanischer Lloyd WindEnergie GmbH, May 26, 2005.

[68] A. C. David J. Laino , Hansen, "USER ' S GUIDE to the Wind Turbine Aerodynamics Computer Software Aerodyn.

[69] Suzuki, A. and Hansen, A.C., June 1999, 'Dynamic Inflow Models with Nonlinear Induced Velocity Distribution for YawDyn/AeroDyn Codes,' Proceedings in CD-ROM, Windpower 1999, Burlington, VT, U.S.A., American Wind Energy Association.

[70] G. Bir, "User ' s Guide to BModes (Software for Computing Rotating Beam Coupled Modes)", 2005.

[71] Sale, D.C. and Li,Y., 2010. 'Preliminary results from a design methodology and optimization code for horizontal axis wind and hydrokinetic turbines'. The 29th International Conference on Ocean, Offshore And Arctic Engineering.

[72] P. Giguère and M. S. Selig, "Blade Design Trade-Offs Using Low-Lift Airfoils for Stall-

Regulated HAWTs, ASME/AIAA Wind Energy Symposium Reno, Nevada, January 11-14, 1999.

[73] Grasso, F., 'Multi-Objective Numerical Optimization Applied to Aircraft Design', Ph.D. Thesis, Dip. Ingegneria Aerospaziale, Università di Napoli Federico II, Napoli, Italy, December 2008.

[74] J. D. Tangler, J., Kocurek, "Wind Turbine Post-Stall Airfoil Performance Characteristics Guidelines for Blade-Element Momentum Methods,Report NREL/CP-500-36900," 2005.